

Inga Lindemark Solheim

Analysis of the FlipCage aquaculture concept

Master's thesis in Marine Technology

Supervisor: Svein Sævik, Marthe Almeland Mohn and Lars
Laukeland

June 2019

Inga Lindemark Solheim

Analysis of the FlipCage aquaculture concept

Master's thesis in Marine Technology

Supervisor: Svein Sævik, Marthe Almeland Mohn and Lars Laukeland
June 2019

Norwegian University of Science and Technology
Faculty of Engineering
Department of Marine Technology



Norwegian University of
Science and Technology



MASTER THESIS SPRING 2019

for

Stud. tech. Inga Lindemark Solheim

Analysis of the FlipCage aquaculture concept

Analyse av FlipCage fiskemerd-konseptet

Aker Solutions is involved in the engineering of a new aquaculture plant concept termed, FlipCage for use in non-exposed areas. The major idea is to enable fish cage rotation as a means of improving the salmon lice treatment procedure with fresh water. The present thesis proposal addresses the structural analysis of the concept with focus on different operating load scenarios where the thesis work is to be carried out as a continuation of the project work from fall 2018 and as follows:

1. Literature study focusing on identifying relevant design standards for the concept as well as the methodologies (methods and relevant software) related to performing design analysis of such structures.
2. Identify and describe the relevant environmental conditions to be applied as basis for design analyses.
3. Define critical load scenarios in terms of relevant load cases to be analysed.
4. Establish structural models in Sesam for the relevant load scenarios including careful modelling of the different beam cross-sections and selection of hydrodynamic coefficients.
5. Structural analysis of the selected scenarios for the relevant load cases and perform capacity checks according to the different limit states.
6. If necessary adjust the concept and perform re-analysis to fulfil the design requirements.
7. Conclusions and recommendations for further work

All necessary input data are assumed to be provided by Aker Solutions.

The work scope may prove to be larger than initially anticipated. Subject to approval from the supervisors, topics may be deleted from the list above or reduced in extent.

In the thesis report, the candidate shall present her personal contribution to the resolution of problems within the scope of the thesis work

Theories and conclusions should be based on mathematical derivations and/or logic reasoning identifying the various steps in the deduction.

The candidate should utilise the existing possibilities for obtaining relevant literature.

Thesis report format



The thesis report should be organised in a rational manner to give a clear exposition of results, assessments, and conclusions. The text should be brief and to the point, with a clear language. Telegraphic language should be avoided.

The report shall contain the following elements: A text defining the scope, preface, list of contents, summary, main body of thesis, conclusions with recommendations for further work, list of symbols and acronyms, references and (optional) appendices. All figures, tables and equations shall be numerated.

The supervisors may require that the candidate, in an early stage of the work, presents a written plan for the completion of the work.

The original contribution of the candidate and material taken from other sources shall be clearly defined. Work from other sources shall be properly referenced using an acknowledged referencing system.

The report shall be submitted in electronic format (.pdf):

- Signed by the candidate
- The text defining the scope shall be included (this document)
- Drawings and/or computer models that are not suited to be part of the report in terms of appendices shall be provided on separate (.zip) files.

Ownership

NTNU has according to the present rules the ownership of the thesis reports. Any use of the report has to be approved by NTNU (or external partner when this applies). The department has the right to use the report as if the work was carried out by a NTNU employee, if nothing else has been agreed in advance.

Thesis supervisors:

Prof. Svein Sævik, NTNU
Lars Laukeland, Aker Solutions
Marthe Almeland Mohn, Aker Solutions

Deadline: June 11th , 2019

Trondheim, January 14th , 2019

Svein Sævik

Candidate – date and signature:

07.06.2019

Preface

This thesis is the concluding work to a five year integrated master program in Marine Technology at the Norwegian University of Science and Technology (NTNU). This thesis was proposed by Aker Solutions and includes a study of the fish farming concept FlipCage.

I want to thank Svein Sævik, Professor at the Department of Marine Technology, for his guidance. He has been available throughout the semester for guidance and discussions regarding my thesis. A special thank you to Marthe Almeland Mohn and Lars Laukeland from Aker Solutions, for giving me the opportunity to write this thesis and giving me great industry insight. Are Sandven Kristiansen, Aiwei Su and Andreas Fredborg from Aker Solutions have also been to great help and available at all times. Without you, this thesis would not have been possible.

The work submitted is my own unless otherwise stated. Material taken from other sources is clearly marked throughout the thesis.

June 7, 2019



Inga Lindemark Solheim

Abstract

While the aquaculture industry is growing quickly, it is also facing great challenges connected to fish lice, environmental impact and lack of sheltered locations. To solve some of these challenges, the Norwegian Directorate of Fishery launched a new aquaculture license in 2015. It is awarded to concepts showing considerable innovation and investments. Aker Solutions, on behalf of Norway Royal Salmon, developed a set of aquaculture concepts eligible for this license. One of these concepts is called FlipCage and aims to improve the fresh water treatment of salmon and reduce the environmental footprint of fish farming.

FlipCage is based on an idea of a fish farm being able to rotate 180° about its horizontal axis at the waterline. It consists of one permeable part and one impermeable part. The rotation makes it possible to switch between these two operational states. The permeable part is a cylindrical framework with net panels and the impermeable part is designed as a dome.

This thesis carries out a study of FlipCage. It aims to identify critical load cases and to carry out an ultimate limit state analysis with respect to von Mises stress and buckling. FlipCage is exposed to wind, current and waves. Contribution from wind and current are neglected in the analysis. This is because the reaction forces are absorbed by the mooring system. In addition, wind and current will generate a heeling angle. This is small and will therefore not affect the structural response significantly.

The first method used to determine critical waves was based on a stochastic spectral response analysis. A set of sectional planes was defined on the structure and the hydrodynamic load transfer function was calculated for each of these. In the following step, they were combined with a wave spectrum, and response amplitude operators for each sectional load were estimated. From these results, the waves generating maximum response for each sectional load were identified.

The second method is referred to as a stress peak analysis. It is based on calculating the structural response for a set of unit waves. The waves have periods in the interval between three and twenty seconds, with half a second step size. This was to cover the entire interval of periods in a sea state. In areas where the structure experience high levels of stress, representative elements were chosen. For each element the stress was plotted for all wave periods and directions. This resulted in a set of stress response amplitude operators. From these plots, periods and directions generating the highest levels of stress were identified.

The resulting waves from the two methods were used as input to the ultimate limit state analysis. The capacity checks follows DNV GL's offshore standard Design of Offshore Steel Structures, General - LRFD method [6]. Load and material factors were used in the post-processing of the results. The von Mises yield criteria and the buckling utilisation factor were applied in the design check.

The results from the two design wave analysis indicates that the most critical wave periods are in the interval five to ten seconds. Even though both methods gave a relative similar set of waves, there were some differences that turned out to be critical in the ultimate limit state analysis. The ultimate limit state analysis gave areas with stress levels exceeding the allowable limit. The most critical wave was identified in the stress peak analysis. However, it was not picked up by the statistic design wave analysis. This indicates that the sectional planes chosen did not cover all the critical responses. From the results it may be concluded that a stress peak analysis is a safer choice when the structure has a geometry that is deviating from previous experience.

The ultimate limit state analysis produced stress levels exceeding the allowable limit, and it is therefore necessary to strengthen these areas. In the member capacity check several cross-sections were utilised above their capacity, both with respect to yielding and buckling. It is necessary to redesign and perform a new ultimate limit state check for both these criteria.

An eigenvalue analysis was performed and all eigenfrequencies lies outside what is expected to be experienced in a sea state. It is therefore concluded that excitation of these modeshapes is not a problem.

In general, the concept seems feasible. However, small adjustments to plate thicknesses and beam cross-sections are necessary. In addition, further work includes a local structural analysis with a higher level of detail in the structural modelling. It is also relevant to perform fatigue limit state and accidental limit state analysis.

Sammendrag

Fiskeoppdrett har vært en industri i enorm utvikling de siste årene, men med denne utviklingen har det også dukket opp en rekke utfordringer knyttet til fiskelus, forurensning og mangel på lokasjoner. Fiskeridirektoratet lanserte i 2015 utviklingstillatelser som blir tilegnet oppdrettskonsepter som viser innovasjon og betydelig investering. Aker Solutions, på oppdrag fra Norway Royal Salmon, utviklet en rekke konsepter med tanke på denne lisensen. Et av disse konseptene kalles FlipCage og har som mål å forbedre ferskvannsbehandling av laks og redusere å redusere forurensningen fra fiskeoppdrett.

FlipCage er basert på en idé om en fiskemerde som kan rotere 180° om sin horisontale akse ved vannlinjen. Den består av en permeable og en ikke-permeable del. Rotasjonen gjør det mulig å bytte mellom disse to tilstandene. Den permeable delen består av et sylindrisk rammeverk med nettingpaneler og den ikke-permeable delen er designet som en kuppel.

Denne oppgaven tar for seg en studie av FlipCage. Målet er å identifisere kritiske lasttilfeller og utføre en grenseverdianalyse i forhold til von Mises spenninger og knekking. FlipCage er eksponert for vind, bølger og strøm. I analysen neglisjeres strøm og vind, da det antas at krenningsvinkelen FlipCage får blir liten og resultatkraftene i hovedsak blir tatt opp av forankringssystemet.

Den første metoden som ble brukt for å identifisere kritiske bølger, var basert på en stokastisk-spektral-responsmetode. Et sett med seksjonsplan ble definert på konstruksjonen og den hydrodynamiske last-transferfunksjonen ble beregnet for hvert av disse planene. I neste steg ble disse kombinert med et bølgespektrum og responsamplitudeoperatøren for hver seksjonslast ble estimert. Fra disse resultatene ble bølgen som ga den maksimale responsen for hver seksjonslast identifisert.

Den andre metoden refereres til som en spennings-topp analyse. Den er basert på å beregne den strukturelle responsen for et sett av enhetsbølger. Bølgene har perioder i intervallet mellom tre og tjue sekunder. Dette er for å dekke hele spekteret med perioder som finnes i en sjøtilstand. For hvert valgte element ble spenningen plottet for alle bølgeperioder og retninger. Dette resulterte i et sett av spennings-responsamplitudeoperatorer. Fra disse plottene ble det identifisert perioder og retninger som genererte de høyeste spenningsnivåene. Bølgene fra de to metodene ble brukt som inputverdier i grenseverdianalysen. Grenseverdieneanalysen følger DNV GLs offshore standard Design of Offshore Steel Structures, General - LRFD method [6]. Last og materialfaktorene ble brukt i postprosesseringen av resultatene.

Resultatene fra de to designbølgeanalysene indikerer at de mest kritiske bølgene har perioder i intervallet mellom fem og ti sekunder. Selv om begge metodene ga et relativt lignende sett med bølger, var det noen forskjeller som viste seg å være kritiske i grenseverdianalysen. Grenseverdianalysen ga områder med stressnivåer som overskrider det tillatte spenningsnivået.

Den mest kritiske bølgen ble identifisert i spennings-topp analysen. Den ble i midlertidig ikke plukket opp i den stokastiske analysen. Dette indikerer at de valgte seksjonsplanene ikke dekker alle de kritiske lastene. Fra resultatene kan det konkluderes med at en spennings-topp analyse er et sikrere valg når konstruksjonen har en geometri som avviker fra tidligere erfaringer.

Grenseverdianalysen ga spenningsnivåer som overstiger det tillate nivået, og det er derfor nødvendig å forsterke disse områdene. Kodesjekken viste at flere av tverrsnittene ble utnyttet over sin kapasitet, med hensyn på både knekking og flyt. Det er derfor nødvendig å gjøre endringer på designet av rammeverket slik at det ligger innenfor kravene.

En egenverdianalyse ble utført og alle egenfrekvensene ligger utenfor det som forventes å oppleve i en sjøtilstand. Det konkluderes derfor med at eksitasjon av disse modene ikke er et problem.

Generelt er dette et gjennomførbart konsept. Det er nødvendig med små justeringer av platetykkelser og tverrsnitt. I tillegg kreves det videre arbeid hvor utmatting og ulykkeslaster blir analysert.

Table of Contents

Preface	iii
Abstract	v
Sammendrag	vii
Table of Contents	ix
List of Figures	xiii
List of Tables	xvii
Nomenclature	xix
1 Introduction	1
1.1 Background and Motivation	1
1.2 Objective	1
1.3 Outline of Thesis	2
2 FlipCage	5
2.1 Concept of FlipCage	5
2.2 Main Dimensions	6
2.3 Location and Metocean Data	9
3 Theory	11
3.1 Coordinate System and Rigid-Body Modes	11
3.2 Hydrostatic Stability	12
3.3 Wave Theory	13
3.3.1 Surface Elevation	13
3.3.2 Velocity Potential	14
3.4 Wave Induced Forces	15

3.4.1	Diffraction and Radiation Problem	15
3.4.2	Diffraction Problem	15
3.4.3	Radiation Problem	16
3.4.4	Morison's Equation	16
3.5	Wind Loads	17
3.6	Current Loads	18
3.7	Static Response	18
3.8	Dynamic Response	18
3.9	Solving the Equation of Motion	19
3.10	Wave Statistics	21
3.11	Frequency Domain and Stochastic Response Analysis	23
3.12	Eigenvalues	24
3.13	Buckling of Beams	25
4	Standards and Recommended Practice	27
4.1	Norwegian Law - NYTEK	27
4.2	NS 9415	27
4.3	DNV GL	28
4.4	Applied Standards	28
5	SESAM Software	29
5.1	Introduction to Sesam	29
5.2	GeniE	30
5.3	Presel	30
5.4	HydroD	30
5.5	Wadam - Hydrodynamic Analysis	31
5.6	Postresp - Post-Processor for Statistical Response Calculations	31
5.7	Sestra	32
5.8	Xtract	32
6	Model Description	33
6.1	Structural Model	33
6.1.1	General Specifications	33
6.1.2	Mechanical Properties and Center of Gravity	34
6.1.3	Boundary Conditions	34
6.1.4	Choice of Elements	35
6.2	Super Elements	36
6.3	Hydrodynamic Model	37
6.3.1	Input to HydroD	37
6.3.2	Modelling of Fish Net	38
6.3.3	Morison Properties	38

7	Contribution From Wind and Current	41
7.1	Wind and Current in a Structural Analysis	41
7.2	Calculation of Heeling Angle	41
7.3	Overturning Moment due to Wind	42
7.4	Overturning Moment due to Current	44
7.5	Total Heeling Angle	44
8	Design Waves	45
8.1	Determining Design Waves for a Structure	45
8.2	Wave Data	45
8.3	Statistical Design Wave Analysis	46
8.4	Design Wave Analysis - Stress Peak Analysis	49
9	Global Analysis - Ultimate Limit State	53
9.1	Flow Chart of Structural Analysis	53
9.2	Post-Processing and Load Factors	54
9.3	Yield Check	54
9.4	Buckling Check	55
9.5	Load Case Numbering	55
10	Eigenvalue Problem	57
10.1	Modal Analysis	57
10.2	Contribution from Added Mass	57
11	Results	59
11.1	Results - Eigenvalue Analysis	59
11.2	Model Verification	60
11.3	Convergence Test - Hydrodynamic Model	62
11.4	Convergence Test - Structural Model	63
11.5	Results From Design Wave Analysis	65
11.5.1	Results From Statistical Design Waves	65
11.5.2	Extracting Physical Response of Complex Results	67
11.5.3	Results From Design Wave Analysis - Stress Peak	68
11.5.4	Discussion of Results - Design Wave Analysis	73
11.6	Results from ULS Analysis	74
11.6.1	Static Load Case	74
11.6.2	ULS From Statistical Design Wave Analysis - von Mises Stress	74
11.6.3	ULS From Stress Peak Analysis - von Mises Stress	75
11.6.4	Discussion of ULS Results - von Mises Stress	76
11.7	Buckling Capacity Check	76

12 Conclusion and Further Work	79
12.1 Conclusion	79
12.1.1 Eigenvalue Analysis	79
12.1.2 Design Wave Analysis	79
12.1.3 Ultimate Limit State	80
12.2 Further Work	80
Bibliography	80
A Design Drawings	I
A.1 Global Design	I
B Load case numbering	V
C Results From ULS Analysis	VII
C.1 Results ULS - Stress Peak	VII
C.2 Results ULS - Statistical Response	IX
D Detailed Calculations of Statistical Design Waves	XIII

List of Figures

2.1	Concept model of FlipCage	5
2.2	Conceptual idea of switching between closed and open operation	6
2.3	Main components of FlipCage	6
2.4	Main dimensions of the FlipCage	7
2.5	Principle sketch of I-section	8
2.6	Principle sketch of square section	8
2.7	Location of the FlipCage - close up [29]	9
2.8	Coinciding values for 50-year return period [29]	9
3.1	Coordinate system and rigid-body modes [15]	11
3.2	Definition of metacenter [21]	12
3.3	Definition of different wave parameters [20]	13
3.4	Maximum response for different loading frequencies	20
3.5	Flowchart of how the RAO connects the surface elevation η and the dynamic response	21
3.6	Principle sketch of a Jonswap spectrum	22
5.1	Overview of the Sesam software [11]	29
6.1	Main components of the structure, starting from the left: cylindrical frame work, dome, floating collar and rotation tanks.	33
6.2	Top view of the structural model showing the coordinate system and wave directions	34
6.3	Boundary conditions for the global structural model	35
6.4	Elements assigned by Sestra	35
6.5	Membrane and bending condition of a shell [27]	36
6.6	Illustration of how the structural model is split into three sub models.	37
6.7	Snapshot of the combined model in Presel	37
6.8	Snapshot of the model in HydroD - Statistical Design Waves	38

6.9	Snapshot of the model in HydroD - Stress Peak Analysis	38
6.10	Plot of the water particle velocity.	39
7.1	Wind and current forces affecting FlipCage	42
7.2	Shape coefficients for sphere-shaped structures [9]	43
7.3	Centroid of a hemisphere [25]	43
8.1	Steps in the design wave process [7]	46
8.2	Sectional planes	48
8.3	Flowchart of the statistical design wave analysis	49
8.4	Flowchart of a design wave stress peak analysis.	50
9.1	Flowchart of an ULS analysis.	53
9.2	Load factors recommended by DNVGL-OS-C101 [6]	54
10.1	Added mass for a circular cross-section in the vertical direction [9]	58
10.2	Added mass for a circular cross section in the horizontal direction [9]	58
11.1	Modeshape displacement from eigenperiod 2.128 seconds	60
11.2	Modeshape displacement form eigenperiod 2.123 seconds	60
11.3	Modeshape displacement from eigenperiod 1.499 seconds	60
11.4	Excerpt of hydrodynamic properties from WADAM.LIS	61
11.5	Added mass coefficient, A_{55} , for different mesh sizes	62
11.6	Damping coefficient, B_{55} , for different mesh sizes	63
11.7	Position used in the mesh convergence study for ULS analysis	64
11.8	Result of mesh convergence study for the ULS analysis	64
11.9	RAO SECL1011	65
11.10	RAO SECL1012	65
11.11	RAO SECL1013	65
11.12	RAO SECL3013	65
11.13	RAO SECL3021	66
11.14	RAO SECL3023	66
11.15	RAO SECL3024	66
11.16	RAO SECL3031	66
11.17	RAO SECL3033	66
11.18	RAO SECL3034	66
11.19	Stress variation through a cycle for a complex result case [14]	67
11.20	Areas with high stress peaks	68
11.21	Maximum von Mises stress in element 5205	69
11.22	Maximum von Mises stress in element 3618	69
11.23	Maximum von Mises stress in element 5084	69
11.24	Maximum von Mises stress in element 5511	69

11.25	Maximum von Mises stress in element 3834	70
11.26	Maximum von Mises stress in element 19261	70
11.27	Critical beam elements used in a stress peak analysis	70
11.28	Maximum normal stress through a cycle for element 2	71
11.29	Maximum normal stress through a cycle for element 89	71
11.30	Maximum normal stress through a cycle for element 795	71
11.31	Maximum normal stress through a cycle for element 2215	71
11.32	Maximum normal stress through a cycle for element 3085	72
11.33	Surface pressure - static load case	74
11.34	Color coding of the von Mises stress level given in Pascal	74
11.35	von Mises stress load case 1.02 - ULSA	75
11.36	von Mises stress load case 1.11 - ULSA	75
11.37	von Mises stress load case 1.02 - ULSB	75
11.38	von Mises stress load case 1.11 - ULSB	75
11.39	Load case 2.05 - ULSA	75
11.40	Load case 2.06 - ULSA	75
11.41	Load case 2.05 - ULSB	76
11.42	Load case 2.06 - ULSB	76
11.43	Capacity check of beams from design waves identified in a statistical design wave analysis.	77
11.44	Capacity check of beams from design waves identified in a stress peak analysis.	77
C.1	Load case 2.02 ULSA maximum von Mises stress	VII
C.2	Load case 2.03 ULSA maximum von Mises stress	VII
C.3	Load case 2.04 ULSA maximum von Mises stress	VII
C.4	Load case 2.07 ULSA maximum von Mises stress	VII
C.5	Load case 2.08 ULSA maximum von Mises stress	VIII
C.6	Load case 2.09 ULSA maximum von Mises stress	VIII
C.7	Load case 2.10 ULSA maximum von Mises stress	VIII
C.8	Load case 2.11 ULSA maximum von Mises stress	VIII
C.9	Load case 2.02 ULSB maximum von Mises stress	VIII
C.10	Load case 2.03 ULSB maximum von Mises stress	VIII
C.11	Load case 2.04 ULSB maximum von Mises stress	IX
C.12	Load case 2.07 ULSB maximum von Mises stress	IX
C.13	Load case 2.08 ULSB maximum von Mises stress	IX
C.14	Load case 2.09 ULSB maximum von Mises stress	IX
C.15	Load case 2.10 ULSB maximum von Mises stress	IX
C.16	Load case 2.11 ULSB maximum von Mises stress	IX
C.17	Load case 1.03 ULSA maximum von Mises stress	X
C.18	Load case 1.04 ULSA maximum von Mises stress	X

C.19 Load case 1.05 ULSA maximum von Mises stress	X
C.20 Load case 1.06 ULSA maximum von Mises stress	X
C.21 Load case 1.07 ULSA maximum von Mises stress	X
C.22 Load case 1.08 ULSA maximum von Mises stress	X
C.23 Load case 1.09 ULSA maximum von Mises stress	XI
C.24 Load case 1.10 ULSA maximum von Mises stress	XI
C.25 Load case 1.03 ULSB maximum von Mises stress	XI
C.26 Load case 1.04 ULSB maximum von Mises stress	XI
C.27 Load case 1.05 ULSB maximum von Mises stress	XI
C.28 Load case 1.06 ULSB maximum von Mises stress	XI
C.29 Load case 1.07 ULSB maximum von Mises stress	XII
C.30 Load case 1.08 ULSB maximum von Mises stress	XII
C.31 Load case 1.09 ULSB maximum von Mises stress	XII
C.32 Load case 1.08 ULSB maximum von Mises stress	XII

List of Tables

2.1	Main dimensions - FlipCage	7
2.2	Profiles for the different structural members	8
2.3	Properties of the cross-sections	8
2.4	Material properties	9
6.1	Modified densities	34
6.2	Stiffness of the fish farm	35
6.3	General input values to HydroD	38
6.4	Drag velocity calculations	39
6.5	Properties of the Morison cross-sections	39
7.1	Calculations of wind force	43
7.2	Calculations of current force	44
7.3	Total heeling angle due to wind and current forces	44
8.1	Wave directions for design wave analysis	45
8.2	Numbering of degrees of freedom	47
8.3	Naming of sectional planes	48
8.4	Forces and moments checked for the different sectional planes	48
8.5	Jonswap spectra used for design wave analysis	49
10.1	Modified densities including contribution from added mass	58
11.1	Eigenperiods and frequencies from the free vibration analysis	59
11.2	Properties of design waves - Statistical analysis	67
11.3	Corresponding element number to stress peak area	69
11.4	Corresponding element number to stress peak area	71
11.5	Design waves from a stress peak analysis	72

Nomenclature

Abbreviations

NS	Norwegian Standard
NDF	Norwegian Directorate of Fishery
NRS	Norway Royal Salmon
CFD	Computational Fluid Dynamics
COB	Center of Buoyancy
COG	Center of Gravity
DNV GL	Det Norske Veritas and Germanischer Lloyd
FEM	Finite Element Method
JONSWAP	Joint North Sea Wave Project
RAO	Response Amplitude Operator
ULS	Ultimate Limit State

Symbols

Φ	Eigenvector
A	Added mass matrix
B	Damping matrix
C	Restoring matrix

C_D	Drag coefficient matrix
$H(\omega)$	Response transfer function
K	Stiffness matrix
M	Mass matrix
R	Load matrix
V	Velocity vector of the wave field
ϵ_n	Phase angle
η	Surface elevation
γ_M	Material factor
λ	Wave length
$F(t)$	Time dependent external load vector
ω	Wave frequency
ϕ	Velocity potential
ρ	Density of sea water
ρ_a	Density of air
σ	Projected area of a Morison element
σ_a	Parameter in the Jonswap spectra
σ_b	Parameter in the Jonswap spectra
σ_s	Standard deviation
σ_x	Standard deviation of parameter x
σ_x	Stress in the x-direction
σ_y	Stress in the y-direction
σ_{vM}	von Mises stress
τ_{xy}	Shear stress

θ	Heeling angle
ζ	Wave elevation
ζ_a	Wave amplitude
A_W	Waterplane area
C_D	Drag coefficient
C_s	Shape coefficient
D	Diameter
E	Wave energy
F_w	Wind force
g	Acceleration of gravity
H	Wave height
h	Water depth
H_s	Significant wave height
k	Wave number
N_{waves}	Number of waves in a sea state
p	Dynamic pressure
p	Percentile level for exceeding a maximum value
S	Projected area
S	Steepness criteria
$S(\omega)$	Wave spectrum
T	Wave period
T_p	Peak period in a sea state
T_z	Zero upcrossing period
u	Horizontal water particle velocity

v	Current velocity
V_{max}	Linearising velocity amplitude
$V_{T,z}$	Wind velocity
M_θ	Restoring moment
∇	Displaced volume
I_{xx}	Moment of inertia

Introduction

1.1 Background and Motivation

The aquaculture industry roots back to the stone age [22] and has become one of Norway's leading industries. In 2017 it produced a first-hand value of fish for approximately 65 NOK billion [34]. According to the Norwegian Directorate of Fishery (NDF) there are 1044 registered locations for fish farming and 1015 licenses for edible fish in Norway [16].

NDF is responsible for issuing fish farming licenses. In 2015 they released a new type called developing licenses [17], these are awarded to concepts showing considerable innovation and investment. The purpose is to develop new technologies that can solve one, or more, of the challenges the industry is facing. These are connected to environmental footprint, lice and a lack of available sheltered locations [23].

Aker Solutions developed a set of concepts on behalf of Norway Royal Salmon (NRS) that would be eligible for the development license. One of the concepts is FlipCage which aims to reduce the environmental footprint of fish farming.

NYTEK [18] is the Norwegian regulation addressing the technical requirements for floating fish farms. Together with the standard NS 9415 [30], it sets the technical safety level.

1.2 Objective

Aker Solutions and Norway Royal Salmon applied for a development license for FlipCage in November 2017. As it is not yet approved by NDF, only a preliminary study of the concept has been conducted. The objective is to identify critical load scenarios, analyze these.

Two methods are used to identify the critical load scenarios. First a standard design wave

analysis as described by DNV GL [7] is used. This method uses short term statistics to determine the most critical load scenarios in a sea state. The second is referred to as a stress peak analysis and is based on checking the structural response for a set of directions and periods from a unit wave. By locating areas with stress peaks and plotting the stress as a function of period, a set of critical periods and directions is found. The thesis will look at benefits and disadvantages with the two methods and compare the results. An ultimate state capacity check for von Mises stress and buckling is performed based on the results from the design wave analysis. Furthermore, an eigenvalue analysis is executed.

The software used, does not support composite materials. As FlipCage's dome is made of a composite material, it is not of interest in the analysis.

1.3 Outline of Thesis

Chapter 1 gives a brief overview of the fish farming industry and the objective of the thesis.

Chapter 2 gives a description of FlipCage.

Chapter 3 provides the necessary background theory to perform and interpret a design wave and ultimate limit state analysis.

Chapter 4 describes which standards and regulations that are used throughout the thesis.

Chapter 5 describes the software used in the analysis.

Chapter 6 provides a description of how FlipCage is modeled by the Sesam software.

Chapter 7 describes how the contribution from wind and current is included in the analysis.

Chapter 8 presents the steps behind the two different design wave approaches.

Chapter 9 presents the requirements for an ultimate limit state analysis.

Chapter 10 describes the modelling and method behind the eigenvalue analysis.

Chapter 11 presents the results and discussion of the design wave, ULS and eigenvalue analysis.

Chapter 12 presents the final conclusions and further work.

Bibliography includes all literature used.

Appendix contains additional results, input files and design sketches.

Digital appendix contains files used in the analysis. The following folders are used for the different analysis,

- *FishFarm*: Main structural model in Genie, where all submodels are exported from. Includes the eigenvalue analysis.
- *FC*: used in the statistical design wave analysis
- *FC_Metode2*: used in the stress peak design wave analysis
- *FC_static*: used in the ULS analysis with the waves from the statistical design wave analysis
- *FC_ULS*: used in the ULS analysis with the waves from the stress peak analysis as input.
- *Member_Check*: used in the buckling analysis with design waves from the statistical method.
- *Member_Check2*: used in the buckling analysis with design waves from the stress peak method

FlipCage

2.1 Concept of FlipCage

FlipCage is a fish farming concept developed by Aker Solutions based on an idea from Norway Royal Salmon (NRS). A model of FlipCage can be found in Figure 2.1. The application to the Norwegian Directorate of Fishery includes three fish farms connected to one barge.

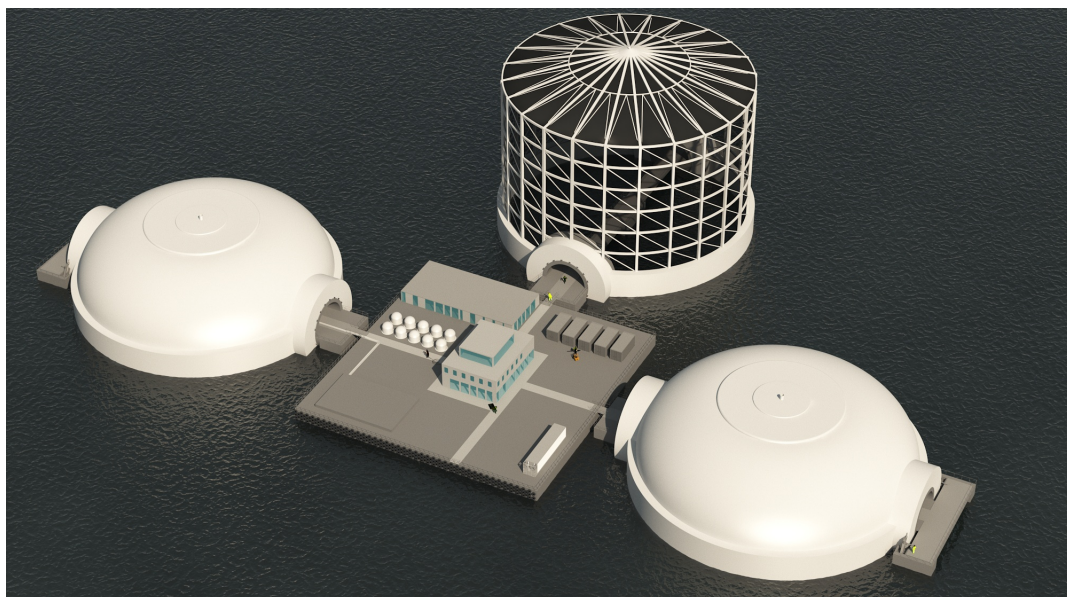


Figure 2.1: Concept model of FlipCage

FlipCage is based on an idea of a fish farm that is able to rotate 180° about its horizontal axis close or at the waterline. It consists of a permeable and a non-permeable part, this allows it to switch between closed and open operation. Open operation is defined as fluid contact between the water inside and outside the fish farm and closed as no contact between the fluids.

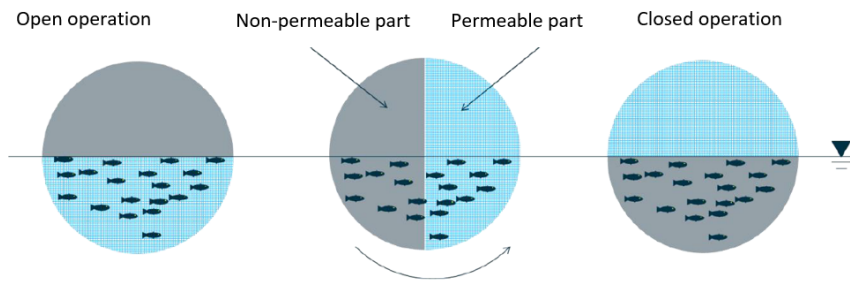


Figure 2.2: Conceptual idea of switching between closed and open operation

Freshwater treatment of salmon, in relation to delousing, is one of the operations that is exposed to the most risk in fish farming. These include fish escape, fish welfare and mortality. By rotating the fish farm around its horizontal axis, fish can be moved from open to closed operation in a gentle way without the use of crowding, well boat or pumping of the fish. It is also thought to utilize the rotation for the following operations,

- Remove fouling through air drying of permeable part.
- Crowding and sorting of fish.
- Use closed operation when treating the fish with oral medicines that can affect the environment.
- Inspection, maintenance and replacement of structural elements.

2.2 Main Dimensions

Figure 2.3 shows FlipCage in closed operation and specifies main components. Main dimensions are given in Table 2.1 and Figure 2.4.

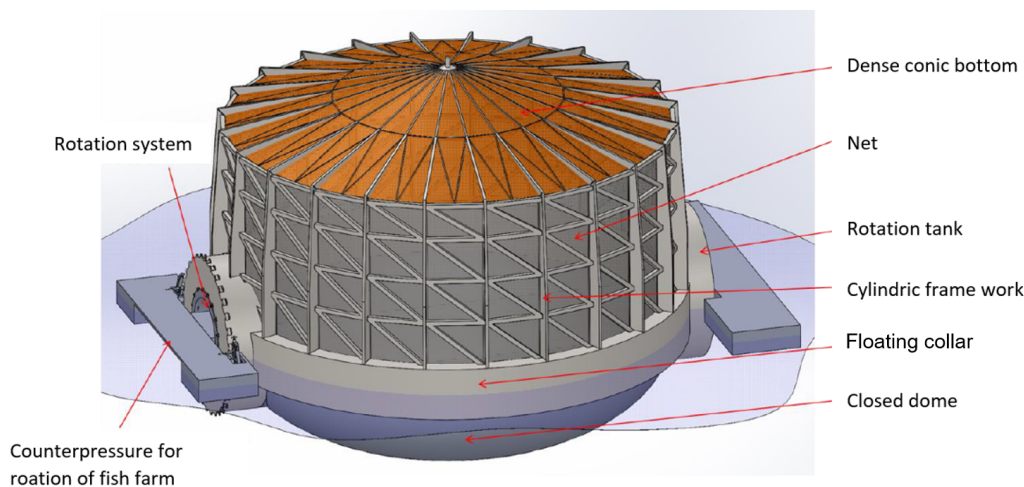


Figure 2.3: Main components of FlipCage

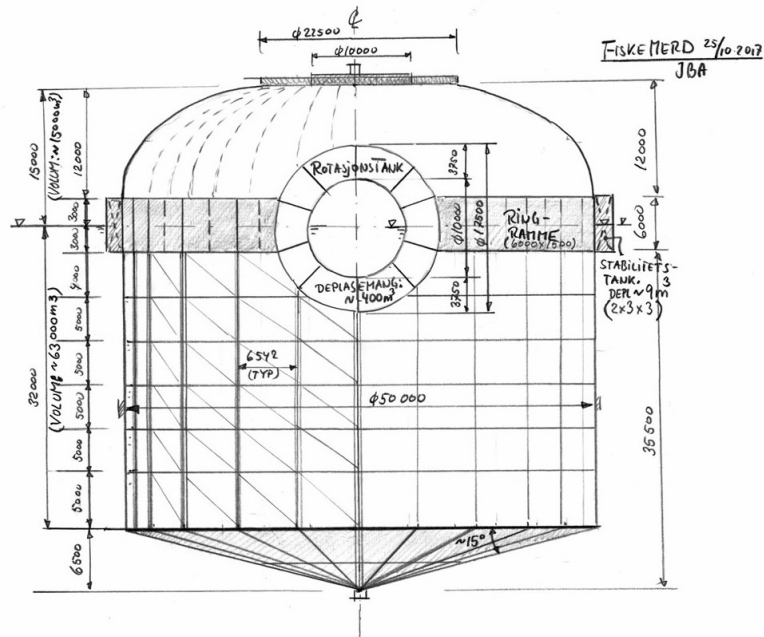


Figure 2.4: Main dimensions of the FlipCage

Table 2.1: Main dimensions - FlipCage

Component	Size	Unit
Diameter of floating collar	50	m
Thickness floating collar	1.5	m
Height of floating collar	6	m
Plate thickness	10	mm
Outer diameter rotation tank	17	m
Inner diameter rotation tank	10	m
Height of closed dome	12	m
Height of cylindrical frame work	29	m
Inner diameter frame work	50	m
Height conic bottom	6.5	m

Center of gravity is estimated to be in the center of the fish farm and -3.2 meters below the waterline. Profiles of the different structural members are given in Table 2.2. Cross-sectional properties for the cylindrical framework are given in Table 2.3.

Table 2.2: Profiles for the different structural members

Structural member	Profile type
Vertical profiles	HEB340
Horizontal profiles	HEB450
Horizontal profiles - reinforced	RHS 300x300x16
Diagonals	RHS 300x300x12.5
Diagonals - reinforced	RHS 300x300x16
Radials	HEA200
Ring 1	HEA180
Ring 2	HEA160
Ring 3 and 4	HEA120

Table 2.3: Properties of the cross-sections

Profile name	Profile type	h [mm]	b [mm]	r [mm]	tw [mm]	tf [mm]
HEB340	I-section	340	300	27	12	21.5
HEB450	I-section	450	300	27	14	26
HEA200	I-section	190	200	18	6.5	10
HEA120	I-section	114	120	12	5	8
HEA160	I-section	152	160	15	6	9
HEA180	I-section	171	180	15	6	9.5
RHS300x300x16	Rectangular hollow section	300	300	24	16	
RHS300x300x12.5	Rectangular hollow section	300	300	18.8	12.5	

A principle sketch of I-section and rectangular hollow cross-section are given in Figure 2.5 and 2.6.

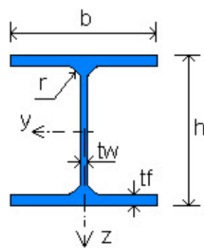


Figure 2.5: Principle sketch of I-section

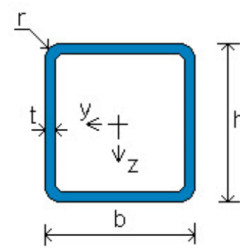


Figure 2.6: Principle sketch of square section

Mechanical properties for the different materials are given in Table 2.4. The floating collar is made out of steel and the framework is made of aluminum. The dome is made of a composite material.

Table 2.4: Material properties

Material	Density [kg/m ³]	Yield strength [MPa]	Modulus of elasticity [GPa]
Steel	7850	420	210
Aluminium	2730	350	70

2.3 Location and Metocean Data

FlipCage is thought to be located at Andal in the municipality of Bømlo. The location can be seen in Figure 2.7. This is an inshore location and is sheltered from most of the waves [29]. A site survey is required by NS 9415 [30] and is executed by Noomas Sertifisering AS. Figure 2.8 shows results for wind, wave and current for a 50-year return period. It is wanted that FlipCage is able to withstand a significant wave height, H_s , of 2.5 – 3.5 meters. Therefore, this value will be used in the design wave analysis.

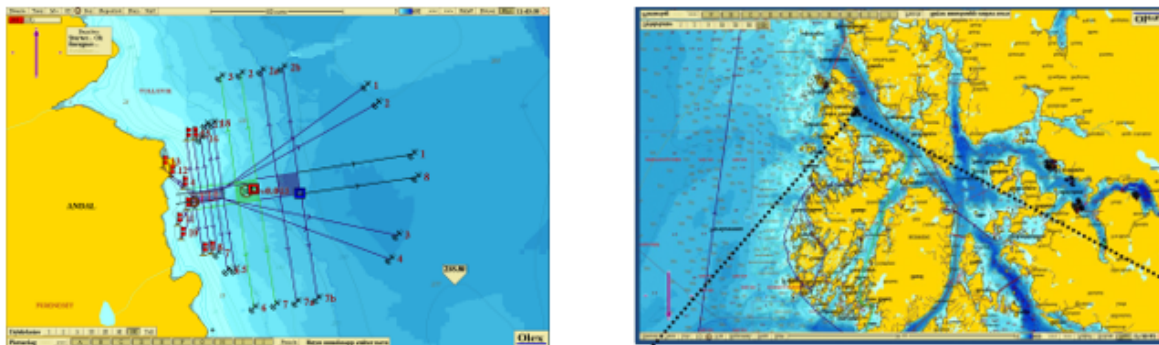


Figure 2.7: Location of the FlipCage - close up [29]

Returperiode 50 år										
Kompassretning			N	NO	O	SO	S	SV	V	NV
Vind, U ₁₀ (tabell 4.1)	Retning fra	m/s	29	20	26	29	33	33	33	33
Strom (tabell 4.2)	5m	cm/sek	62	50	34	47	50	40	37	69
	Retning	°Mot	157.5-202.5	202.5-247.5	247.5-292.5	292.5-337.5	337.5-22.5	22.5-67.5	67.5-112.5	112.5-157.5
	15m	cm/sek	59	33	35	43	14	36	49	57
	Retning	°Mot	157.5-202.5	202.5-247.5	247.5-292.5	292.5-337.5	337.5-22.5	22.5-67.5	67.5-112.5	112.5-157.5
Vindbolger (tabell 4.5)	Hs	m	1.6	1.3	1.8	1.6	1.4	0.8	0.6	1.1
	Tp	s	3.8	3.9	4.2	3.7	3.3	2.2	1.9	2.8
	Retning	°Fra	360	45	90	135	180	225	270	315
Havbolger (se egen rapport)	Hs	m	-	-	-	-	0.2	0.2	-	-
	Tp	s	-	-	-	-	14.3	14.3	-	-
	Retning	°Fra	-	-	-	-	180	225	-	-
Kombinert (tabell 4.6)	Hs	m	-	-	-	-	1.4	0.8	-	-
	Tp	s	-	-	-	-	14.3	14.3	-	-
	Retning	°Fra	-	-	-	-	180	225	-	-

Figure 2.8: Coinciding values for 50-year return period [29]

Theory

3.1 Coordinate System and Rigid-Body Modes

Figure 3.1 shows the coordinate system and rigid-body modes for a floating structure.

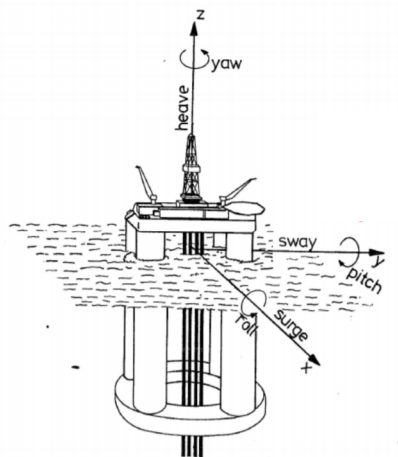


Figure 3.1: Coordinate system and rigid-body modes [15]

There are three translational and three rotational motions, these are defined as

Translational degrees of freedom	Rotational degrees of freedom
---	--------------------------------------

- | | |
|--|--|
| <ul style="list-style-type: none"> • Surge - η_1 • Sway - η_2 • Heave - η_3 | <ul style="list-style-type: none"> • Roll - η_4 • Pitch - η_5 • Yaw - η_6 |
|--|--|

All motions are defined in the inertial reference frame earth-fixed. This is valid in linear seakeeping where it is assumed that motion amplitudes are small. A benefit of using this definition is that Newton's second law can be applied directly [15].

3.2 Hydrostatic Stability

Hydrostatic stability of a floating structure is affected by the geometry and weight. A floating structure in static equilibrium is under the influence of two forces, weight and buoyancy. The points of attack of these two forces, center of gravity (COG) and center of buoyancy (COB), are important, as these will affect the stability. The parameters of interest in the hydrostatic analysis are shown in Figure 3.2.

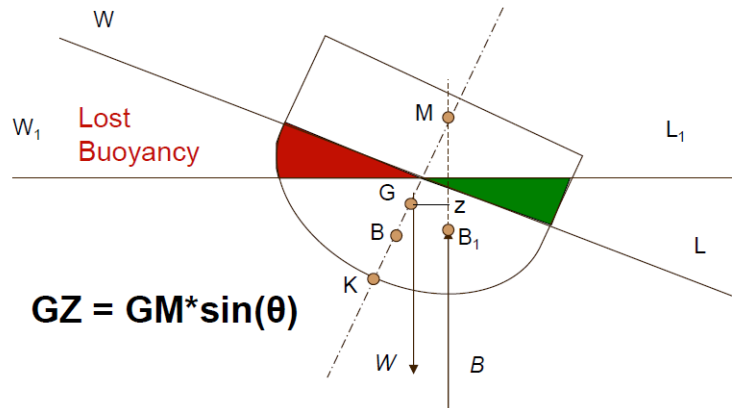


Figure 3.2: Definition of metacenter [21]

K is the keel point, G is the center of gravity, B is the center of buoyancy, M (metacenter) is the point of intersection between the line of buoyancy and center line, GM (metacentric height) is the distance between G and M . For a floating system to be stable, $GM > 0$. The metacentric height is given by equation (3.1).

$$GM = KB + BM - KG \quad (3.1)$$

KB and KG are the distances from center of buoyancy and gravity to the keel of the structure. BM is the distance between the center of buoyancy and the metacenter, given by equation (3.2).

$$BM = \frac{I_{xx}}{\nabla} \quad (3.2)$$

I_{xx} is the second moment of the waterplane area about the x-axis and ∇ is the displaced volume.

GM is dependent on the center of buoyancy and will therefore change as the structure heels. However, for small heeling angles it is assumed that the metacenter does not move. When the metacentric height is found the restoring moment can be found through Equation (3.3).

$$M_{\theta} = GM \Delta \sin(\theta) \quad (3.3)$$

GZ is the righting arm, Δ is the buoyancy and θ is the heeling angle.

3.3 Wave Theory

Theory in this chapter is taken from the book *Sealloads on Ships and Offshore Structures* [15], unless otherwise stated.

3.3.1 Surface Elevation

In mathematics, sine and cosine functions are used to describe wave motions. The surface elevation from one single propagating wave is described, in linear wave theory, by Equation (3.4).

$$\zeta = \zeta_a \sin(kx - \omega t) \quad (3.4)$$

ζ is the wave elevation at a point, ζ_a is the wave amplitude, ω is the wave frequency and k is the wave number given by equation (3.13). x represents the position in reference to the chosen coordinate system and t is a time variable. Figure 3.3 display different properties of a wave.

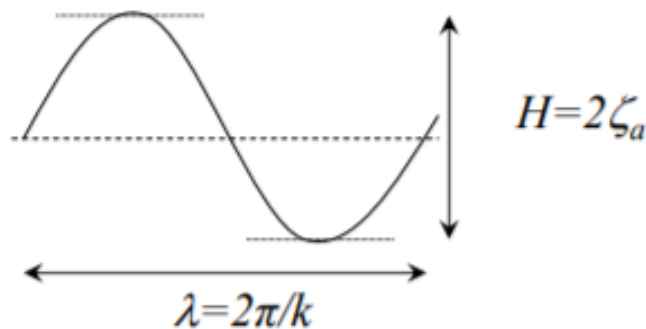


Figure 3.3: Definition of different wave parameters [20]

H is the wave height and λ is the wave length.

A sea state does not consist of one linear regular wave, therefore an approximation has to be used. An approximation of the sea state is made by summing up the contribution from several regular waves. This is represented by Equation (3.5).

$$\zeta(x, t) = \sum_{n=1}^N \zeta_{an} \cos(\omega_n t - k_n x + \epsilon_n) \quad (3.5)$$

ϵ_n is the phase angle and is uniformly distributed between 0 and 2π .

3.3.2 Velocity Potential

In order to calculate hydrodynamic forces acting on a structure, it is necessary to have a general description of the flow field. For an incompressible fluid, the continuity equation is called Laplace's equation, and is given by Equation (3.6)

$$\nabla^2 \phi = 0 \quad (3.6)$$

By assuming that the fluid is inviscid and incompressible, the velocity, V , can be written as the gradient of a scalar variable, ϕ . ϕ is called a velocity potential and has to satisfy Laplace's equation.

$$V = \nabla \phi \quad (3.7)$$

This is a boundary value problem and it is necessary to define the governing equations, boundary conditions and initial conditions. Impermeability at the sea bottom is one of the boundary conditions.

$$\left(\frac{\partial \phi}{\partial z} \right)_{z=-h} = 0 \quad (3.8)$$

h is the water depth and the sea bed is assumed to be horizontal. Furthermore, the velocity potential has to satisfy a dynamic and kinematic boundary conditions, given by Equation (3.9) and (3.10) respectively.

$$g\zeta + \left(\frac{\partial \phi}{\partial t} \right)_{z=0} = 0 \quad (3.9)$$

$$\frac{\partial^2 \phi}{\partial t^2} + g \frac{\partial \phi}{\partial z} = 0 \quad \text{at } z = 0 \quad (3.10)$$

g is the acceleration of gravity.

The solution is a nonlinear velocity potential, however, by assuming small nonlinearities and neglecting these terms, the velocity potential and wave elevation can be linearized and applied at the mean free surface. A benefit of using linear theory is the linear relationship between input, incident wave field, and output, body-motion amplitude [15]. Equation 3.11 gives the velocity potential for deep water. Deep water is assumed when the water depth is larger than twice the wave length.

$$\phi = \frac{g\zeta_a}{\omega} e^{kz} \sin(kx - \omega t) \quad (3.11)$$

By differentiating the velocity potential with respect to x , y and z , the wave particle velocity in the respective direction can be found. Wave particle velocity in the x -direction at a certain location is given by Equation 3.12.

$$u = \omega \zeta_a e^{kz} \cos(kx - \omega t) \quad (3.12)$$

Equation 3.13 is denoted as the dispersion relation and is an important parameter because it

relates the wave frequency to the wave length.

$$k = \frac{\omega^2}{g} = \frac{2\pi}{\lambda} \quad (3.13)$$

The dynamic pressure caused by the velocity potential is given by Equation (3.14)

$$p = -\rho \frac{\partial \phi}{\partial t} \quad (3.14)$$

3.4 Wave Induced Forces

Theory in this section is taken from the book Sealoads on Ships and Offshore Structures [15], unless otherwise stated.

3.4.1 Diffraction and Radiation Problem

Due to linearity it is possible to split the calculations of wave induced forces on a structure into two parts. It is split into a diffraction and radiation problem and by summing up the contribution from each sub-problem, the total wave induced force can be found.

3.4.2 Diffraction Problem

The diffraction problem assumes that the structure is fixed and exposed to incident waves. Equation (3.15) is the velocity potential solving the diffraction problem.

$$\phi(x, y, z, t) = \phi_0(x, y, z, t) + \phi_D(x, y, z, t) \quad (3.15)$$

ϕ_0 and ϕ_D represents the incident wave and diffraction velocity potential respectively.

ϕ_0 generates a flow that penetrates the structure with normal velocity $\frac{\partial \phi_0}{\partial n}$. This generates hydrodynamic forces called Froude-Kriloff loads [15]. In order to keep the impermeability of the structure intact, it generates a flow, diffraction waves, which results in ϕ_D . Forces obtained from ϕ_D are referred to as diffraction forces. The sum of these two contributions make up the wave excitation loads. The wave excitation loads are obtained by integrating the pressure from ϕ_0 and ϕ_D along the mean wetted hull surface.

$$F_{exc,k}(t) = - \int_{S_{0B}} \rho \frac{\partial \phi_0}{\partial t} n_k dS - \int_{S_{0B}} \frac{\partial \phi_D}{\partial t} n_k dS \quad k = 1, 2, \dots, 6 \quad (3.16)$$

3.4.3 Radiation Problem

The structure is forced to oscillate with the wave excitation frequency with no incoming waves. This will generate outgoing waves and an oscillating fluid pressure on the body. Integration of the fluid pressure will result in forces and moments on the structure. This force has three contributions, one connected to body acceleration, one connected with body velocity and one with the body motion.

$$F_k(t) = - \int_{S_{0B}} \rho \frac{\partial \phi_R}{\partial t} n_k dS = \sum_{j=1}^6 -A_{kj} \frac{d^2 \eta_j}{dt^2} - B_{kj} \frac{d\eta_j}{dt} - C_{kj} \eta_j \quad k = 1, 2, \dots, 6 \quad (3.17)$$

A_{kj} , B_{kj} and C_{kj} are respectively added mass, damping and hydrostatic restoring coefficients. Added mass and damping are parameters connected to the dynamic pressure caused by the body motions. They depend on body geometry, frequency, vicinity of free surface, water depth, water confinement and the speed of the body.

Added mass:

Added mass is relevant in reducing the body acceleration. It is not a physical mass and does not always have the units of mass. Added mass can for some frequencies be negative.

Damping:

Linear wave-radiation damping coefficients are connected to a structure's ability to generate waves when oscillating. It is proportional to the square power of the amplitude of the generated waves.

Restoring:

A systems stiffness has a hydrostatic contribution in heave, roll and pitch. In heave, stiffness is given by Equation (3.18). In sway, roll and yaw it is connected to the mooring system.

$$C_{33} = \rho g A_w \quad (3.18)$$

C_{33} is the hydrostatic restoring in heave and A_w is the waterplane area.

3.4.4 Morison's Equation

Theory in this section is taken from the Wadam user manual [13], unless otherwise stated. Morison's equation is used to calculate forces for slender parts of a structure modeled as beam elements. It can be used for cross-sections that are sufficiently small enough to allow the gradients of fluid particle velocities and accelerations in the direction normal to the member to be neglected. Morison's equation is a sum of an inertia force proportional to acceleration and a drag force proportional to the velocity squared [9]. Equation (3.19) gives Morison's equation

in matrix form.

$$\mathbf{F} = \omega^2(\mathbf{M} + \rho V_M \mathbf{C}_a) - \omega^2 \rho V_M (\mathbf{C}_a + \mathbf{I}) \mathbf{x} + i\omega \mathbf{B}(\mathbf{x} - \boldsymbol{\zeta}) + \mathbf{f}_c + \mathbf{f}_g + \mathbf{f}_b \quad (3.19)$$

\mathbf{C}_a is the 3 by 3 diagonal added mass matrix, \mathbf{I} is the 3 by 3 identity matrix, ρ is the density of water, V_M is displaced volume of the Morison element, \mathbf{B} is the linearised viscous damping matrix, \mathbf{C}_D is the 3 by 3 diagonal drag coefficient matrix, \mathbf{x} is complex amplitude of the incident wave field, $\boldsymbol{\zeta}$ is complex amplitude of the motion, \mathbf{f}_c fluctuating hydrostatic restoring force representing the first order restoring contributions integrated in the equation of motion, \mathbf{f}_g is the fluctuating gravity force representing the acceleration of gravity calculated in a coordinate system fixed with the Morison model, \mathbf{f}_b is the fluctuating buoyancy force calculated in a coordinate system fixed with the Morison model.

In linear theory it is assumed that a regular wave with frequency ω should give a response at the same frequency and the amplitude should be proportional to the wave amplitude. These are assumptions for use of transfer functions for stochastic response calculation. Since Morison's equation gives a drag force proportional to the velocity squared, these assumptions are not satisfied [31]. It is beneficial to linearize the drag force to preserve the linear relationship between input and output [31].

Furthermore, due to quadratic coupling between the wave induced velocity and the response velocity, it is not possible to split the drag term into a damping and excitation term. The linearised damping contribution from drag is found by linearisation of Equation (3.20). It is obtained by assuming equal work done at resonance by the non-linearised and the equivalent linear damping term.

$$\mathbf{F}_D = \frac{1}{2} \rho \sigma \mathbf{C}_D (\mathbf{v} - \dot{\mathbf{x}}) |\mathbf{v} - \dot{\mathbf{x}}| = \frac{1}{2} \rho \sigma \mathbf{C}_D \frac{8}{3\pi} V_{max} (\mathbf{v} - \dot{\mathbf{x}}) = \mathbf{B}(\mathbf{v} - \dot{\mathbf{x}}) \quad (3.20)$$

σ is the projected area of the Morison element and V_{max} is a linearising velocity amplitude.

3.5 Wind Loads

A wind field will generate a pressure force on a structure, primarily it is a force normal to the structure and in some cases a tangential friction force. The load is generally time dependent due to fluctuations in wind velocity. If this period is close to the eigenperiod, a dynamic analysis using a wind frequency spectrum should be carried out. DNV GL recommends using a time-averaged velocity for wind loads when analysing a structure [9].

Equation (3.21) can be used to calculate the wind force, F_w , acting normal on a structural surface.

$$F_w = \frac{1}{2} \rho_a V_{T,z}^2 S C_s \quad (3.21)$$

ρ_a is the density of air, $V_{T,z}$ is time-averaged the wind velocity over a period T and at height z , S is the projected area of the structural surface and C_s is the shape coefficient [9]. C_s depends on the geometry of the structural surface.

3.6 Current Loads

Current forces on slender structures will mainly be due to viscous effects and can be calculated using the drag term in Morison's equation.

$$F_c(z) = \frac{1}{2} \rho_s C_D D v |v| \quad (3.22)$$

ρ_s is the density of sea water, C_D is the drag coefficient D is the cross-sectional diameter and v is the current velocity.

3.7 Static Response

A static analysis is solved using displacement-based nodal finite element method. Equation (3.23) is the governing equation that needs to be solved.

$$\mathbf{K} \mathbf{x} = \mathbf{R} \quad (3.23)$$

\mathbf{K} is the global stiffness matrix, \mathbf{x} is the unknown displacement and \mathbf{R} is the load matrix.

The nodal displacement is found by solving the governing equation with respect to \mathbf{x} , as shown in equation (3.24).

$$\mathbf{x} = \mathbf{K}^{-1} \mathbf{R} \quad (3.24)$$

3.8 Dynamic Response

A floating structure can be modelled as a mass-spring-damper system. The governing equation is the equation of motion given by (3.25).

$$(\mathbf{M} + \mathbf{A})\ddot{\mathbf{x}} + \mathbf{C}\dot{\mathbf{x}} + \mathbf{K}\mathbf{x} = \mathbf{F}(t) \quad (3.25)$$

\mathbf{x} , $\dot{\mathbf{x}}$ and $\ddot{\mathbf{x}}$ are the displacement vector, velocity vector and acceleration vector respectively. \mathbf{M} , \mathbf{A} , \mathbf{C} and \mathbf{K} are the mass, added mass, damping and stiffness matrix respectively. $\mathbf{F}(t)$ is the external load vector.

Damping

Damping is split into three contributions, hydrodynamic, structural (small) and aerodynamic. Hydrodynamic damping comes from drag, radiation (frequency dependent) and wave drift (second order effect).

3.9 Solving the Equation of Motion

Theory in this section is taken from lecture notes in the course Design of Floating Structures [26]. The external force, $\mathbf{F}(t)$, is modelled as a harmonic load as shown in Equation (3.26).

$$\mathbf{F}(t) = \mathbf{F}_0 e^{i\omega t} \quad (3.26)$$

\mathbf{F}_0 is the amplitude of the external force.

From this a response on the form given in Equation (3.27) is assumed.

$$\mathbf{x}(t) = \mathbf{x}_0 e^{i\omega t} \rightarrow \dot{\mathbf{x}}(t) = i\omega \mathbf{x}_0 e^{i\omega t} \rightarrow \ddot{\mathbf{x}}(t) = -\omega^2 \mathbf{x}_0 e^{i\omega t} \quad (3.27)$$

The force from Equation (3.26) and the displacement, velocity and acceleration from Equation (3.27) are inserted into Equation (3.25).

$$-\omega \mathbf{x}_0 e^{i\omega t} (\mathbf{M} + \mathbf{A}) + i\omega \mathbf{x}_0 e^{i\omega t} \mathbf{C} + \mathbf{x}_0 e^{i\omega t} \mathbf{K} = \mathbf{F}_0 e^{i\omega t} \quad (3.28)$$

$$(-\omega^2 (\mathbf{M} + \mathbf{A}) + i\omega \mathbf{C} + \mathbf{K}) \mathbf{x}_0 = \mathbf{F}_0 \quad (3.29)$$

$$\mathbf{x}_0 = \mathbf{H}(w) \mathbf{F}_0 \quad (3.30)$$

$\mathbf{H}(w)$ is called a response transfer function and is given by Equation (3.31). It is only valid for linear systems.

$$\mathbf{H}(w) = \frac{1}{-\omega^2 (\mathbf{M} + \mathbf{A}) + i\omega \mathbf{C} + \mathbf{K}} \quad (3.31)$$

Figure 3.4 illustrates a typical transfer function for a floating structure. The response can be divided into three categories; inertia dominated, damping dominated and stiffness dominated.

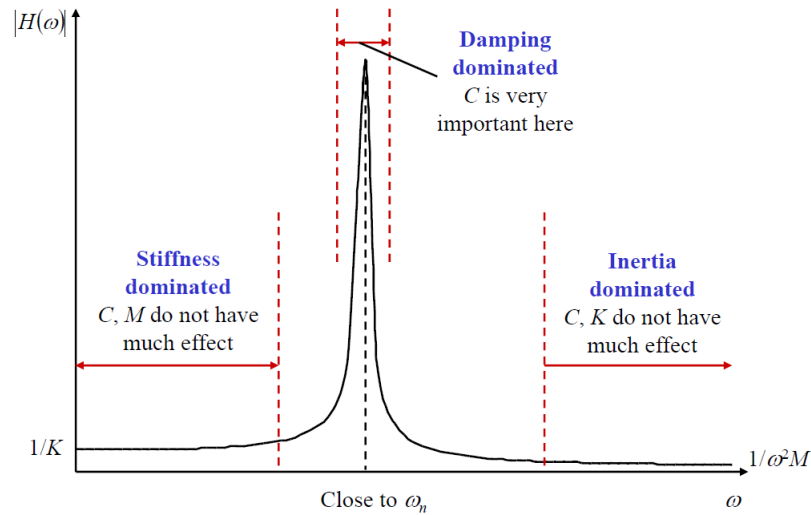


Figure 3.4: Maximum response for different loading frequencies

Damping dominated system

$$K - \omega^2 M = 0 \rightarrow \omega = \sqrt{\frac{K}{M}} = \omega_n \quad (3.32)$$

ω is the excitation frequency and ω_n is the natural frequency. If the excitation frequency is equal to the natural frequency, $H(\omega)$ will go to infinity if damping is zero. This means that damping is the only thing that prevents infinite response. This is not a wanted scenario, but not always avoidable. The energy in the sea, with respect to period, lies between five and twenty seconds. When designing floating structures it is beneficial keep the eigenperiod outside this interval.

Stiffness dominated system

$$K \gg \omega^2 M \rightarrow \omega_n \gg \omega \quad (3.33)$$

For this type of system mass and damping is relatively unimportant. The load frequency is lower than the natural frequency of the structure. The load variations are slow and the structure behaves quasi-static.

Inertia dominated system

$$K \ll \omega^2 M \rightarrow \omega_n \ll \omega \quad (3.34)$$

For this type of system, stiffness and damping are relatively unimportant. The load frequency is significantly higher than the natural frequency and the structure has too large inertia for the displacements to become large enough to get a response from the restoring forces.

The Response Amplitude Operator (RAO) connects the surface elevation of the incoming wave and the dynamic response. It is modeled as a complex number because it is easier to handle mathematically and preserves information about the amplitude and phase. Figure 3.5 illustrates how the surface elevation η is connected to the dynamic response x . x is an arbitrary dynamic response, for example displacement, velocity, excitation force etc.

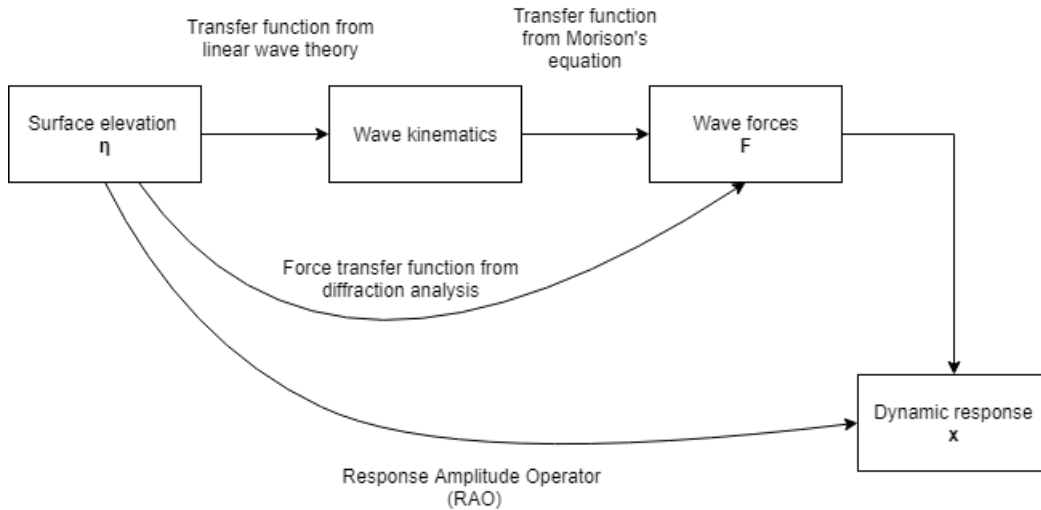


Figure 3.5: Flowchart of how the RAO connects the surface elevation η and the dynamic response

The phase of the RAO represents the time lag between the wave crests passes through a reference point and the structure reaches maximum response. The RAO is obtained in the following way,

$$\mathbf{F} = \mathbf{T}(\omega)\zeta_a e^{i\omega t} \quad (3.35)$$

$$\mathbf{x} = \mathbf{H}(\omega)\mathbf{F}(\omega) \quad (3.36)$$

$$\mathbf{RAO}(\omega) = \mathbf{H}(\omega)\mathbf{T}(\omega) \quad (3.37)$$

$$\mathbf{x} = \mathbf{H}(\omega)\mathbf{T}(\omega)\zeta_a e^{i\omega t} = \mathbf{RAO}(\omega)\zeta_a e^{i\omega t} \quad (3.38)$$

$\mathbf{T}(\omega)$ is the load transfer function.

3.10 Wave Statistics

Theory in this chapter is taken from lecture notes in the course Marine Dynamics [28]. The principle behind wave statistics is to establish a relationship between the energy in a sea state

and the wave frequency. The total amount of energy in a sea state is given by Equation (3.39).

$$\frac{E}{\rho g} = \sum_{n=1}^N \frac{1}{2} \zeta_{An}^2(\omega_n) \quad (3.39)$$

$\zeta_{An}^2(\omega_n)$ is the wave amplitude of the linear wave component with frequency ω_n . A spectrum of $\zeta(t)$, called $S(\omega)$, is defined so that the the area inside a frequency interval $\Delta\omega$ is equal to the energy of all the wave components within this interval. The relationship between the wave spectrum and the wave amplitude is given by Equation (3.40).

$$\frac{1}{2} \zeta_{An}^2 = S(\omega_n) \Delta\omega \quad (3.40)$$

The total amount of energy can be found by summing up the contribution from all the frequency intervals.

$$\frac{E}{\rho g} = \sum_{n=1}^N \frac{1}{2} \zeta_{An}^2 = \sum_{n=1}^N S(\omega_n) \Delta\omega \quad (3.41)$$

By assuming that $N \rightarrow \infty$ and $\Delta\omega \rightarrow 0$, the total amount of energy is given by Equation (3.42).

$$\frac{E}{\rho g} = \sum_{n=1}^N \frac{1}{2} \zeta_{An}^2 = \int_0^{\infty} S(\omega) d\omega \quad (3.42)$$

NS 9415 [30] requires that a Joint North Sea Wave Project (Jonswap) spectra is used when designing fish farms. It is a wave spectra based on measurements from shallow areas in the North Sea close to shore. NS 9415 also says that a fully developed sea state is to be assumed [30]. Figure 3.6 shows a principle sketch of a Jonswap spectrum. Jonswap is a five parameter spectrum with γ , α , σ_a , σ_b and ω_p as input parameters.

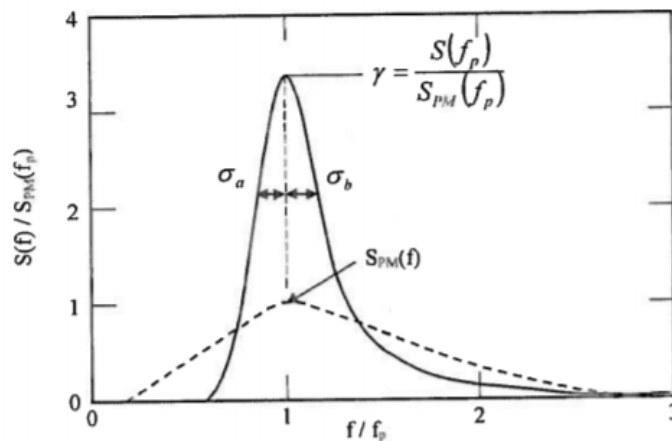


Figure 3.6: Principle sketch of a Jonswap spectrum

The shape of the Jonswap spectra is given by Equation (3.43).

$$S(\omega) = \frac{A}{\omega^5} \exp\left[-\frac{B}{\omega^4}\right] \quad (3.43)$$

A and B are given by Equation (3.44) and (3.45) respectively.

$$A = \alpha g^2 \quad (3.44)$$

α determines the spectrum shape in the high frequency range.

$$B = \frac{5}{4} \omega_p^4 \quad (3.45)$$

ω_p is the peak frequency of the sea state.

By inserting (3.44) and (3.45) into Equation (3.43) and multiply it with a factor given in Equation (3.46), Equation (3.47) is obtained.

$$\gamma \exp\left[\frac{1}{2} \left(\frac{\omega - \omega_p}{\sigma \omega_p}\right)^2\right] \quad (3.46)$$

$$S(\omega) = \alpha \frac{g^2}{\omega^5} \exp\left[-\frac{5}{4} \left(\frac{\omega_p}{\omega}\right)^4\right] \quad (3.47)$$

γ is a non-dimensional peak shape parameter and σ is given by Equation (3.48).

$$\sigma = \begin{cases} \sigma_a & \text{for } \omega \leq \omega_p \\ \sigma_b & \text{for } \omega > \omega_p \end{cases} \quad (3.48)$$

Average values for σ_a and σ_b are by DNV GL given as 0.07 and 0.09 respectively [9].

The peak shape parameter γ is proportional to the ratio between the maximum energy in the Jonswap spectrum and the maximum energy in a Pierson-Moskowitz spectrum. γ has a mean value of 3.3.

3.11 Frequency Domain and Stochastic Response Analysis

Theory in this chapter is taken from lecture notes in the course Design of Floating Structures at the National University of Singapore [26]. By combining wave statistics and the RAO from the dynamic response, a frequency domain analysis of a structure can be conducted. The procedure of a frequency domain analysis is as following.

Let $I(\omega)$ = input signal, $J(\omega)$ = output signal, $S_{II}(\omega)$ = input spectrum and $S_{JJ}(\omega)$ = output

spectrum.

$J(\omega) = G(\omega)I(\omega)$, where $G(\omega)$ is the transfer function. The key formula in spectral analysis is given by equation (3.49).

$$S_{JJ}(\omega) = |G(\omega)|^2 S_{II}(\omega) \quad (3.49)$$

Lets assume that input $I =$ wave elevation ζ , output $J =$ vessel motion x and the transfer function $G = RAO$. In order to find out how large the motions are, the variance of x can be calculated.

$$S_{xx}(\omega) = |RAO(\omega)|^2 S_{\zeta\zeta}(\omega) \quad (3.50)$$

It is now possible to find the standard deviation in the specter, shown in Equation (3.51). It can be used further in calculations of extreme response values.

$$\sigma_x^2 = \int_0^{\infty} S_{xx}(\omega) d\omega = \int_0^{\infty} |RAO(\omega)|^2 S_{\zeta\zeta}(\omega) d\omega \quad (3.51)$$

3.12 Eigenvalues

Theory in this chapter is taken from the lecture notes Dynamic Response of Marine Structures [24]. A system exposed to harmonic loading can experience resonance if the frequency of the harmonic load is equal to its eigenfrequencies. The method for determining eigenfrequencies is based on virtual work and energy methods.

An eigenfrequency analysis starts with the equation of motion for a dynamic system.

$$\mathbf{M}\ddot{\mathbf{r}} + \mathbf{C}\dot{\mathbf{r}} + \mathbf{K}\mathbf{r} = \mathbf{Q}(t) \quad (3.52)$$

\mathbf{M} is the mass matrix and includes both the added mass and structural mass, \mathbf{C} is the damping matrix, \mathbf{K} is the stiffness matrix, \mathbf{r} is the displacement vector, $\dot{\mathbf{r}}$ is the velocity vector, $\ddot{\mathbf{r}}$ is the acceleration vector and \mathbf{Q} is the excitation force.

Eigenvalues are found from an undamped free vibration analysis, where damping and excitation forces are set to zero. Equation (3.52) can then be written as Equation (3.53)

$$\mathbf{M}\ddot{\mathbf{r}} + \mathbf{K}\mathbf{r} = 0 \quad (3.53)$$

For harmonic vibration the displacement vector is given by Equation (3.54).

$$\mathbf{r} = \Phi \sin \omega t \quad (3.54)$$

By inserting Equation (3.54) into Equation (3.53) the following equation is obtained.

$$(\mathbf{K} - \omega_i^2 \mathbf{M}) \Phi_i = 0 \quad \text{for } i = 1, \dots, n \quad (3.55)$$

n is the number of degrees of freedom in the system.

Equation (3.55) is the general form of the eigenvalue problem. The number of equations is equal to the number of degrees of freedom. Each equation will have a corresponding eigenfrequency ω_i^2 and an eigenvector or modeshape ϕ . One is most often interested in the lowest eigenvalues as these contributes most in the dynamic amplification.

3.13 Buckling of Beams

Theory in this section is taken from the compendium in the course TMR4167 Marin Teknikk 2 [4]. A beam in compression will experience axial strain and it will be shortened without bending deformations. At a certain strain level buckling will occur. This implies that the beam bends out and gets an unlimited lateral deformation without an increase in load level. For elastic buckling theory the load cannot be increased due to a buckling shape $w(x)$ which creates an equilibrium between inner and outer forces for all amplitudes w_{max} . In reality the amplitude will be limited by non-linear forces and plastic strain.

Two beams of different material will buckle at the same level of strain, buckling is therefore considered to be a geometrical problem. A central parameter of a buckling analysis is therefore Young's modulus.

$$\epsilon_{cr} EA = \sigma_{cr} A = P_{cr} \quad (3.56)$$

ϵ_{cr} is the critical strain level, σ_{cr} is the critical stress level, E is Young's modulus, A is the cross-sectional area and P_{cr} is the critical buckling load.

For a given geometry, ϵ_{cr} is the same for all materials, however P_{cr} increases proportionally with Young's modulus. If a beam is exposed to bending, this has to be accounted for in addition to the compression. Critical load for elastic buckling of a beam is given by Equation (3.57), called Euler's equation.

$$P_{cr} = \frac{\pi EI}{l_k^2} \quad (3.57)$$

E is Young's modulus, I is the moment of inertia and l_k is the effective buckling length. The effective buckling length depends on the boundary conditions. Another important parameter of buckling is the slenderness ratio, given by Equation (3.58).

$$\lambda = \frac{l_k}{r} \quad (3.58)$$

λ is the slenderness ratio and r is the radius of gyration, given by Equation (3.59).

$$r = \sqrt{\frac{I}{A}} \quad (3.59)$$

I is the moment of inertia and A is the cross-sectional area.

Standards and Recommended Practice

4.1 Norwegian Law - NYTEK

NYTEK [18] and NS 9415 [30] addresses the technical safety level for fish farms. The scope of NYTEK is given in §1 (translated from Norwegian):

The regulation shall contribute to preventing fish escape from floating aquaculture plants through securing a satisfactory technical standard of the plants [18].

§4 in NYTEK says (translated from Norwegian):

When this regulation refers to NS-9415:2009, it refers to Norwegian Standard NS 9415 - Marine Fish Farms - or European or other international standard with an equivalent safety level as NS-9415:2009 [18]

The regulation opens up for alternative standards, given that it provides at least the same safety level as in NS 9415 [30].

4.2 NS 9415

The first edition of NS 9415 came out in 2003. In 2009 a revision of the standard from 2003 was published and is the one used for this thesis. It has 7 main focus areas:

- Site surveys
- Load and load combinations
- General requirements regarding main components and marine fish farms
- Requirements regarding net pens
- Requirements regarding the floating collar

- Requirements regarding rafts
- Requirements for mooring

4.3 DNV GL

DNV GL - RU - OU - 0503 [8] is a standard for offshore fish farming and can be used as an alternative to NS 9415[30], provided that the safety level is equal or higher than in NS 9415. It can only be applied to fish farms where the floating collar is made of steel. Ocean Farm 1 [32] and Arctic Offshore Farming [2] are examples of fish farms where standards from DNV GL are used [33].

DNV GL - RU - OU - 0503 [8] refers to existing standards from DNV GL that are intended for the offshore industry. The risk of human life is greater on an offshore platform, compared to a fish farm. Using DNV GL's offshore standards may therefore provide a higher safety level than what is required by NYTEK.

4.4 Applied Standards

In this Thesis a combination of NS 9415 and a selection of standards from DNV GL is used. An overview of which standards from DNV GL are used for the different segments follows,

DNV GL-RP-C103 Column Stabilized Units [7] is mainly used for the stochastic design wave analysis.

DNVGL-RP-H103 Modelling and Analysis of Marine Operations [10] is used to model added mass coefficients.

DNVGL-RP-C205 Environmental conditions and environmental loads [9] is used to calculate wind and current forces.

DNVGL-OS-C101 Design of Offshore Steel Structures, General - LRFD Method [6] is used in the ULS analysis.

DNVGL-CG-0128 Buckling [5] is used for capacity check of beam members.

SESAM Software

5.1 Introduction to Sesam

DNV GL’s software Sesam is used for analysis of FlipCage throughout this Thesis. Figure 5.1 shows an overview of the different software and their function. Software used in this thesis are marked with a red circle.

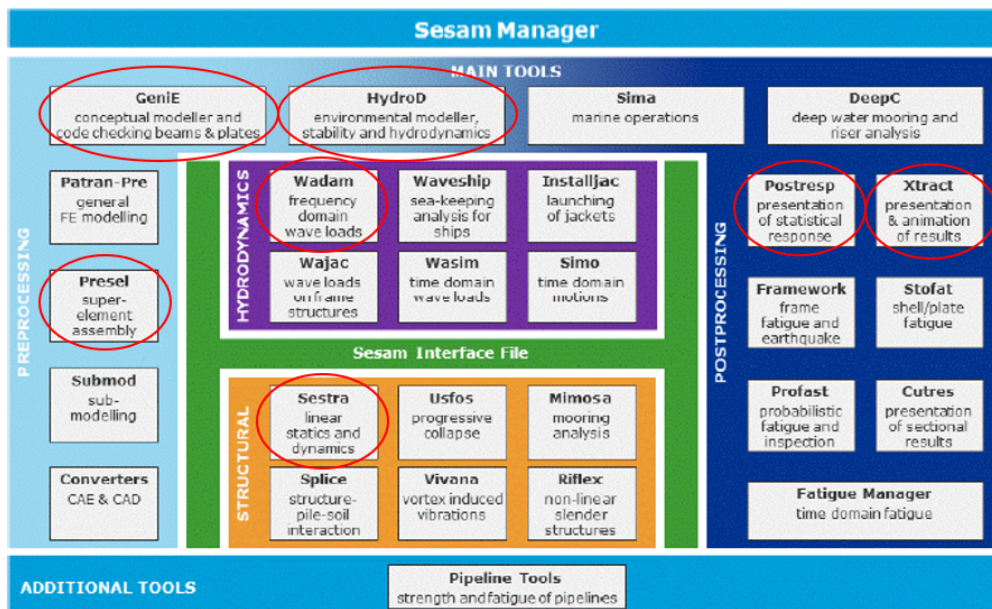


Figure 5.1: Overview of the Sesam software [11]

5.2 GeniE

The structure is modeled in GeniE where all mechanical properties are applied. Boundary conditions are defined and mesh is applied to the structural model. The surfaces exposed to water pressure, needs to be defined and exported as a separate model. This is called a panel model.

The super element technique is used in order to map the forces from the Morison model to the structural model. In order to use super elements, it is necessary to define a super element boundary condition at all connection points between the different models, except the panel model. That means that a super boundary condition is placed at every joint and where beams are attached to plates. Each sub-model is given its own super element number, this is set in GeniE before the mesh is generated.

5.3 Presel

Presel is used to assemble the top super element as a new .FEM file from the first level super elements generated in GeniE. The .FEM files connected to the different super elements, except for the panel model, are imported in Presel.

In addition, it is necessary to preallocate the load cases used in the hydrodynamic analysis. The first load case is the hydrostatic load case and then the load cases for the different wave combinations follows. As HydroD operates with unit waves, a load factor is defined for all load cases which includes a wave. The value of this load factor corresponds to the wave amplitude. It is also necessary to specify which combination of wave period and direction applies for each load case. This numbering is defined by HydroD.

5.4 HydroD

HydroD calculates static and hydrodynamic forces. Hydro D takes in three different models, the structural model made in Presel, the Morison model and the panel model.

The structural model contains information about the mass. The panel model consists of the wet surfaces and is included into HydroD. HydroD uses this model to calculate buoyancy and to apply the water and wave pressure.

The Morison model is used to calculate the drag force and damping contribution. Morison properties are defined for the different beam elements in the Morison model.

5.5 Wadam - Hydrodynamic Analysis

Wadam is used in the hydrodynamic analysis and is launched through HydroD. It provides an automatic load transfer to the finite element model for further structural analysis and includes; inertia loads, line loads for structural beam element analysis, pressure loads for structural shell/solid element analysis and pressure loads up to the free surface [13].

Wadam uses potential theory to calculate first order radiation and diffraction effects on large volume structures. The diffraction analysis is based on first and second order potential theory. Morison's equation is used to calculate forces on beams and slender members. Drag velocity is used to calculate the linearised damping from the Morison equation. In Wadam it is constant for all sea states and should therefore have a velocity corresponding to the natural frequency of the structure in heave. This is because damping is most critical around the natural frequency.

In this report Wadam is used for two different types of analysis. It is used in a design wave analysis where it generates load transfer functions used in a statistical response calculation. It is also used to calculate the load from waves which is used in a static FEM analysis. Which type of analysis Wadam runs is specified in the input file.

5.6 Postresp - Post-Processor for Statistical Response Calculations

Wadam generates transfer functions in frequency domain which are exported to Postresp. Postresp combines the transfer functions with a spectra to make an RAO. The RAO's are treated statistically and includes calculating the standard deviation, exceedance probability and number of waves in the sea state.

Postresp supports several different wave spectra, including Jonswap. If Jonswap spectra is used necessary input is significant wave height, zero upcrossing period and the parameters γ , σ_a and σ_b , described in Chapter 3.10.

Postresp creates a response spectrum for the defined load sections and generates two Excel files containing the standard deviation for all defined spectra and directions and RAO values for all periods and directions. These values are used to identify the waves that gives the maximum response for each load section.

5.7 Sestra

Sestra imports the load files from Wadam and applies loads to the structure. The linear static analysis is conducted using displacement-based nodal finite element method.

Furthermore, Sestra creates a result file containing the reaction force sums, load sums and force balances for each load case [12]. Sestra produces a result file which is opened in Xtract. Appropriate element types are assigned to the different parts of the structure by Sestra.

5.8 Xtract

Xtract is a post-processor for presentation, animation and reporting of results [14]. It is the visualization program of Sesam and can display, animate and tabulate results from the FE-analysis. Contour plots of different stress components, displacements and reaction forces can be made. It is also used to apply load factors and combine different load cases. The program can make a scan of different results, which makes it easier to evaluate the results.

Model Description

6.1 Structural Model

6.1.1 General Specifications

According to DNV GL's rules for finite element modelling, a global model should represent the global stiffness [19]. All members that do not contribute to the overall stiffness can be omitted from the structural model. A global model is used to calculate nominal stresses in areas away from stress concentrations.

The structural model consists of four main parts; the cylindrical frame work, floating collar, two rotation tanks and dome. These are shown in Figure 6.1 and is taken from the structural model in GeniE.

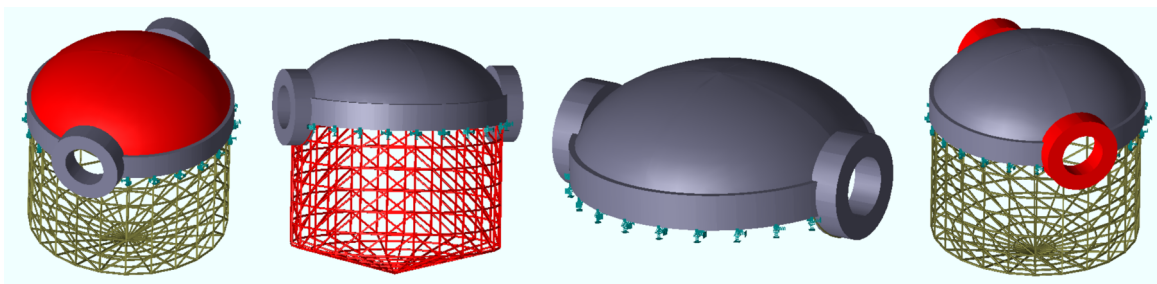


Figure 6.1: Main components of the structure, starting from the left: cylindrical frame work, dome, floating collar and rotation tanks.

The coordinate system is defined so that the center of the fish farm is at $x = 0$ and $y = 0$ meters, and $z = 0$ lies at the waterline, at the middle of the floating collar. A top view of the structural model showing the coordinate system and wave direction definitions can be found in Figure 6.2.

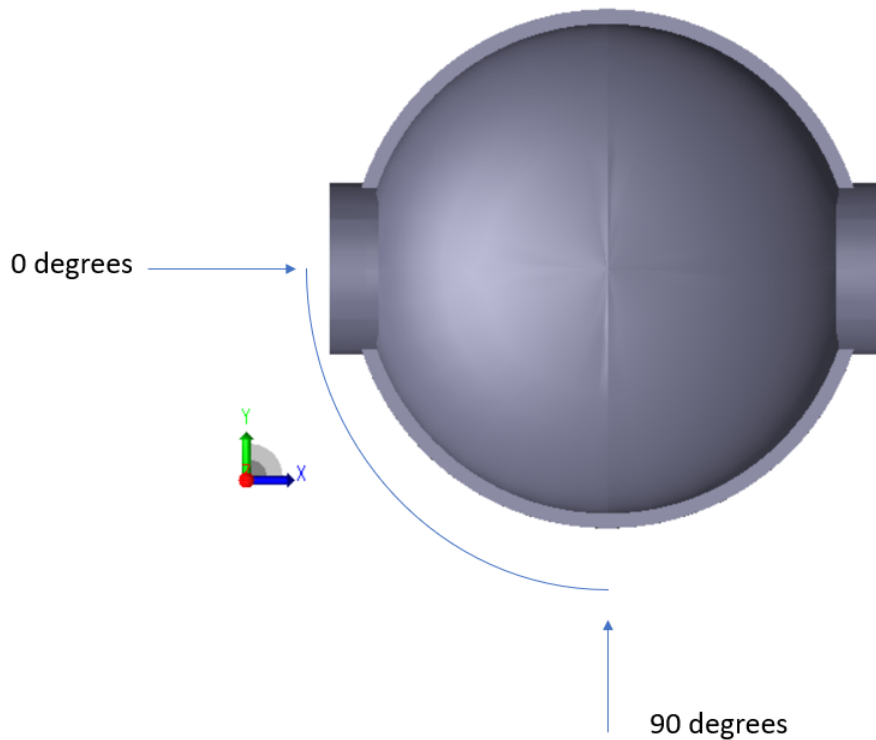


Figure 6.2: Top view of the structural model showing the coordinate system and wave directions

6.1.2 Mechanical Properties and Center of Gravity

In a structural analysis ballasting is not used, the weight is therefore adjusted by modifying the densities of the materials, while keeping the center of gravity at the correct position. The material of the cylindrical framework is aluminium and the floating collar is made out of steel. As the dome is of little interest in the analysis, its material is given the same density as the floating collar. Modified densities for both materials are given in Table 6.1.

Table 6.1: Modified densities

Material	Density [kg/m^3]
Steel	15920
Aluminium	6870

6.1.3 Boundary Conditions

The following points should be considered when choosing boundary conditions for a global model; avoid built in stresses, prevent rigid body motion, small reaction forces and keep fixation points away from areas of interest[19].

Boundary conditions in the z-direction are defined as springs with stiffness equal to the

hydrostatic stiffness in heave, Equation (3.18). Boundary conditions in the x- and y-direction are also modeled as springs with stiffness equal to 10% of the stiffness in the z-direction. The water plane area and the stiffness in the different directions can be found in Table 6.2.

Table 6.2: Stiffness of the fish farm

Water plane area	262.4 m^2
Stiffness z-direction	2.64 MN/m
Stiffness x- and y-direction	0.264 MN/m

By using springs, the boundary conditions will not produce rigid body motions. The supports are distributed to several points around the floating collar so that it is not only restricted at one point. The fish farm is free to rotate in the x-, y- and z-direction. The supports are attached at the bottom of the floating collar, as can be seen in Figure 6.3. One boundary condition is marked with a red circle.

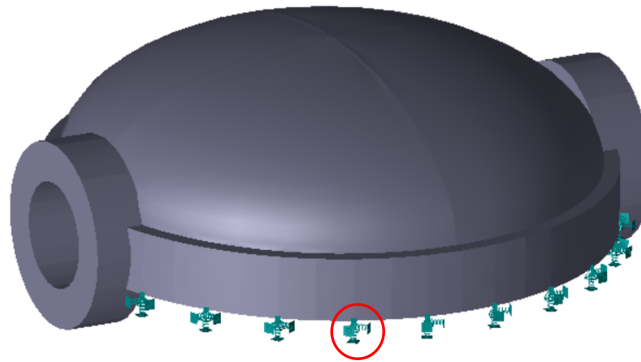


Figure 6.3: Boundary conditions for the global structural model

6.1.4 Choice of Elements

DNV GL recommends using mainly shell elements (4-/8-noded) in the structural model [19]. Beam elements can be used to model stiffeners and girder flanges. The elements assigned to the model can be found in Figure 6.4 and is taken from the output file from Sestra called SESTRALIS.

```
The following basic elements are given:
    20  1 node spring elements      GSPR
    40  3 node beam elements        BTSS
    556 6 node curved shell elements SCTS
    21697 8 node curved shell elements SCQS
```

Figure 6.4: Elements assigned by Sestra

The model contains curved shell elements with 6 and 8 nodes. In addition, due to the boundary conditions, it contains spring elements. The boundary conditions are modeled as 20 springs, and this is consistent with the number of spring elements generated by Sestra.

A shell element is a curved surface and is characterized by carrying the loads by a combination of in-plane forces and bending moments. The pressure loading of marine structures will often result in an overall bending which will result in membrane forces for curved plates. The bending condition of a shell can be seen in Figure 6.5. A general rule is that shell elements carry loads as in-plane forces. Bending effects can occur if the boundary conditions or geometry do not match the variation of the loading [27].

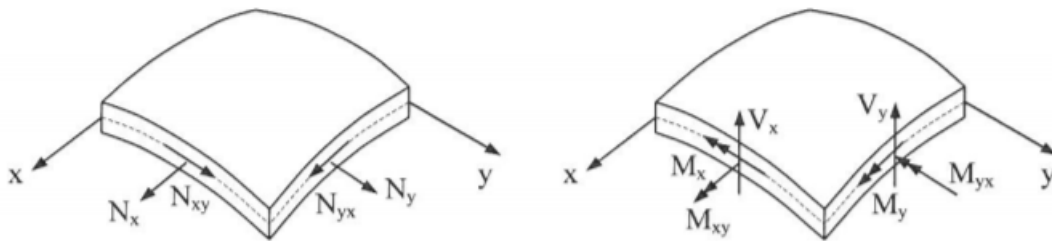


Figure 6.5: Membrane and bending condition of a shell [27]

6.2 Super Elements

From the main model, three sub models, shown in Figure 6.6, are exported as super elements. A description of the different structural models follows,

- Morison model: contains all the beam elements, but with no density and low stiffness.
- Beam model: same as Morison model, but with mechanical properties.
- Model without Morrison elements: all the members that need to have second order elements, which is the dome and the floating collar in this case. This model also contains the boundary conditions.
- Panel model: the part of the model with plates elements which have a wet surface and should not have any mechanical properties.

A snapshot from the combined model in Presel is shown in Figure 6.7. As the figure shows, Presel has read 3 super elements and the boundary conditions are modeled as springs.

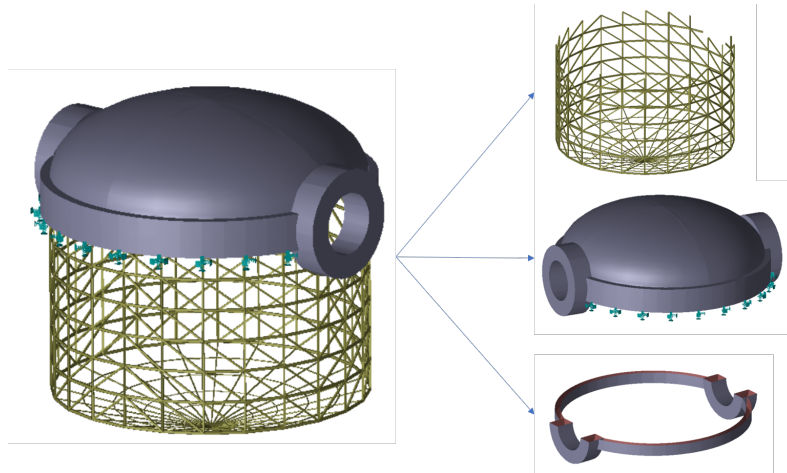


Figure 6.6: Illustration of how the structural model is split into three sub models.

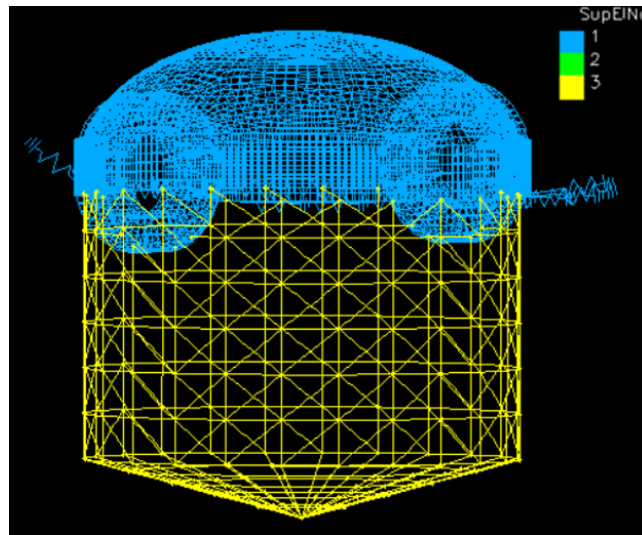


Figure 6.7: Snapshot of the combined model in Presel

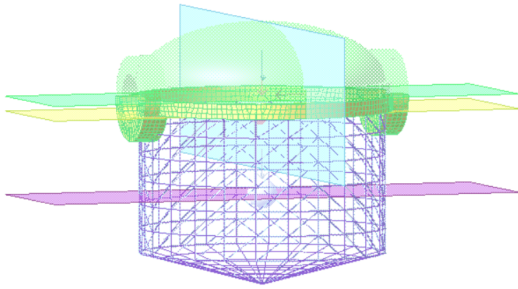
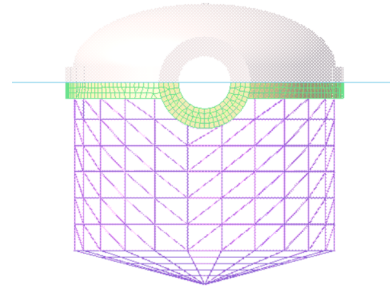
6.3 Hydrodynamic Model

6.3.1 Input to HydroD

The input to HydroD varies with the type of analysis that is run. However, there are some general input values that are equal for all types of analysis. In the input file, three different models are included (structural from Presel, Morison model and panel model) and the hydrodynamic properties are defined. Hydrodynamic properties are given in Table 6.3. A snapshot of the model in HydroD is shown in Figure 6.8 and 6.9 and are used in the statistical design wave and stress peak analysis respectively.

Table 6.3: General input values to HydroD

Property	Value	Unit
Gravity	9.80665	m/s^2
Density sea water	1025	kg/m^3
Kinematic viscosity	$1.19 \cdot 10^{-6}$	m^2/s

Figure 6.8: Snapshot of the model in HydroD
- Statistical Design WavesFigure 6.9: Snapshot of the model in HydroD
- Stress Peak Analysis

6.3.2 Modelling of Fish Net

In hydrodynamic analysis it is important to model the structure correctly in order to obtain accurate calculations of the response. A fish net represents millions of twines, making computational fluid dynamics (CFD) methods extremely expensive. In general, two different methods are used to model a fish net, Morison type and screen models. The advantage of the Morison method is its simplicity and that it is a well known method for calculating forces on slender structures. Disadvantages of using this method is that it largely over-predicts the drag force for large inflow angles [3].

A Morison model is used to model the fish net in HydroD. FlipCage has a fish net consisting of a frame work with net panels in each frame. The drag contribution from the fish net is accounted for in the equivalent diameter of the beam elements in the framework.

6.3.3 Morison Properties

In HydroD a drag velocity has to be specified, this velocity will be used to calculate the linearised drag damping for all frequencies. This velocity is set to the wave particle velocity for an incident wave with the same period as FlipCage's eigenperiod in heave. Equation (3.12) is used to calculate the velocity and it can be seen that the velocity varies exponentially with the water depth. In order to get an average value of the velocity it is taken at the center of area of

the velocity function. A plot of the water particle velocity as a function of water depth can be seen in Figure 6.10. The center of area for the velocity distribution is at $z = -5.85$ meters. Table 6.4 shows input values and results from the computations.

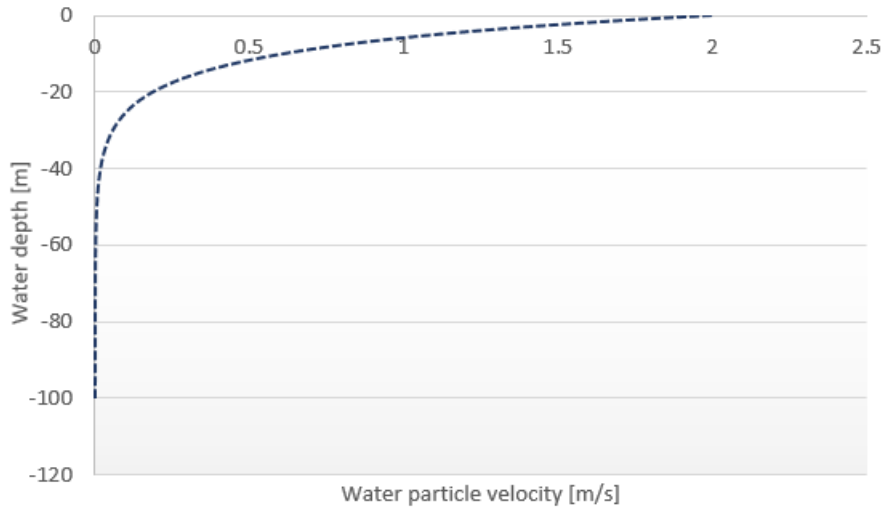


Figure 6.10: Plot of the water particle velocity.

Table 6.4: Drag velocity calculations

Wave period [s]	Wave frequency [1/s]	Wave length [m]	Wave number [1/m]	Water depth [m]	Amplitude [m]	Wave particle velocity [m/s]
5.828	1.078	53.022	0.119	-5.85	2	1.078

For each Morison cross-section it is necessary to specify an equivalent diameter. The drag contribution from the fish net is accounted for in the equivalent diameter. These values are provided by Aker Solutions and are presented in Table 6.5.

Table 6.5: Properties of the Morison cross-sections

Cross section	Diameter [m]	Drag coefficient y	Drag coefficient z
HEA180	0.707426758	0.7	0.7
RHS12.5	0.135287913	3.4	1.33
HEA120	0.055394109	0.7	0.7
HEA160	0.068488059	0.7	0.7
HEB340	0.144784727	0.7	0.7
HEA200	0.080621882	1.33	3.4
RHS16	0.152126276	0.7	0.7
HEB450	0.164185958	0.7	0.7

Contribution From Wind and Current

7.1 Wind and Current in a Structural Analysis

FlipCage is exposed to wind and current forces. They create a heeling moment and the reaction forces are mainly absorbed by the mooring system. In a global structural analysis the contribution from wind and current is therefore modeled as a heeling moment. If the angle is small, it will not affect the structural response significantly and can be neglected. It is therefore necessary to determine the heeling angle due to current and wind. This is based on the theory described in Chapter 3.2, 3.5 and 3.6.

7.2 Calculation of Heeling Angle

The largest heeling moment will occur when the wind force and current force acts in opposite directions. A principle sketch of the points of attack for the wind and current force is given in Figure 7.1. It is assumed that the wind and current velocity is constant.

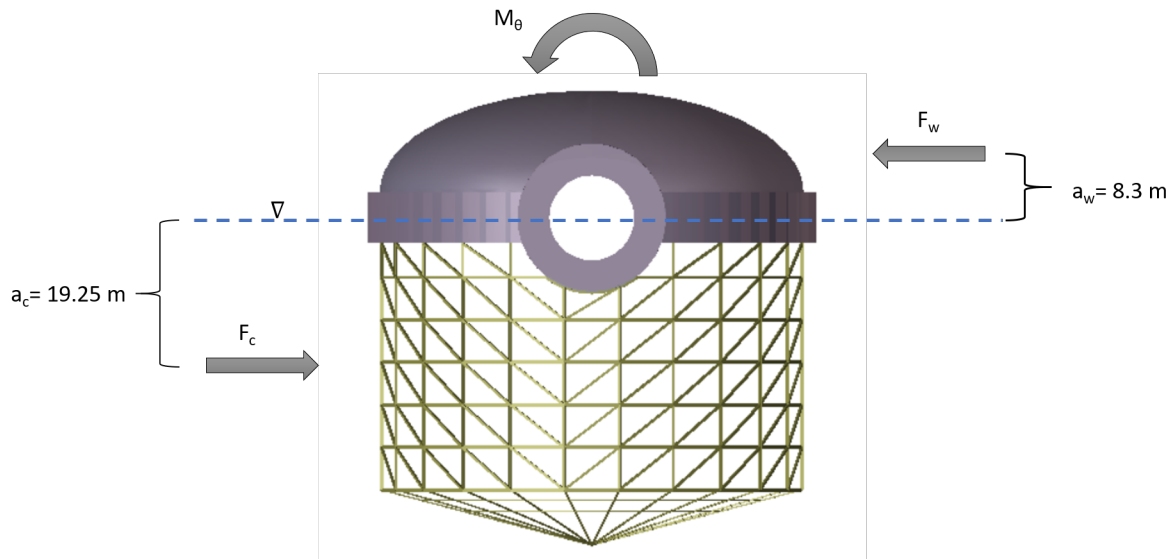


Figure 7.1: Wind and current forces affecting FlipCage

F_w is the wind force, F_c is the current force, a_c is the distance between the waterline and point of attack of the current force, a_w is the distance between the waterline and point of attack of the wind force. The heeling moment, M_θ , is the sum of the moment generated by wind and current.

$$M_\theta = F_w l_w + F_c l_c \quad (7.1)$$

l_w and l_c are the distances between the metacenter and point of attack of the wind force and current force, respectively.

7.3 Overturning Moment due to Wind

The wind force is calculated based on theory from Chapter 3.5. It is the top three meters of the floating collar and the dome that are exposed to the wind field. The projected area of these two components is modeled as a hemisphere. Shape coefficients for different sphere-shaped structures can be found in Figure 7.2.

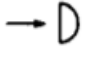
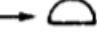
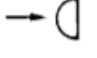
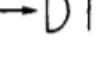
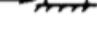
Table 5-3 Shape coefficients C for sphere-shaped structures		
	Structures	Shape coefficient
	Hollow hemisphere, concavity to wind	1.40
	Hollow hemisphere	0.35
	Hollow or solid hemisphere, concavity to leeward	0.40
	Solid hemisphere and circular disc	1.20
	Hemisphere on horizontal plane	0.50

Figure 7.2: Shape coefficients for sphere-shaped structures [9]

The overturning moment due to the wind force is generated due to the distance between the metacenter and point of attack of the wind force. The point of attack is at the centroid of the projected area. The centroid of a hemisphere is given by Equation (7.2) and defined in Figure 7.3. Properties used to calculate the overturning moment due to wind are given in table 7.1.

$$\bar{y} = \frac{4b}{3\pi} \quad (7.2)$$

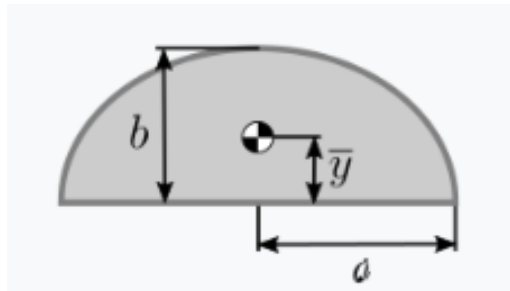


Figure 7.3: Centroid of a hemisphere [25]

Table 7.1: Calculations of wind force

Shape coefficient	0.5
Area [m^2]	499.51
$U_{T,z}$ [m/s]	35
ρ_a [kg/m^3]	1.225
Wind force [kN]	187.40
a_c [m]	8.31
l_w [m]	43.96

7.4 Overturning Moment due to Current

The force due to current is calculated based on theory from Chapter 3.6. It is necessary to define a drag coefficient for the fish net. This input is provided by Aker Solutions and from experience with similar nets it is set to 0.7. It is assumed that the point of attack of the current force is in the middle of the submerged volume. Properties used to calculate the overturning moment due to current are given in Table 7.2.

Table 7.2: Calculations of current force

Drag coefficient	0.7
Area [m^2]	1925
v [m/s]	0.65
ρ [kg/m^3]	1025
Force [kN]	291.78
a_w [m]	19.25
l_c [m]	73.02

7.5 Total Heeling Angle

The total heeling angle due to wind and current forces is given in table 7.3.

Table 7.3: Total heeling angle due to wind and current forces

COG [m]	2.86
GM [m]	55.13
Displacement [m^3]	1495
Moment [MN]	29.54
Angle [$^\circ$]	1.965

The heeling angle is of importance for structures with a deep draught. This is because it will create a global bending moment and shear forces in the hull. It is therefore necessary to take this into account in the design of the hull structure. A SPAR-platform is an example of a deep draught structure where the heeling angle is of importance. The global bending moment and shear forces due to the heeling angle is small for a structure with a draught similar to FlipCage. It is therefore concluded that the contribution from wind and current can be neglected in the structural analysis.

Design Waves

8.1 Determining Design Waves for a Structure

As explained in Chapter 3.3, a sea state is described as a sum of regular waves with different amplitudes, directions and periods. It is not possible to analyse all waves in a sea state. Therefore, there are established methods to determine a set of waves that will generate the most critical response. This is called a design wave analysis and two different methods are used in this thesis, one is a statistical design wave approach and the other is a stress peak analysis.

8.2 Wave Data

A set of wave directions are input variables to both design wave analysis. Due to symmetry it is sufficient to choose wave headings from 0 to 90 ° with 15° spacing. This is given in Table 8.1 and the directions are defined in Figure 6.2.

Table 8.1: Wave directions for design wave analysis

Direction [°]						
0	15	30	45	60	75	90

In addition, there is a limitation on the wave height due to wave steepness, given by Equation (8.1) [7]. This value should be within the limits given in Equation (8.2). It is necessary to check that all the design waves meet the criteria.

$$S = \frac{H}{\lambda} = \frac{2\pi H}{gT^2} \quad (8.1)$$

$$S \leq \frac{1}{7} \quad (8.2)$$

8.3 Statistical Design Wave Analysis

The first method uses wave statistics and a stochastic response analysis to determine the waves that leads to the extreme critical response. It follows the recommended practice by DNV GL DNVGL-RP-C103 Column-stabilized units [7].

The first step is to determine characteristic response parameters. These are global responses, design loads, that are critical for the structure, for example global bending moments, shear forces etc. A chosen wave spectra is combined with the transfer functions from these design loads. The standard deviation and RAO's are then calculated as described in chapter 3.10. An outline of the procedure is given in Figure 8.1.

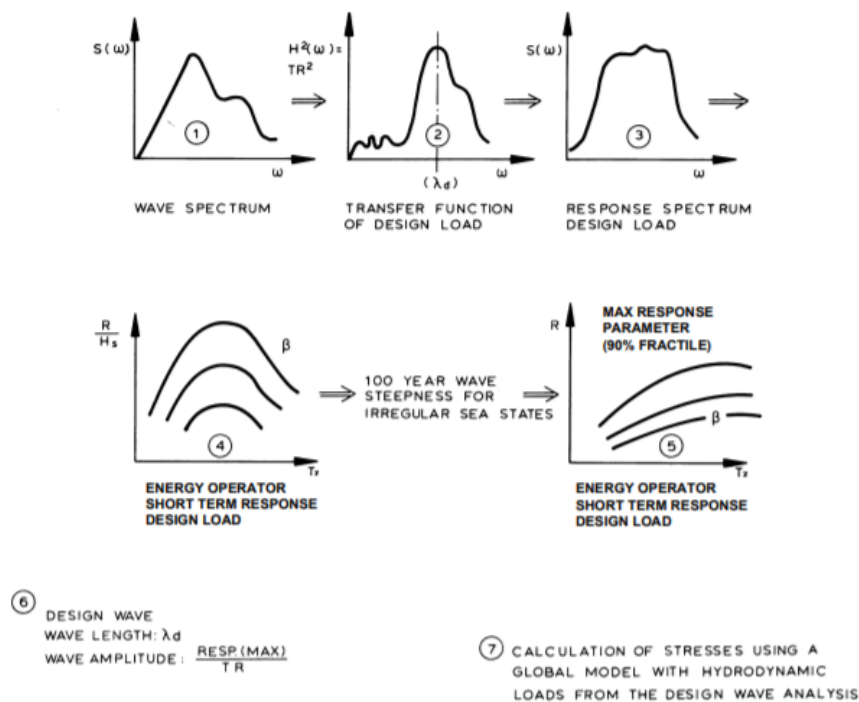


Figure 8.1: Steps in the design wave process [7]

The following steps are used to identify the design waves

- Identify the largest standard deviation, σ_s
- Identify the average zero-up-crossing period, T_z . From T_z the number of waves in the sea state, N_{waves} , can be calculated.

- Calculate the load level using Equation (8.3)
- Find the maximum RAO-value corresponding to the wave direction
- Calculate the wave amplitude by using Equation (8.4)
- Identify the period corresponding to the maximum RAO-value

$$Resp(max) = \sigma_s \sqrt{-0.5 \ln(1 - p^{\frac{1}{N}})} \quad (8.3)$$

p represents the percentile level, $1 - p$ gives the probability of exceeding the maximum load value. The design wave amplitudes are found by Equation (8.4).

$$Amplitude = \frac{Resp(max)}{RAO} \quad (8.4)$$

Critical responses are obtained by defining a set of sectional planes in the hydrodynamic model. For these sectional planes, forces and moments are estimated by integrating hydrodynamic pressures in addition to drag and inertia forces. Choice of sectional planes and load components will highly influence the design wave analysis. It is therefore important to choose these planes carefully. They should be selected based on a knowledge of global structural response. Typical responses that needs to be covered are global bending moments, shear forces and normal forces. The sectional planes used in the analysis are shown in Figure 8.2. Each load section has a name SECL&##*

- '&' is the section normal
- '#' is the section number
- '*' is the degree of freedom

There are six degrees of freedom and they are numbered as given in Table 8.2.

Table 8.2: Numbering of degrees of freedom

Number	Degree of freedom
1	Force in x-direction
2	Force in y-direction
3	Force in z-direction
4	Moment about x-axis
5	Moment about y-axis
6	Moment about z-axis

The names of the different sectional planes are given in Table 8.3

Table 8.3: Naming of sectional planes

Plane	Description	Section name
YZ-plane	Blue	SECL101*
XY-plane	Black	SECL303*
XY-plane	Red	SECL302*
XY-plane	Yellow	SECL301*

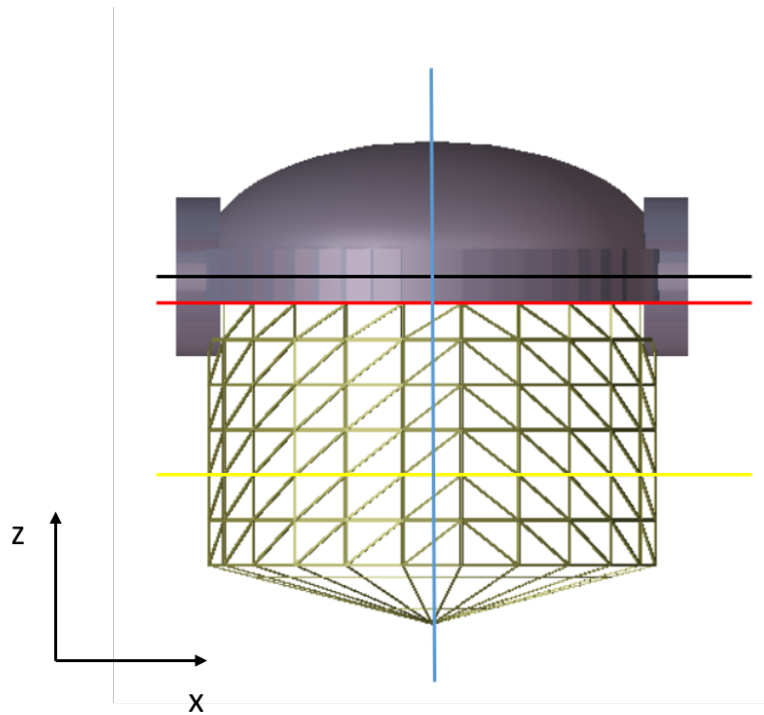


Figure 8.2: Sectional planes

The following forces and moments are checked for the different sectional planes.

Table 8.4: Forces and moments checked for the different sectional planes

Section name	Load component
SECL1011	Force in x-direction
SECL1012	Force in y-direction
SECL1013	Force in z-direction
SECL3013	Force in z-direction
SECL3021	Force in x-direction
SECL3023	Force in z-direction
SECL3024	Moment about x-axis
SECL3031	Force in x-direction
SECL3033	Force in z-direction
SECL3034	Moment about x-axis

Jonswap spectra is used to describe the sea state, the peak shape parameter γ is set to 3.3 as this is the average value. Table 8.5 describes the Jonswap spectra that are used in the design wave analysis. Each spectra is combined with the wave directions given in Table 8.1.

Table 8.5: Jonswap spectra used for design wave analysis

H_s [m]	T_p [s]	γ
0.5	1.48	3.3
1.0	2.17	3.3
1.5	2.88	3.3
2.0	3.27	3.3
2.5	4.00	3.3
3.0	4.45	3.3
3.5	5.00	3.3

A flowchart of the statistical design wave analysis in Sesam can be found in Figure 8.3.

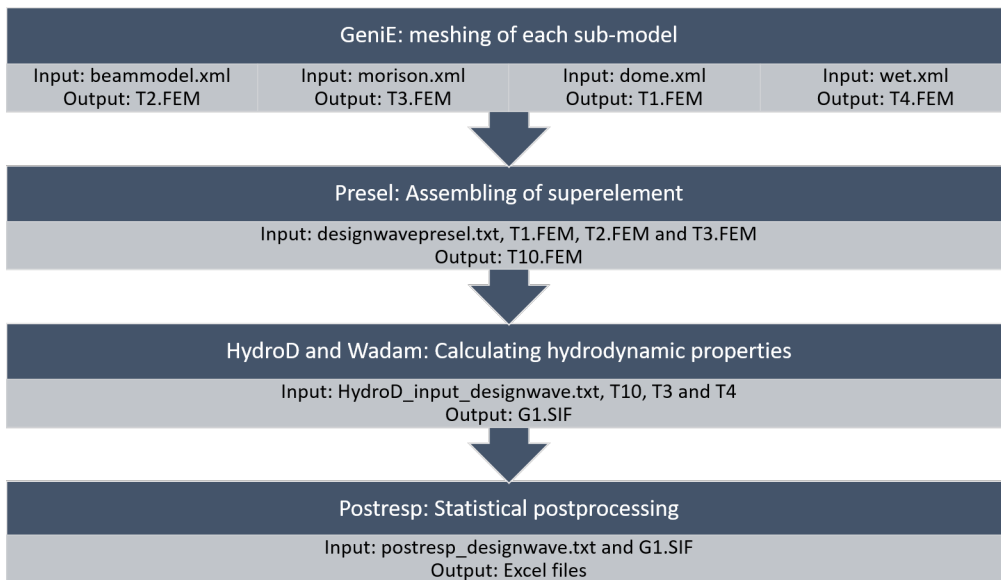


Figure 8.3: Flowchart of the statistical design wave analysis

8.4 Design Wave Analysis - Stress Peak Analysis

The second method is referred to as a stress peak analysis. It is based on calculating the structural response for a set of unit waves. In this analysis, required input is a set of wave periods and directions. To cover the wave periods found in a sea state, periods in the interval from three to twenty seconds, with half a second step size are used. In areas where the structure gets high levels of stress, elements are chosen. For each element, the stress is plotted for all periods and directions. This results in a set of stress RAO's. An outline of the method follows;

- Run a hydrodynamic analysis for a set of directions and periods.
- Run a FEM analysis and locate areas on the structures that seem to be the most critical.
- For critical areas choose representative elements and plot the stress for all directions and periods.

From the different RAO plots it is now possible to determine which directions and periods that are most critical, these will make up the design waves. A flowchart of the statistical design wave analysis in Sesam can be found in Figure 8.4.

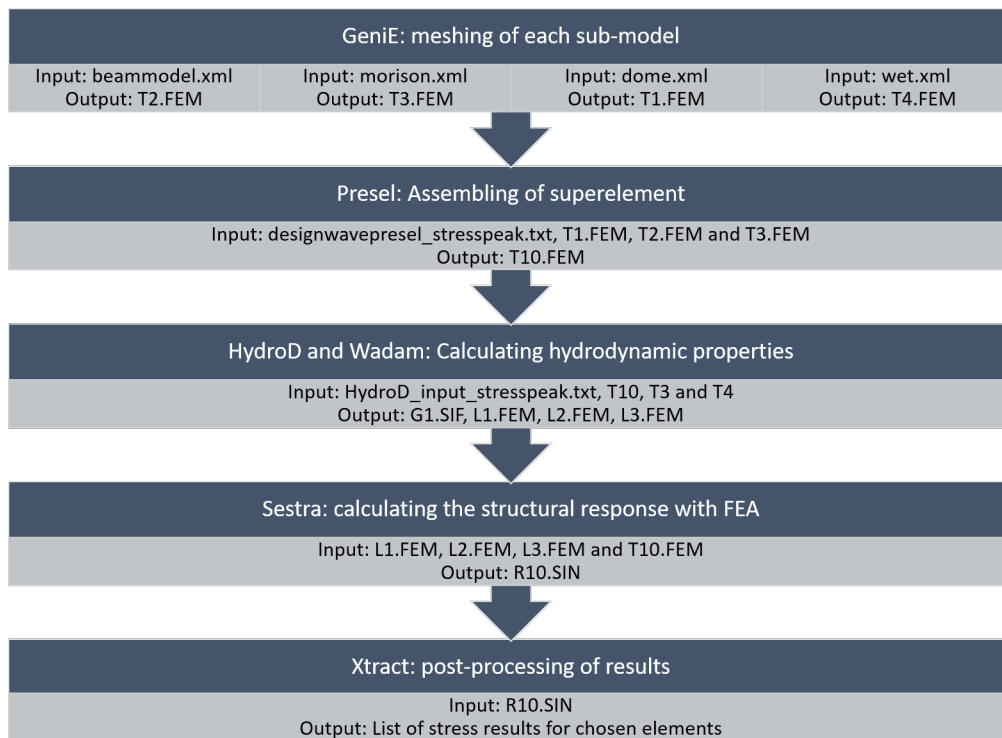


Figure 8.4: Flowchart of a design wave stress peak analysis.

HydroD combines each period and direction and creates a load case, this gives 246 load cases, including the static analysis. In areas where stress peaks are present, an element is chosen and the stress listed for each dynamic load case. Where FlipCage is modeled as plates von Mises stress is measured and where it is modeled as beam elements the normal stress is checked.

When choosing areas to use in the stress peak analysis, it is beneficial to have an idea of which parts of the structure that will be critical. From hydrodynamic theory, an increase in pressure occurs where the water particle velocity is decelerated. Therefore, before executing an analysis it is possible to make an assumption of which parts of the structure that will experience stress peaks.

When a wave approaches FlipCage, depending on its direction, it hits the the floating collar or rotation tank first. The water particles cannot move through the structure and are decelerated.

This results in a higher water pressure and the structure may experience higher level of stress in these areas. This is also the case for the inside of the floating collar and rotation tank.

Unlike the statistical approach, this method does not directly compute a wave amplitude for each design wave. The wave height is therefore taken as the minimum value of the wave height limited by the steepness criteria, Equation (8.2), and the statistical relationship between H_s and H_{max} , Equation (8.5).

$$H_{max} = 1.9 H_s \quad (8.5)$$

Global Analysis - Ultimate Limit State

9.1 Flow Chart of Structural Analysis

An ultimate limit state analysis (ULS) is executed to control that the design meets the performance requirements for the most critical load cases. The ULS analysis follows DNV GL's offshore standard Design of offshore steel structures, general - LRFD [6]. Both yield and buckling should be assessed using a rational, justifiable engineering approach. Figure 9.1 gives a flowchart of the global stress analysis.

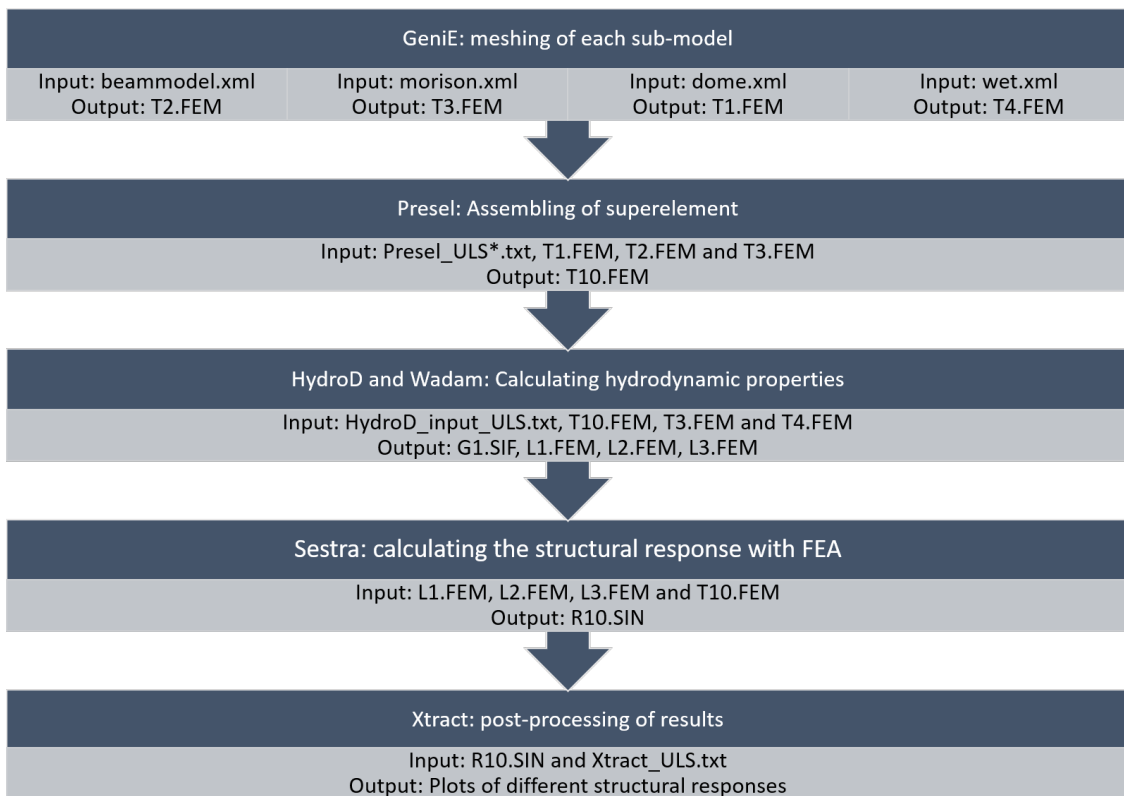


Figure 9.1: Flowchart of an ULS analysis.

Results from the design wave analysis are input in a structural analysis of FlipCage. Two separate ULS analysis are conducted, one with the results from the stochastic response analysis and one with the results from the stress peak analysis.

9.2 Post-Processing and Load Factors

In Xtract each design wave is combined with the static load case and corresponding load factors. DNV GL operates with two sets of load factors, an a) and a b) combination shown in Figure 9.2. Both load factor combinations are applied to each load case. It is required to use a material factor, γ_M , which is set to 1.15 [6].

Combination of design loads	Load categories			
	G	Q	E	D
a)	1.3	1.3	0.7	1.0
b)	1.0	1.0	1.3	1.0

Load categories are:
 G = permanent load
 Q = variable functional load
 E = environmental load
 D = deformation load
 For description of load categories see [Sec.2](#).

Figure 9.2: Load factors recommended by DNVGL-OS-C101 [6]

9.3 Yield Check

According to DNV GL, von Mises equivalent design stress for plated structures shall not exceed the design resistance. von Mises stress is given by Equation (9.1). The floating collar is made out of steel with a yield strength of 420MPa . When applying the material factor, stress levels should not exceed 365MPa . Local stress peaks in areas with considerable geometrical changes, may exceed the yield stress, provided that adjacent structural parts have capacity for the redistributed stresses [6].

$$\sigma_{vM} = \sqrt{\sigma_x^2 + \sigma_y^2 - \sigma_x \sigma_y \tau_{xy}^2} \quad (9.1)$$

9.4 Buckling Check

DNV GL requires that cross-sections exposed to axial compression and/or bending are checked for local buckling [6]. Buckling control follows the class guideline from DNV GL, DNVGL-CG-0128 Buckling [5]. Buckling limit state for members under compression is estimated by using "European buckling curves." Extensive experimental and theoretical investigations have resulted in a set of buckling curves for different geometries and materials.

The framework is classified as beam-columns because it is subjected to simultaneous bending and compression [5]. The utilisation factor for members exposed to axial load and bending is given in Equation (9.2).

$$\eta = \frac{\sigma_a}{\sigma_{acr}} + \frac{\sigma_b}{\left(1 - \frac{\sigma_a}{\sigma_E}\right)\sigma_{bcr}} \quad (9.2)$$

σ_a is the axial stress due to compression, σ_b is the effective axial stress due to bending, σ_{acr} is the characteristic buckling stress for axial compression, σ_E is the minimum elastic buckling stress about weak axis and σ_{bcr} is the characteristic buckling stress for pure bending.

GeniE has a built-in capacity check that controls buckling for all beam elements. GeniE imports the .FEM file of the beam model and the .SIN result file generated by Sestra. By combining these results, GeniE is able to calculate the utilisation factor of each beam. All load cases from the two design wave analysis are used in the buckling capacity check. Each load case is combined with the static load case with load factors as described in Figure 9.2. For each member the load case that results in the highest utilisation factor is listed.

9.5 Load Case Numbering

The load cases from the statistical design wave analysis have the numbering 1.01 to 1.11, where the two last digits refers to which wave in Table 11.2 is combined with the static load case. The load cases from the stress peak analysis have numbering 2.01 to 2.11, where the two last digits refers to which wave in Table 11.5 is combined with the static load case. The first load case in each analysis, 1.01 and 2.01, refers to the static load case. In addition, two load factor combinations are used, these will have the abbreviations ULSA and UL SB. ULSA is interpreted as, ultimate limit state with load factor combination a) from Figure 9.2. UL SB will interpreted as, ultimate limit state with load factor combination b).

Eigenvalue Problem

10.1 Modal Analysis

Modeshape analysis has become an important tool in the engineering of floating structures. It is used to determine the dynamic behaviour of a structure when it is exposed to oscillating loads, such as waves. The modal analysis indicates which frequencies coincides with the natural modes of the system. If the load frequencies are similar to these frequencies, it will cause resonance and potentially large displacements.

Sestra is the structural solver and uses Lanczo's method to solve the eigenvalue problem. This has an advantage for medium sized problems where only a few modes are required. It is often only the first modes that are of interest, because these contribute most in the dynamic response.

10.2 Contribution from Added Mass

It is necessary to include added mass in the eigenvalue analysis. Added mass is, for some cross-sections, frequency independent. Two-dimensional added mass coefficients may be combined with strip theory to obtain an approximation to the three-dimensional added mass coefficients [15]. These two assumptions, frequency independent added mass and strip theory, are used to calculate added mass for the framework in the eigenvalue analysis.

As this is an approximation and the structure have different added mass coefficients depending on the direction of motion and force component, two-dimensional added mass coefficients are used. Added mass coefficients used are given in Figure 10.1 and 10.2 respectively. Added mass is included in the analysis by changing the densities of the materials for each cross-section. Table 10.1 gives the densities for the different cross-sections when added mass is included.

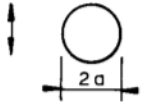
Table A-1 Analytical added mass coefficient for two-dimensional bodies, i.e. long cylinders in infinite fluid (far from boundaries). Added mass (per unit length) is $A_{ij} = \rho C_A A_R$ [kg/m] where A_R [m ²] is the reference area				
Section through body	Direction of motion	C_A	A_R	Added mass moment of inertia [(kg/m)*m ²]
		1.0	πa^2	0

Figure 10.1: Added mass for a circular cross-section in the vertical direction [9]

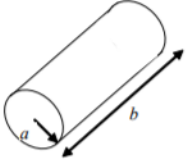
Table A-2 Analytical added mass coefficient for three-dimensional bodies in infinite fluid (far from boundaries). Added mass is $A_{ij} = \rho C_A V_R$ [kg] where V_R [m ³] is reference volume (Continued)				
Body shape	Direction of motion	C_A		V_R
		$b/2a$	C_A	
Right circular cylinder 	Vertical			$\pi a^2 b$
		1.2	0.62	
		2.5	0.78	
		5.0	0.90	
		9.0	0.96	
		∞	1.00	

Figure 10.2: Added mass for a circular cross section in the horizontal direction [9]

Table 10.1: Modified densities including contribution from added mass

Profile	h [m]	Added Mass [kg/m]	Cross-sectional area [m ²]	Density-added mass [kg/m ³]	Material Densities [kg/m ³]	Total [kg/m ³]
RHS 0.0125	0.3	72.45	0.0142	5102.32	2730	7832
HEA180	0.171	94.16	0.0045	20808.82	2730	23539
HEA160	0.152	74.40	0.0039	19189.56	2730	21920
HEA120	0.114	41.85	0.0025	16514.93	2730	19245
HEA200	0.19	116.25	0.0054	21595.17	2730	24325
HEB450	0.45	163.02	0.0218	7478.63	2730	10209
HEB340	0.34	93.06	0.0171	5445.40	2730	8175

Results

11.1 Results - Eigenvalue Analysis

The eigenfrequencies from the free vibration analysis are presented in Table 11.1. Twenty eigenfrequencies were calculated, and six of these will represent the degrees of freedom. Only the six first eigenfrequencies are presented, because it is the first modes that are of most interest.

Table 11.1: Eigenperiods and frequencies from the free vibration analysis

Frequency [Hz]	Period [s]
0.470	2.128
0.471	2.123
0.667	1.499
0.667	1.499
0.674	1.484
0.807	1.238

All eigenfrequencies lies outside the interval where the wave energy is concentrated, that is between 5-20 seconds.

In Xtract it is also possible to visualize the modeshapes and the displacements. It is mainly the bottom of the fish farm that experience displacements. Figure 11.1, 11.2 and 11.3 displays the modeshape displacement for the three first eigenperiods. The modeshapes show that it is the bottom of FlipCage that gets displacements.

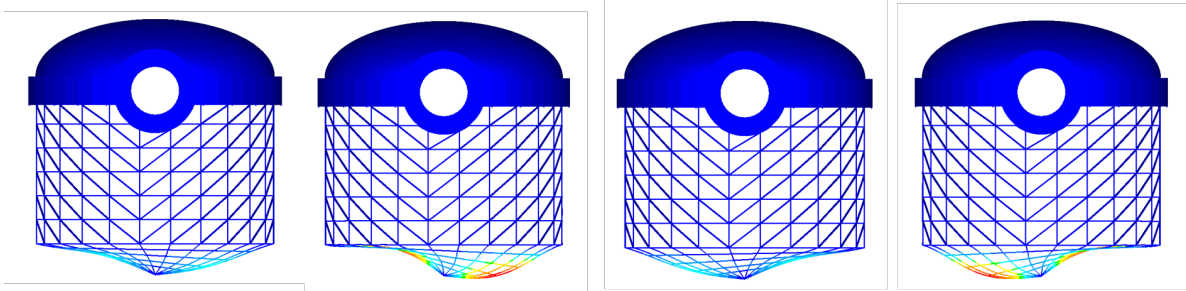


Figure 11.1: Modeshape displacement from eigenperiod 2.128 seconds

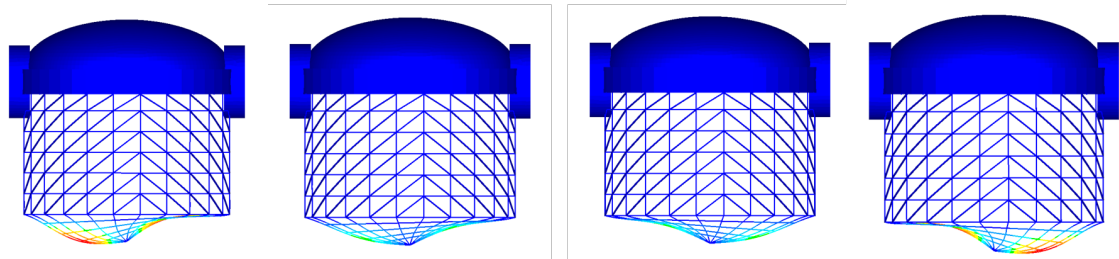


Figure 11.2: Modeshape displacement from eigenperiod 2.123 seconds

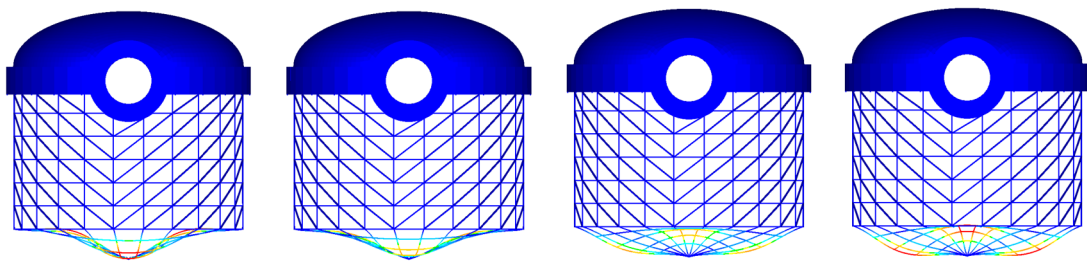


Figure 11.3: Modeshape displacement from eigenperiod 1.499 seconds

In second order theory, high frequency waves are found. The effect of waves are reduced exponentially with a factor kz . Waves with frequencies close to the eigenfrequencies have relatively short wavelengths and the wave number k is therefore large. The effect of these waves are extremely small at the position of the bottom of the framework and are not able to excite the modeshapes.

11.2 Model Verification

Wadam calculates the hydrodynamic properties of the structure. These have to be controlled so that they are consistent with the design. These values can be found in the WADAM.LIS file and an excerpt of the most important properties is found in Figure 11.4.

```

GEOMETRY DATA:
-----
DISPLACED VOLUMES OF THE PANEL MODEL      VOL 1    = 1.38069E+03    [L**3]
                                           VOL 2    = 1.54420E+03
                                           VOL 3    = 1.38729E+03

MASS PROPERTIES AND STRUCTURAL DATA:
-----
MASS OF THE STRUCTURE                      M        = 1.47438E+06    [M]
WEIGHT OF THE STRUCTURE                    M*G      = 1.44588E+07    [M*L/T**2]
CENTRE OF GRAVITY                          XG       = -1.66622E-07   [L]
                                           YG       = -4.40090E-06   [L]
                                           ZG       = -3.17629E+00 [L]

HYDROSTATIC DATA:
-----
DISPLACED VOLUME                          VOL       = 1.43833E+03    [L**3]
MASS OF DISPLACED VOLUME                  RHO*VOL   = 1.47429E+06    [M]
WATER PLANE AREA                          WPLA      = 2.67476E+02    [L**2]
CENTRE OF BUOYANCY                        XCB       = 5.50324E-05    [L]
                                           YCB       = 8.24825E-05    [L]
                                           ZCB       = -3.83362E+00 [L]

EQUILIBRIUM OF STATIC FORCES AND MOMENTS:
-----
CORRESPONDING VERTICAL TRANSLATION        = -3.54829E-04    [L]
TRIM ANGLE IN ROLL                        ALFAX     = 8.72678E-05    [DEG]
TRIM ANGLE IN PITCH                       ALFAY     = -4.64398E-05    [DEG]

```

Figure 11.4: Excerpt of hydrodynamic properties from WADAM.LIS

Geometry data

Displaced volume of the panel model is the result of integrating the volume of the panel model in the x-, y- and z-direction. If the panel model is correctly meshed and modeled these should be in the same order of magnitude. Looking at VOL 1, VOL2 and VOL3 they are all coherent with this.

Mass properties and structural data

As can be seen the center of gravity is in the center of the model and approximately -3.2 meters below the waterline. This is consistent with how FlipCage is designed.

Hydrostatic data

From the mass properties it can be seen that the mass of the structure is 1.474×10^6 kilograms and from the hydrostatic data the mass of the displaced volume, buoyancy, is 1.474×10^6 kilograms. This implies a neutrally buoyant model. The centre of buoyancy is also an important parameter for a floating structure, it can be seen that this lies in the center of the model and 3.8 meters below the waterline. This is consistent with what is calculated in the concept development study [1].

Equilibrium of static forces and moments

The vertical translation can also be used to verify that the model is neutrally buoyant. If the model is not neutrally buoyant it will either move in the positive or negative vertical direction. The corresponding vertical translation is 0.35 millimeters, implying that the model is neutrally buoyant. If the model was in some way not stable in the rotational degrees of freedom, roll and pitch, it would obtain a heeling angle to balance out this. The trim angle in both roll and pitch are very small and it is therefore concluded that the hydrodynamic model is stable.

11.3 Convergence Test - Hydrodynamic Model

A convergence test is performed to ensure that a change in the mesh size of the hydrodynamic model will not influence the results. Added mass and damping are two properties calculated based on the hydrodynamic model, and can therefore be used in the convergence test. A reduction in mesh size will increase the accuracy of the results, but will increase computational time.

The convergence test was executed by reducing the mesh size stepwise, while measuring a hydrodynamic property. Added mass and damping coefficient in pitch, A_{55} and B_{55} , were used because they will experience a large change in water surface pressure. Figure 11.5 and 11.6 are plots of added mass and damping for different mesh sizes. Added mass and damping are frequency dependent parameters, therefore they have to converge for all periods used in the design wave analysis. Wadam calculates added mass and damping coefficients and presents them as dimensionless coefficients. Wadam uses the panel model to calculate hydrodynamic properties, it was therefore only necessary to change the mesh of this model.

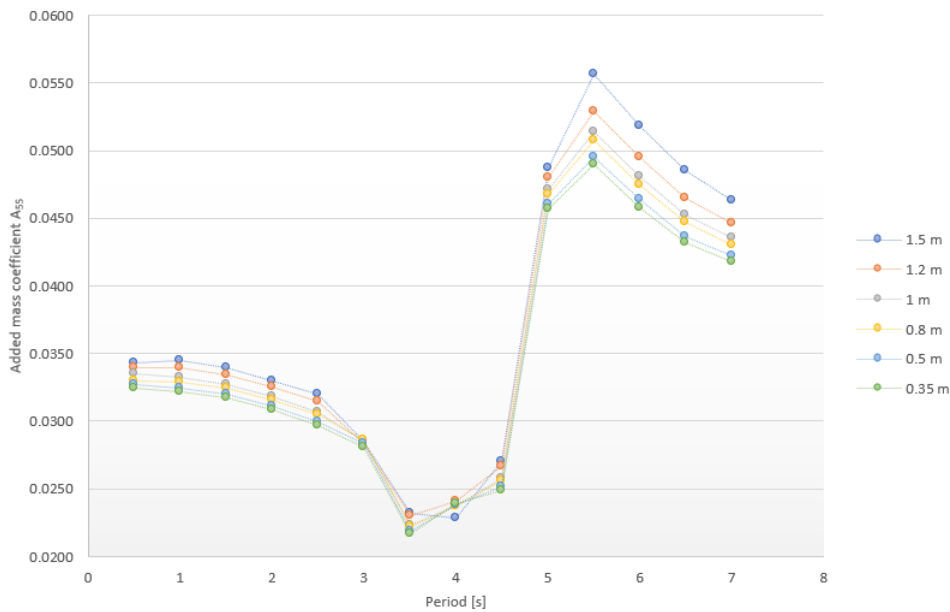


Figure 11.5: Added mass coefficient, A_{55} , for different mesh sizes

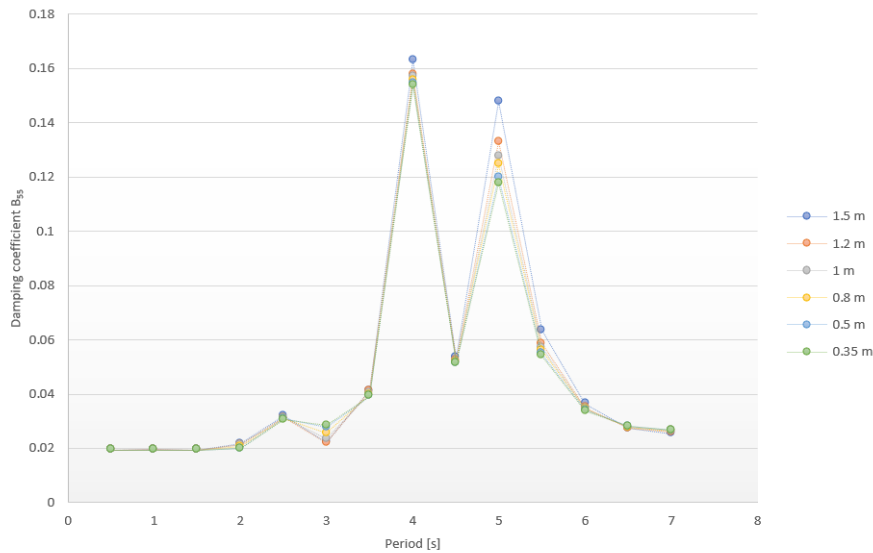


Figure 11.6: Damping coefficient, B_{55} , for different mesh sizes

Added mass and damping converges for smaller mesh sizes, A_{55} and B_{55} converged at different mesh sizes for different frequencies. This implies that some frequencies are more sensitive to a change in mesh size than others. When the mesh size is reduced from 1.5 meters to 1.2 meters, the change in hydrodynamic coefficients are for some frequencies 10%. However, when the mesh is reduced further to 1 meter, the change in A_{55} and B_{55} is less than 5%. It is therefore seen as sufficient to use a mesh size of 1 meter.

11.4 Convergence Test - Structural Model

It is necessary to perform a convergence test on the structural model to ensure that the results are correct. This was performed by measuring the von Mises stress at the same point on the structure while reducing the mesh size. As for the hydrodynamic model, a reduction in mesh size will increase the computational time. Therefore it is a trade off between the accuracy of the results and the time it takes to obtain them.

The position used for the mesh convergence test is inside the rotational tank, as this area has high levels of stress, it is more sensitive to mesh size. Figure 11.7 shows the point on the structure that was used in the mesh convergence study. von Mises stress for the static load case and for one dynamic load case were used. The result is presented in Figure 11.8.

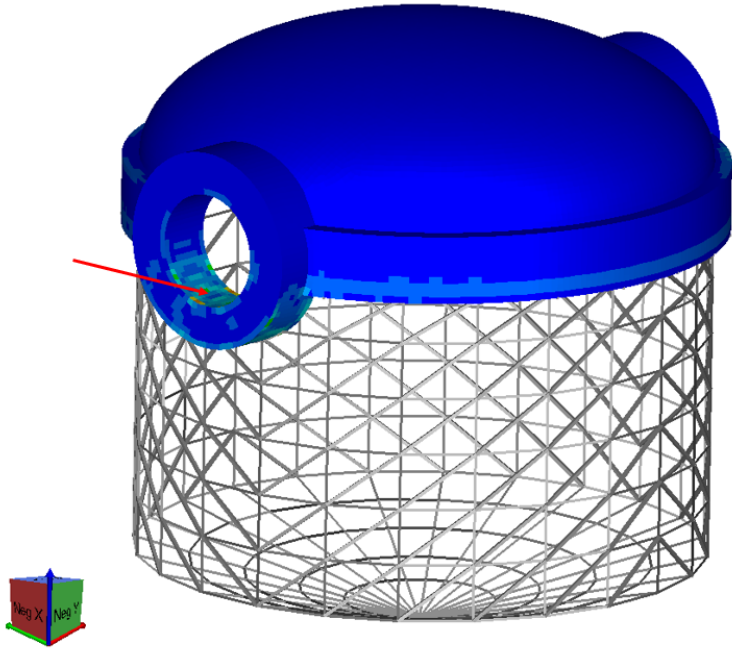


Figure 11.7: Position used in the mesh convergence study for ULS analysis

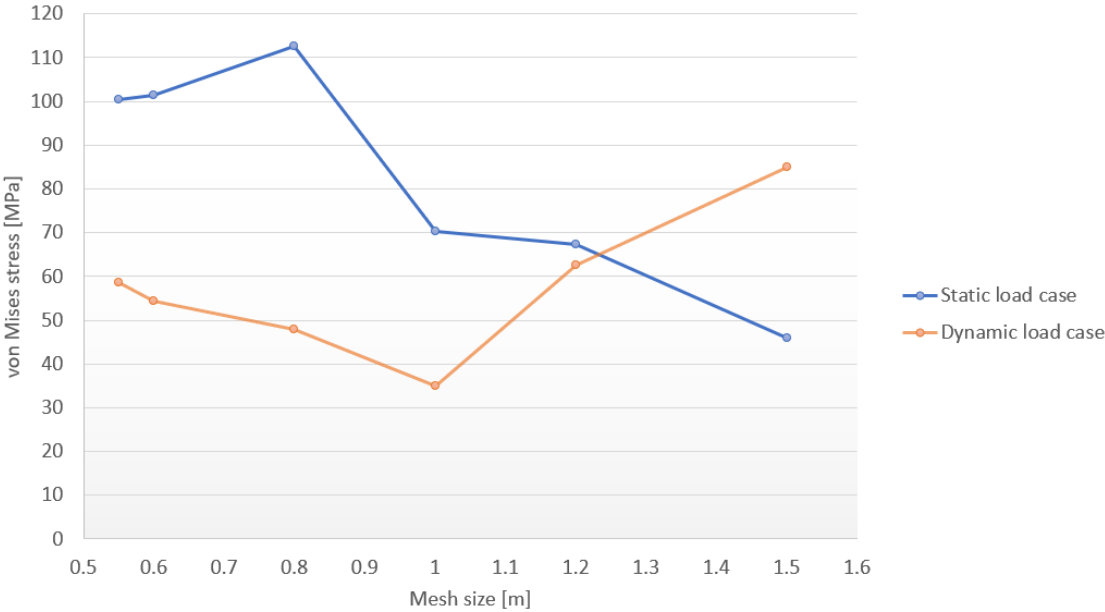


Figure 11.8: Result of mesh convergence study for the ULS analysis

The convergence test started with a mesh size of 1.50 meters before it was reduced stepwise from 1.20, 1.00, 0.80, 0.60 to 0.55 meters. At this point the change in von Mises stress was 7% for the dynamic load case and 1% for the static load case. This was seen as sufficient in a global analysis, as these areas have to be modeled in greater detail in a local analysis on a later point in the design process. It is also possible to reduce the mesh size further in areas with high stress peaks as these areas require a finer mesh size than areas without stress peaks, in order to obtain

the same level of accuracy. This will also lead to a reduction in the overall computational time. If different mesh sizes are used it is important to have a gradual reduction of mesh size.

11.5 Results From Design Wave Analysis

11.5.1 Results From Statistical Design Waves

Postresp calculates the RAO-values for the different sectional loads and these can be found in figures 11.9 to 11.18.

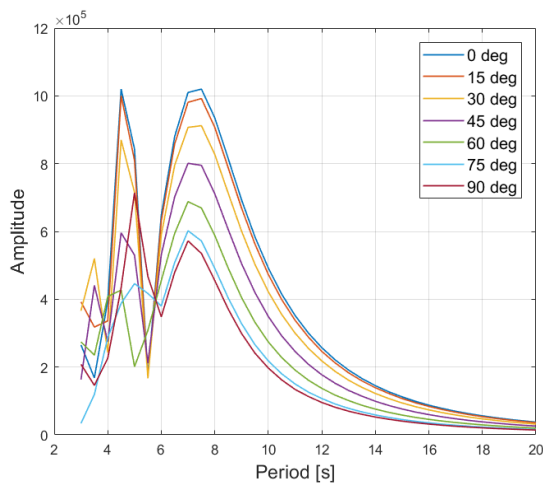


Figure 11.9: RAO SECL1011

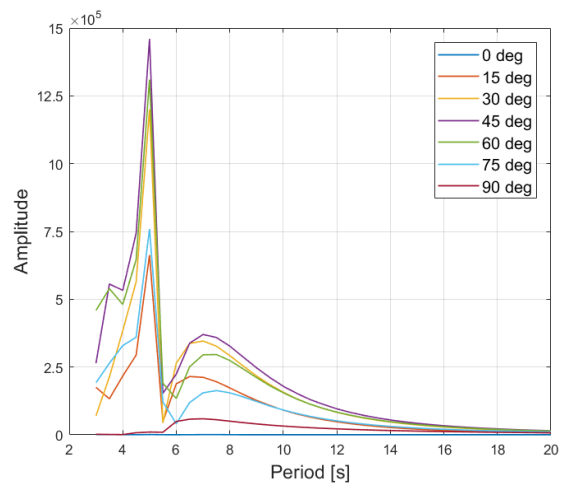


Figure 11.10: RAO SECL1012

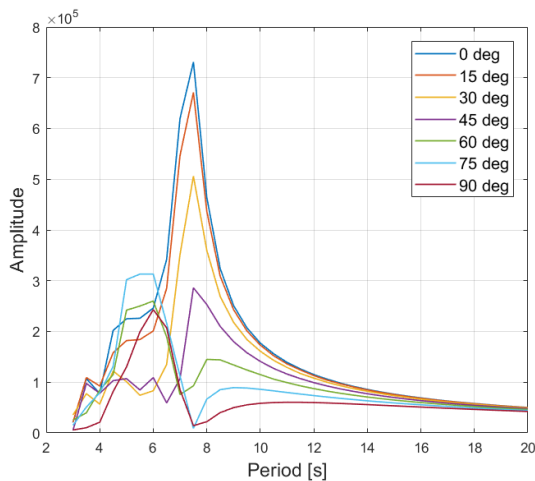


Figure 11.11: RAO SECL1013

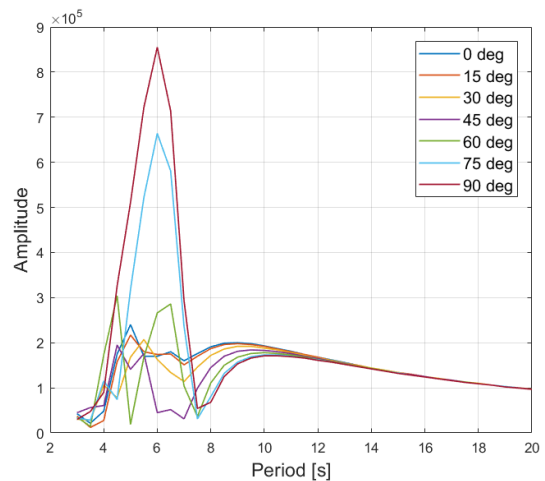


Figure 11.12: RAO SECL3013

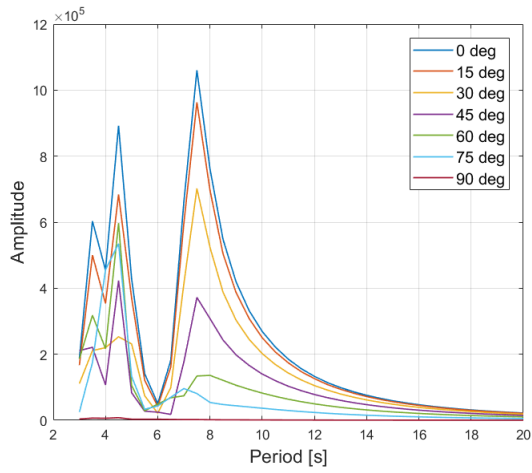


Figure 11.13: RAO SECL3021

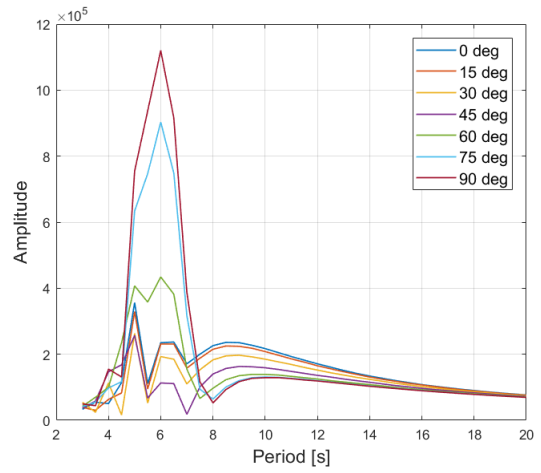


Figure 11.14: RAO SECL3023

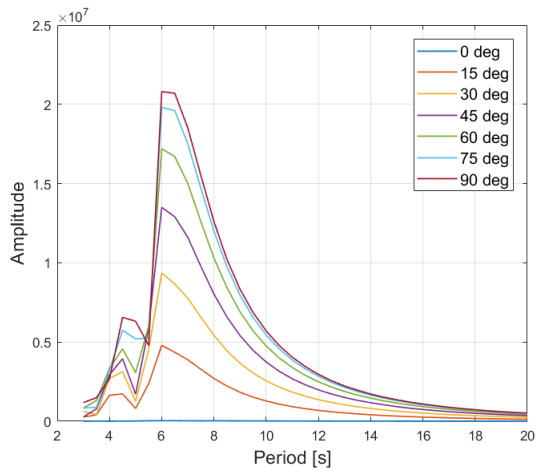


Figure 11.15: RAO SECL3024

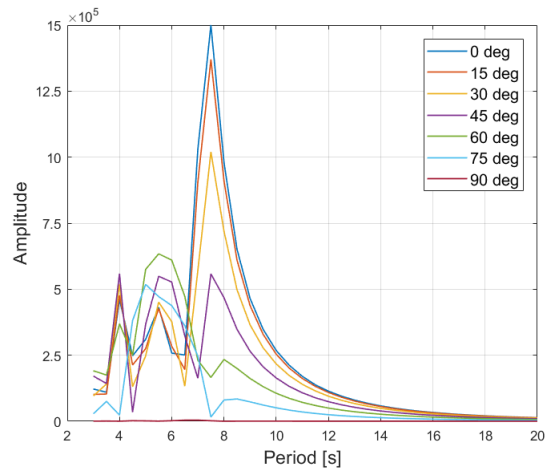


Figure 11.16: RAO SECL3031

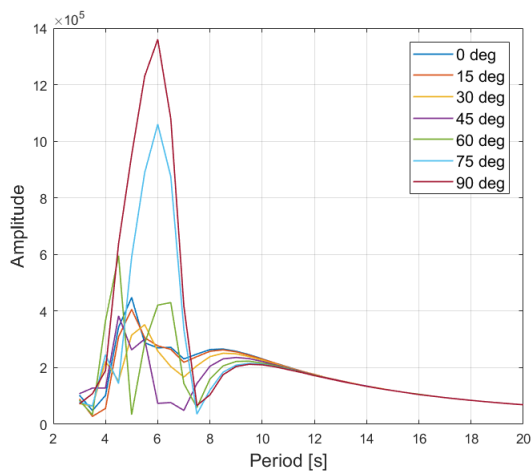


Figure 11.17: RAO SECL3033

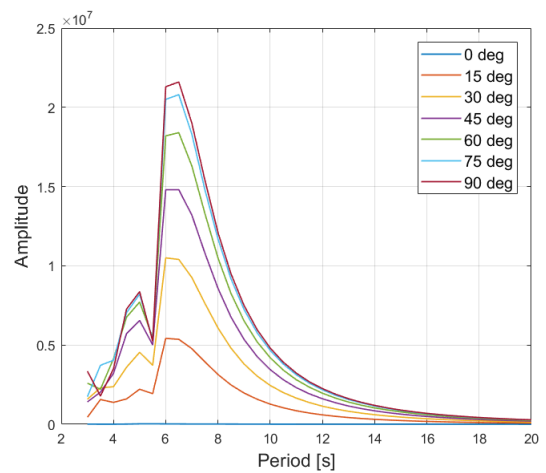


Figure 11.18: RAO SECL3034

The results show that all the RAO's have a peak in the interval between 5 and 10 seconds. For longer periods the response approaches zero. This is because waves with significantly longer period than the natural period of the system will give minimal dynamic response. Table 11.2 presents the resulting design waves from the statistical design wave analysis.

Table 11.2: Properties of design waves - Statistical analysis

Load case	Section	Direction	Most prob	N	Load max	RAO-Value	Amplitude	Period	Wave length	Steepness
2	SECL1011	0	5.09.E+06	1798	5.81E+06	1.02E+06	2.84	7.5	87.82	0.065
3	SECL1012	45	3.88.E+06	2264	4.41E+06	1.46E+06	1.51	13.5	284.55	0.011
4	SECL1013	0	2.37.E+06	1643	2.71E+06	7.31E+05	1.85	7.5	87.82	0.042
5	SECL3013	90	3.90.E+06	1817	4.45E+06	8.55E+05	2.60	10	156.13	0.033
6	SECL3021	0	3.12.E+06	1969	3.55E+06	1.06E+06	1.68	7.5	87.82	0.038
7	SECL3023	90	5.06.E+06	1810	5.77E+06	1.12E+06	2.57	10	156.13	0.033
8	SECL3024	0	1.03.E+08	1697	1.17E+08	2.08E+07	2.82	10	156.13	0.036
9	SECL3031	0	3.75.E+06	1625	4.28E+06	1.50E+06	1.42	7.5	87.82	0.032
10	SECL3033	90	6.27.E+06	1842	7.15E+06	1.36E+06	2.62	10	156.13	0.034
11	SECL3034	90	1.07.E+08	1708	1.22E+08	2.16E+07	2.82	6.5	65.97	0.085

In the last column in Table 11.2 wave steepness is calculated. This is to ensure that the waves are physically realistic. All of the design waves meet the steepness criteria and can be used further in a structural analysis. The periods 7.5 and 10 seconds stands out as most critical for several sectional loads.

11.5.2 Extracting Physical Response of Complex Results

A wave is modeled as a complex number due to its harmonic nature. This will also produce a complex result case, comprised of a real and an imaginary part. The two parts describe the harmonic, sinusoidal, response. Basic stress components, as well as displacements and forces, are harmonic. The derived von Mises stress and the principal stresses are non-linear combination of the basic stress components and therefore non-harmonic [14]. This is illustrated in Figure 11.19.

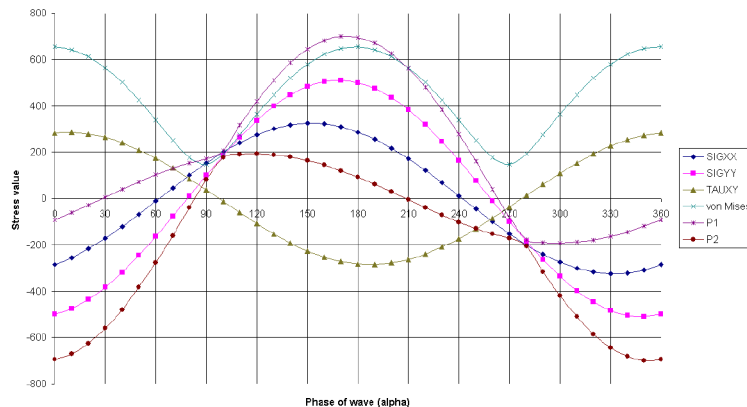


Figure 11.19: Stress variation through a cycle for a complex result case [14]

The phase shift of the response, phase lag between wave and response, is given by Equation (11.1).

$$\varphi = \tan^{-1}\left(\frac{I}{R}\right) \tag{11.1}$$

I is the imaginary part of the response and R is the real part of the response.

The magnitude, amplitude of the response, is found by using Equation (11.2) and represents the maximum value of the component through the cycle.

$$M = \sqrt{R^2 + I^2} \tag{11.2}$$

11.5.3 Results From Design Wave Analysis - Stress Peak

Plate elements

In Figure 11.20, the areas used in the stress peak analysis are marked. Table 11.3 presents which element corresponds to the different stress peak areas. As von Mises stress is non-harmonic, the maximum value through a cycle is used. As could be expected, the rotation tank and floating collar experience the highest levels of stress. The position depends on the wave direction, as this decides which part of the floating collar that is hit first.

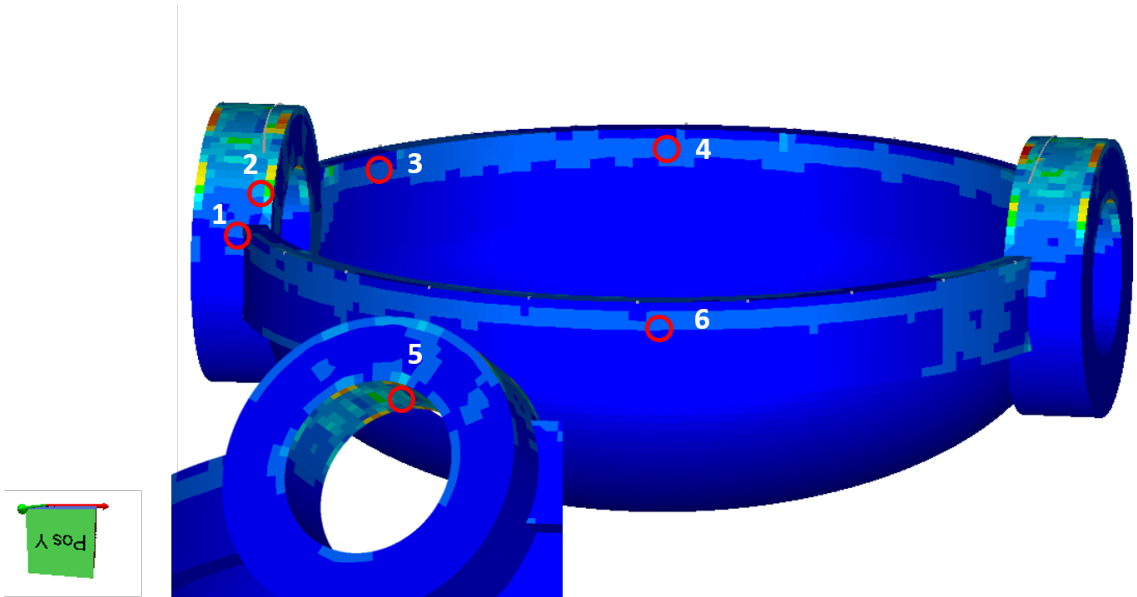


Figure 11.20: Areas with high stress peaks

Table 11.3: Corresponding element number to stress peak area

Area number	Element number
1	5205
2	3618
3	5084
4	5511
5	3834
6	19621

Figure 11.21 to 11.26 presents the stress RAO's for the chosen elements in the stress peak analysis.

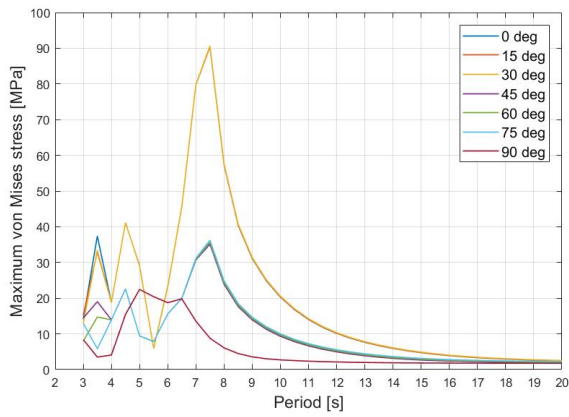


Figure 11.21: Maximum von Mises stress in element 5205

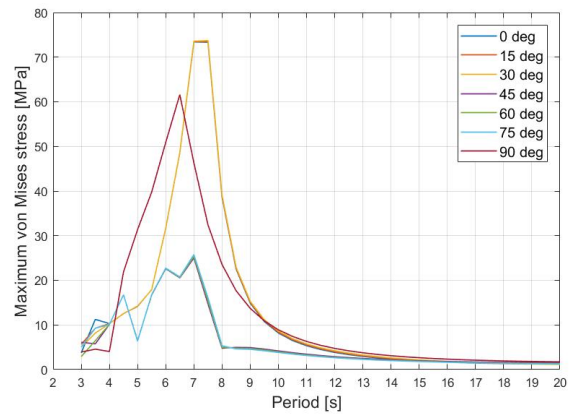


Figure 11.22: Maximum von Mises stress in element 3618

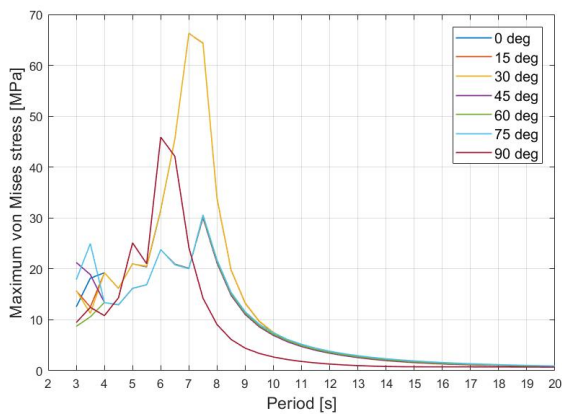


Figure 11.23: Maximum von Mises stress in element 5084

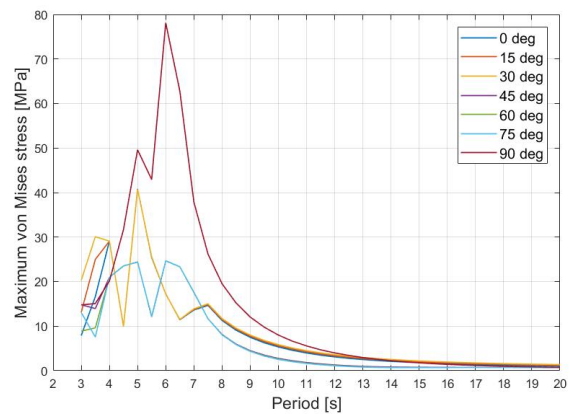


Figure 11.24: Maximum von Mises stress in element 5511

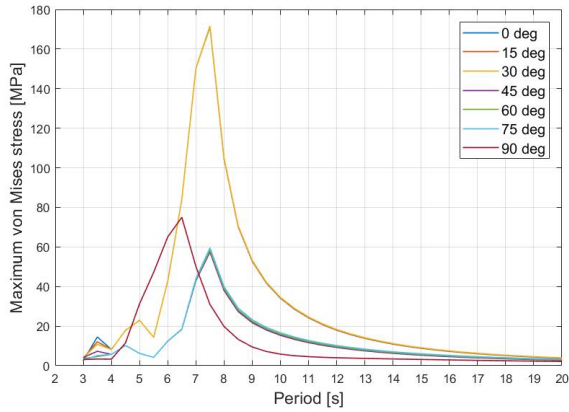


Figure 11.25: Maximum von Mises stress in element 3834

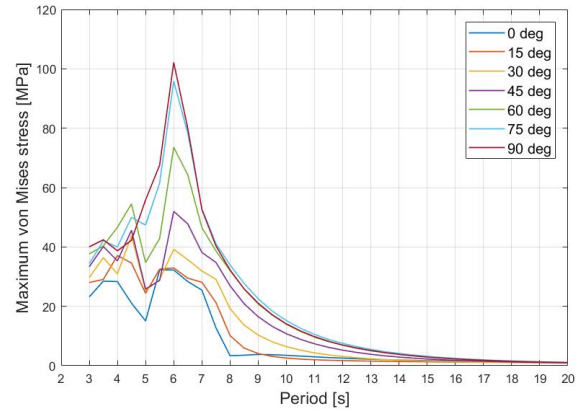


Figure 11.26: Maximum von Mises stress in element 19261

Beam elements

For beam elements, normal stress is used in the stress peak analysis. This is a harmonic load and the maximum value of the component through the cycle is used, calculated by Equation (11.2). For the beam elements the highest stress occurs in the top two rows of the framework especially those supporting the two rotation tanks. Information about critical beam elements and their location is given in Figure 11.27 and Table 11.4.

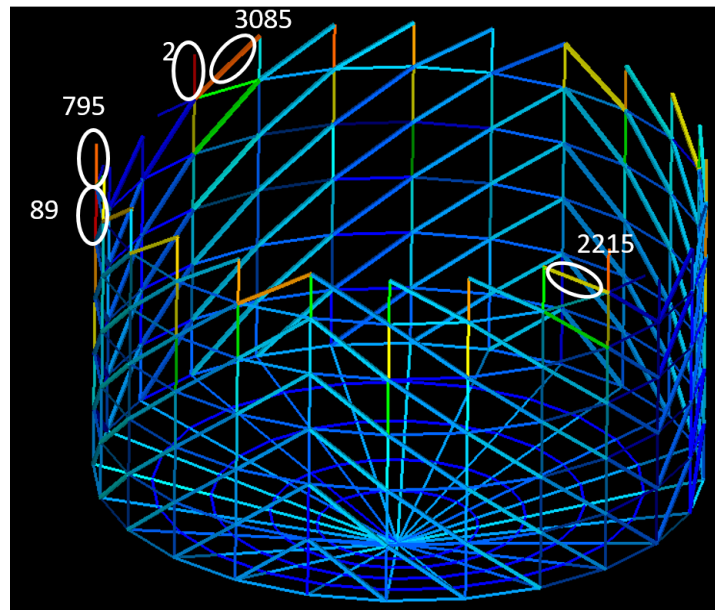


Figure 11.27: Critical beam elements used in a stress peak analysis

Table 11.4: Corresponding element number to stress peak area

Area number	Element number
1	2
2	89
3	795
4	2215
5	3085

Figure 11.28 to 11.32 presents the stress transfer functions for the chosen beam elements.

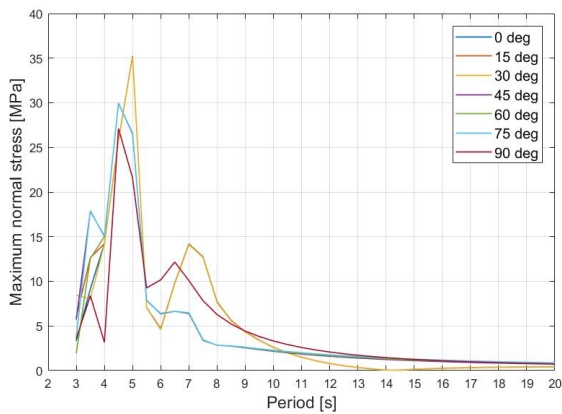


Figure 11.28: Maximum normal stress through a cycle for element 2

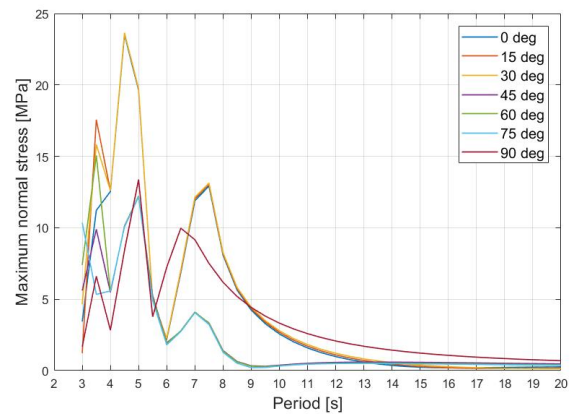


Figure 11.29: Maximum normal stress through a cycle for element 89

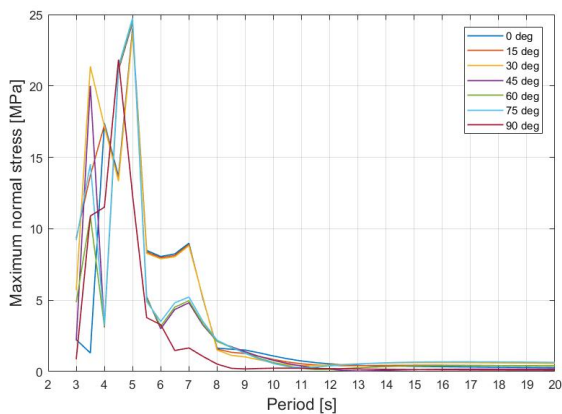


Figure 11.30: Maximum normal stress through a cycle for element 795

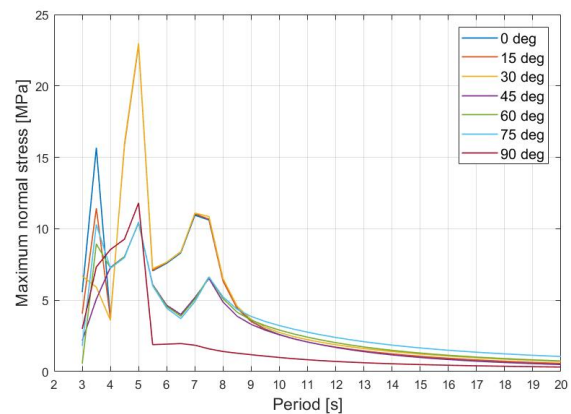


Figure 11.31: Maximum normal stress through a cycle for element 2215

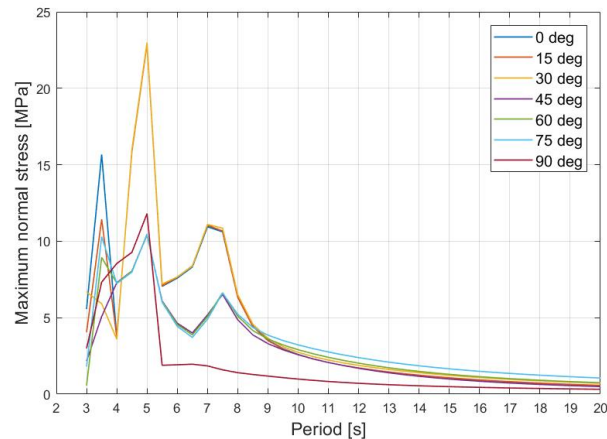


Figure 11.32: Maximum normal stress through a cycle for element 3085

Summary of stress RAO's from stress peak analysis

Peaks in the stress RAO's for plate elements occurs mainly for wave directions 30° and 90° and periods between 5 and 8 seconds.

For beam elements a wave direction of 30° stands out as the most critical direction. In addition, 0° and 75° stands out as critical directions. The stress peak occurs for periods between 4 and 6 seconds.

From the stress RAO's plots, it is apparent that it is a difference in peak period for the framework and floating collar. This may be a result of a small dynamic amplification of the beam elements. For the floating collar stiffness and geometric relations are more dominating and the peak period increases.

For different parts of the structure, different directions and periods dominates as most critical. From the stress RAO's it is clear that periods between three and nine second will produce the most stress. Longer periods will give larger wave lengths, a floating structure will, for large periods and wave lengths, follow the wave motion and therefore not be subjected to large dynamic forces. This theory is consistent with the stress transfer functions for FlipCage. The resulting design waves from a stress peak analysis is given in Table 11.5.

Table 11.5: Design waves from a stress peak analysis

direction [°]	Period [s]	Wave length [m]	H_{max} due to steepness [m]	H_{max} due to H_s [m]	Wave amplitude [m]	Load case number
30	7.5	87.82	12.55	6.65	3.33	81
15	7	76.50	10.93	6.65	3.33	45
90	6.5	65.97	9.42	6.65	3.33	219
90	6	56.21	8.03	6.65	3.33	218
15	7.5	87.82	12.55	6.65	3.33	46
0	5	39.03	5.58	6.65	2.79	6
15	5	39.03	5.58	6.65	2.79	41
30	5	39.03	5.58	6.65	2.79	76
75	5	39.03	5.58	6.65	2.79	181
0	4.5	31.62	4.52	6.65	2.26	5

11.5.4 Discussion of Results - Design Wave Analysis

The main difference between the two methods is that the statistical approach requires more knowledge about the response in advance. This is because the chosen sectional loads will affect the outcome of the analysis. For a structure with an unfamiliar geometry it is difficult to be aware of all global responses and include the correct sectional planes in the analysis.

The standard used, DNV GL-RP-C103 [7], is mainly meant for column-stabilised units such as semi-submersible rigs. The response of a semi-submersible is thoroughly studied and since the geometry does not vary a lot, it is easy to make a general approach. However, for structures that vary a lot in geometry and design, the structural response is not well known. It is therefore difficult to ensure that all critical sectional planes are included in the design wave analysis. The benefit of the statistical method is that, for a well known geometry, it can produce a set of design waves and ensure a sufficient safety level.

For a stress peak analysis, the benefit is that the structural response is known before making decisions that will affect the design waves significantly. By looking at the result of the load cases, areas that experience high levels of stress can be located. Choosing elements in these areas and plotting the stress for all directions and periods, gives a better overview of the response. It is therefore less likely that critical design waves are missed. In this case seven directions and thirty-five periods were combined, making it a total of 245 load cases. Checking all the load cases for different stress components is time consuming and certain responses can be missed.

The statistical approach resulted in design waves with significantly longer periods than the stress peak analysis. The periods ranges up to 13.5 seconds, while the longest period for the stress peak analysis is 7.5 seconds. It is SECL1012, which estimates the largest shear force in a vertical plane, that produces the longest period. Looking at the stress RAO's from the stress peak analysis the von Mises and normal stress is minimal at this period.

Comparing the two methods may indicate that the second method may be safer and more conservative. Given that FlipCage has a geometry that is quite different from a semi-submersible, it is difficult to know that all the correct sectional planes and loads are included in the analysis. A stress peak analysis can therefore be more beneficial in this case. Looking at the result, it is also clear that the statistical design wave approach missed some of the critical responses. It may be the case that different parts of the structure has different design waves, and that this is missed in the statistical design wave approach. For FlipCage, the statistical design wave analysis missed directions and periods that produced areas with significant levels of stress.

11.6 Results from ULS Analysis

11.6.1 Static Load Case

According to theory, the hydrostatic load case should show a linearly increasing surface pressure below the waterline. Figure 11.33 is a plot of the surface pressure from the load case where only the static water pressure is applied. The pressure starts at the waterline, at the middle of the floating collar. As can be seen from the color plot, the surface pressure increases linearly with the water depth. The magnitude is consistent with the hand calculations of the hydrostatic pressure.

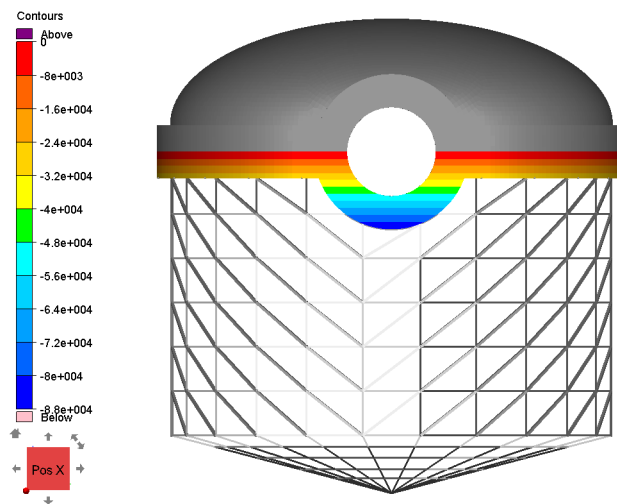


Figure 11.33: Surface pressure - static load case

11.6.2 ULS From Statistical Design Wave Analysis - von Mises Stress

Figure 11.35 to 11.38 shows the two most critical load cases from each load factor combination. The rest of the load cases can be found in the Appendix C.2. The contour color values of the von Mises stress are shown in Figure 11.34.



Figure 11.34: Color coding of the von Mises stress level given in Pascal

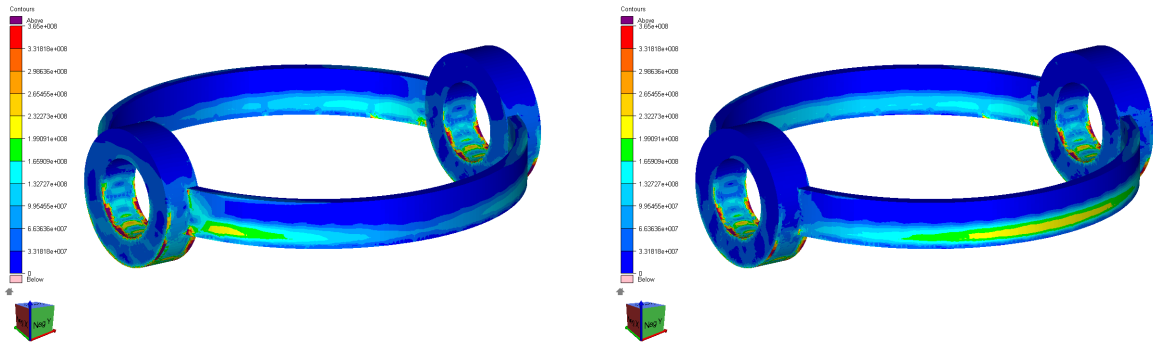


Figure 11.35: von Mises stress load case 1.02 - Figure 11.36: von Mises stress load case 1.11 - ULSA

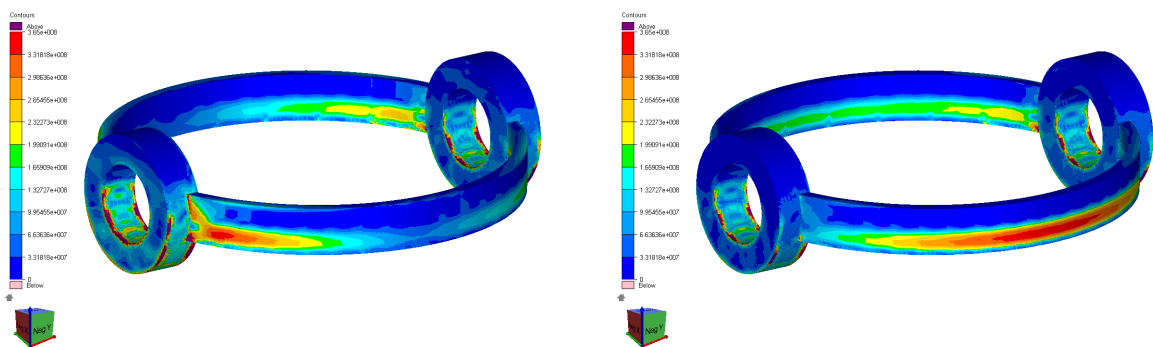


Figure 11.37: von Mises stress load case 1.02 - Figure 11.38: von Mises stress load case 1.11 - ULNB

11.6.3 ULS From Stress Peak Analysis - von Mises Stress

Figure 11.39 to 11.42 shows a plot of von Mises stress from the load cases that produced the most critical loading conditions. The rest of the load cases can be found in Appendix C.1. The color represents the level of stress and the scale spans between 0 and 365 MPa, for details see Figure 11.34.

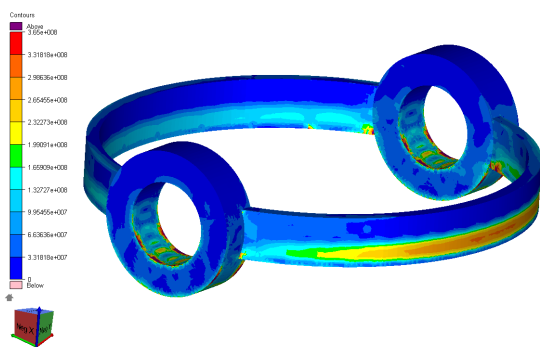


Figure 11.39: Load case 2.05 - ULSA

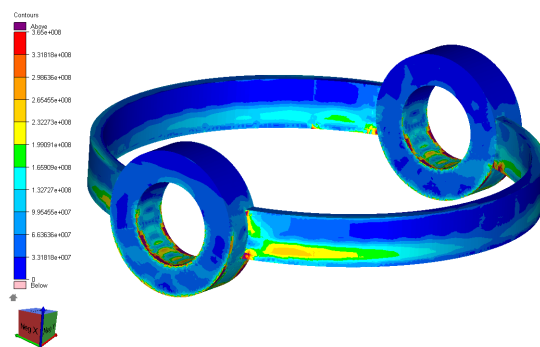


Figure 11.40: Load case 2.06 - ULSA

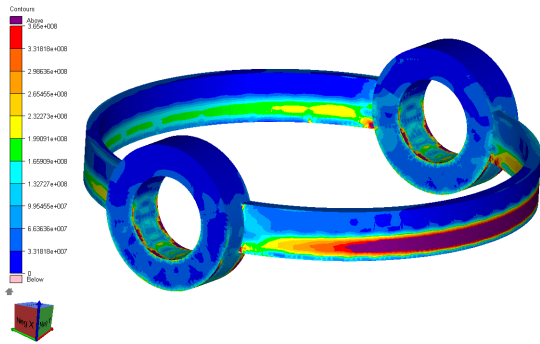


Figure 11.41: Load case 2.05 - ULSB

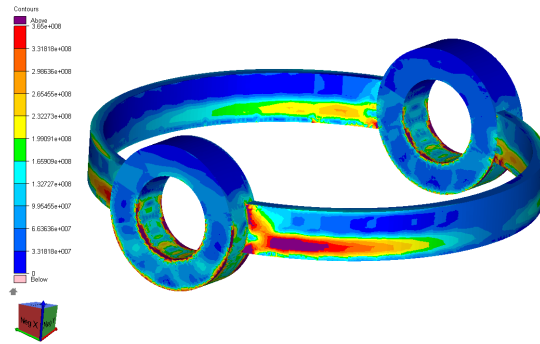


Figure 11.42: Load case 2.06 - ULSB

11.6.4 Discussion of ULS Results - von Mises Stress

It is apparent, when comparing the results from the two design wave analysis, that the two methods gave different results for the most critical design waves. Comparing the results from the ULS analysis, it is clear that the statistical method missed some important responses. An important note is that the stress peak analysis is more conservative, as it assumes a maximum wave height in the sea state. The statistical design wave approach calculates an amplitude based on maximum response and the corresponding RAO value.

Load case combination 2.05, direction 90° and a period of six seconds, gave the highest von Mises stress out of all waves checked. This wave was found by using the stress peak analysis. If this wave is compared to the result from the statistical design waves, load case 1.11 gave a wave with period 6.5 seconds and a direction of 90° . The RAO for for this sectional load is given in Figure 11.18, from this it is seen that there is only a small difference in the amplitude between 6 and 6.5 seconds.

The response from these two waves are given in Figure 11.41 and 11.38 and the difference in response is significant as the wave with period 6.5 seconds results in a von Mises stress which is within the allowable limit, and the wave with period 6 seconds does not. However, this may be due to the wave heights which in load case 2.05 and 1.11 is 3.3 meters and 2.82 meters, respectively. Furthermore, the wave length for a wave with period 6 seconds is much closer to the diameter of FlipCage. This may be the reason that a change in period of 0.5 seconds gives a significant change in the level of stress.

11.7 Buckling Capacity Check

A buckling capacity check is executed for the design waves from both methods. The result is presented in Figure 11.43 and 11.44 . The color coding refers to the utilisation factor of the cross section. If the utilisation factor is greater than 1, it implies that buckling will occur and the beam has to be reinforced.

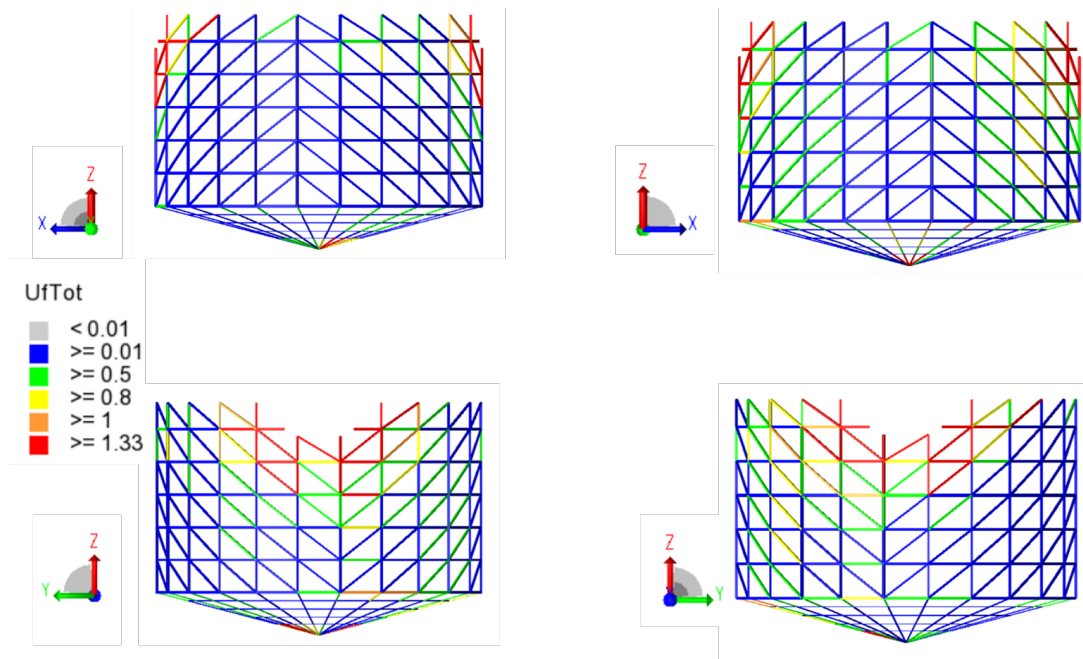


Figure 11.43: Capacity check of beams from design waves identified in a statistical design wave analysis.

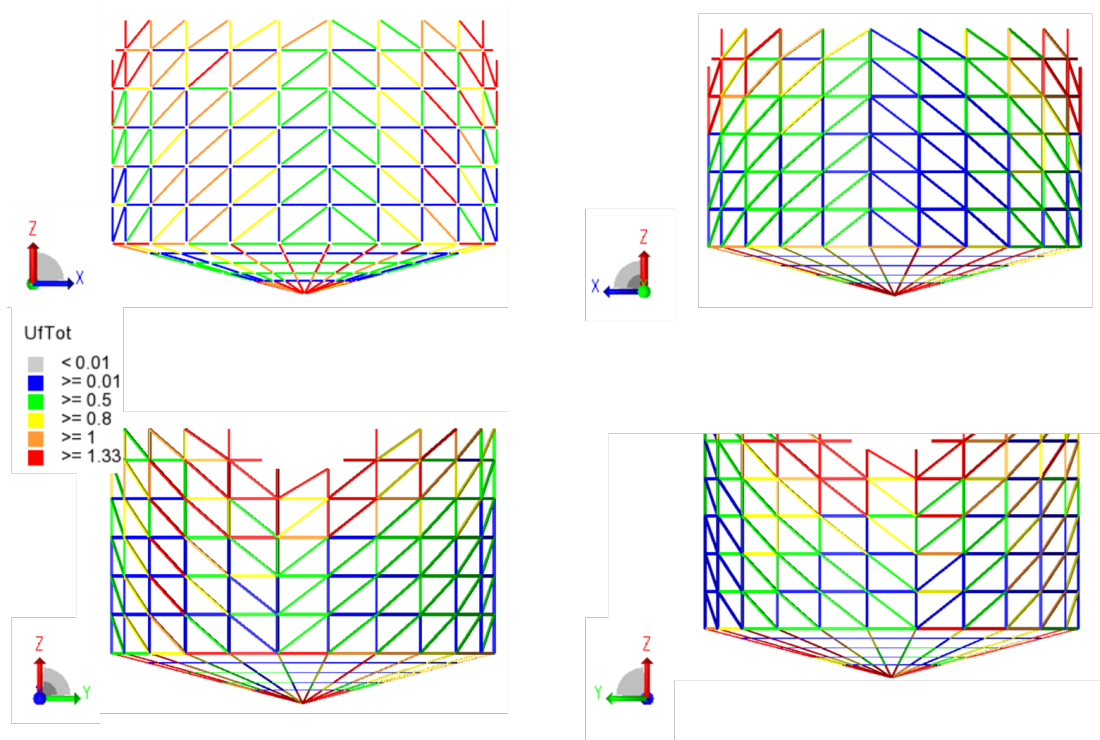


Figure 11.44: Capacity check of beams from design waves identified in a stress peak analysis.

In order to ensure structural integrity, beams with a utilisation factor greater than 1 needs to be redesigned. As could be expected, the most critical members are those supporting the rotation tanks. From Figure 11.43 and 11.44 it can be seen that, in general, the utilisation factor is higher in the capacity check with design waves from the stress peak analysis.

The waves from the stress peak analysis produced a greater set of beams with a utilisation factor greater than 1, compared to the design waves from the stochastic response analysis. In the stress peak analysis beam elements were evaluated separately. They resulted in waves with significantly lower periods than for the elements chosen on the floating collar. The design waves from the statistical approach had waves with significantly longer periods than the stress peak analysis. Looking at which load cases are most critical for each beam member, there were a significant amount that failed due to load cases generated by the stress peak analysis of beam elements. This may be the reason that the stress peak analysis produced a greater set of beams with a utilisation factor greater than 1.

Conclusion and Further Work

12.1 Conclusion

12.1.1 Eigenvalue Analysis

The results from the eigenvalue analysis show that the dynamic amplification of the load effects of this structure will be insignificant.

12.1.2 Design Wave Analysis

The result from the design wave analysis clearly shows that the statistical design wave analysis missed some critical responses. This is because the analysis is based on evaluating the forces at sections selected based on previous experience from structures having a different geometry. With a standard set of sectional planes, it is possible to include the most critical responses for the system. However, when using this method for other types of structures, predicting which sectional planes to include in the analysis is difficult.

In the offshore industry the same type of platforms are used; semi-submersible, tension leg platform, SPAR or FPSO. Having a set of design rules for each of these structures is possible because within each platform type there are only small differences in the main geometry. The benefit of having standard design rules, is that you ensure that critical responses are dimensioned for and it is easier to set the safety level.

Fish farming concepts that have applied for the development license varies a lot in size and geometry. Developing a set of design rules for these is therefore difficult as their response will vary with the design. In a stress peak analysis, more information about the structural response is available before having to make choices that will affect the outcome of the design waves. From the results it is also apparent that the stress peak analysis identifies critical waves the

statistical design wave analysis misses. It can therefore be concluded that for a structure with an unfamiliar geometry, it is better to use a stress peak analysis approach to determine critical load cases.

12.1.3 Ultimate Limit State

von Mises stress

The results from the ultimate limit state capacity check show that the von Mises stress exceeds the allowed limit for certain wave periods and directions. Therefore, it is necessary to strengthen these areas through increasing the plate thickness of the material. Overall the stress levels are within allowed limits, indicating that no major changes to the design is necessary. Load factor combination b) produced the result cases with the highest stress values.

Buckling check

The buckling check showed that several cross-sections were utilized above their capacity. This is critical for the structure, and these have to be redesigned in order to ensure the structural integrity. This can be done through changing the cross-section of the beams or adjusting the framework so that the length of critical members are reduced.

12.2 Further Work

It is necessary to redesign the beams that showed a utilisation factor above 1 in the code check. This can either be done through changing the cross-sectional properties, the material or the design of the framework.

Furthermore, it is necessary to increase the plate thickness in parts of the structure to reduce the von Mises stress for areas where it exceeds the allowable limit. Girders and stiffeners were not modeled, by including these, stress levels may be reduced further. In areas with stress concentrations, it is necessary to create a local structural model. In the local model the level of detail increases and the displacement and stresses from the global model works as boundary conditions.

Fatigue limit state (FLS) is important for structures experiencing dynamic loading. Dynamic loading causes an oscillation in stress levels which can lead to fatigue in certain parts of the structure. Each part of the structure needs to meet the lifetime requirements.

Accidental limit state (ALS) are accidental loads due to e.g. ship collision from well boats. There are certain requirements for the level of impact a structure is required to absorb before capsizing. ALS is especially important due to the danger of fish escape, as this can lead to severe environmental impact and cause a risk to wild salmon stock.

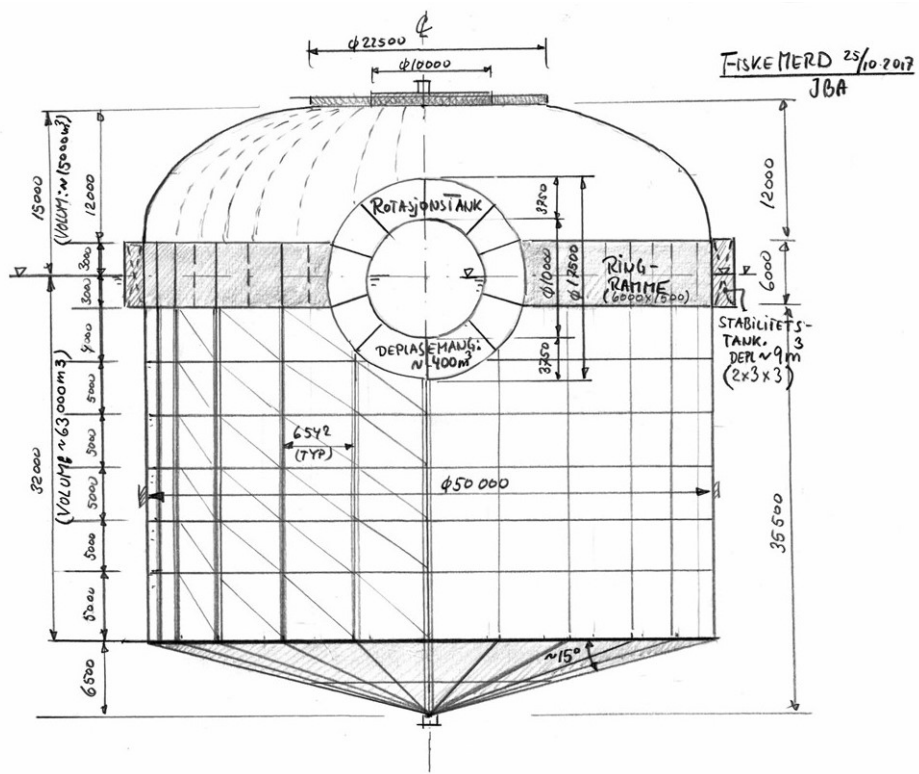
Bibliography

- [1] Aker Solutions. *Konseptutviklingsstudie roterbart merdkonsept*. 2018.
- [2] *Arctic Offshore Farming*. URL: <https://www.arcticoffshorefarming.no/>.
- [3] P. Bore, J. Amdahl, and D. Kristiansen. “Modelling of Hydrodynamic Loads on Aquaculture Net Cages by a Modified Morison Model”. In: May 2017.
- [4] K. S. Carl Larsen Jørgen Amdahl. *Marinteknikk 2 : kompendium : B. 2*. nor. Trondheim, 2006.
- [5] DNV GL. *DNVGL-CG-0128 Buckling*. 2015.
- [6] DNV GL. *DNVGL-OS-C101 Design of offshore steel structures, general - LRFD method*. 2016.
- [7] DNV GL. *DNVGL-RP-C103 Column-stabilised units*. 2017.
- [8] DNV GL. *DNVGL-RU-OU-0503, Offshore fish farming units and installations*. 2017.
- [9] DNV GL. *DNV-RP-C205 Environmental conditions and environmental loads*. 2017.
- [10] DNV GL. *DNV-RP-H103: Modelling and Analysis of Marine Operations*. 2011.
- [11] DNV GL. *Sesam User Manual: Sesam Manager*. May 2017.
- [12] DNV GL. *Sesam User Manual: Sestra*. May 2018.
- [13] DNV GL. *Sesam User Manual: Wadan*. Oct. 2017.
- [14] DNV GL. *Sesam User Manual: Xtract*. Oct. 2017.
- [15] O. Faltinsen. *Sea Loads on Ships and Offshore Structures*. Cambridge University Press, 1990.
- [16] Fiskeridirektoratet. “Nøkkeltall fra norsk havbruksnæring 2017”. In: Downloaded 2.12.2018. 2018.
- [17] Fiskeridirektoratet. *Utviklingstillatelser*. (accessed: 02.10.2018). Jan. 2016. URL: <https://www.fiskeridir.no/Akvakultur/Tildeling-og-tillatelser/Saertillatelser/Utviklingstillatelser>.

-
- [18] *Forskrift om krav til teknisk standard for flytende akvakulturanlegg (NYTEK-forskriften)*. URL: <https://lovdata.no/dokument/SF/forskrift/2011-08-16-849>.
- [19] S. N. Godø and F. Bratbak. “Lectuer note: Advanced Analysis of Marine Structures”. In: TMR4305 - Advanced Analysis of Marine Structures - Norwegian University of Science and Technology, Sept. 2018.
- [20] M. Greco. “Lecture Notes: TMR4214 Sealoads”. In: Department of Marine Hydrodynamics, NTNU, Aug. 2012.
- [21] J. Halkyard. *Handbook of Offshore Engineering*. Elsevier, 2005.
- [22] A. Hallenstvedt. *Norsk fiskerihistorie – Store norske leksikon*. URL: https://snl.no/Norsk_fiskerihistorie.
- [23] D. Kristiansen et al. “Classification of Aquaculture Locations in Norway With Respect to Wind Wave Exposure”. In: *OMAE2017* OMAE2017-61659 (June 2017).
- [24] I. Langen and R. Sigbjörnsson. *Dynamisk analyse av konstruksjoner*. Tapir, 1986.
- [25] *List of centroids*. Apr. 2019. URL: https://en.wikipedia.org/wiki/List_of_centroids.
- [26] L. Y. Min. “Lecture note: Dynamic Analysis under Regular Waves”. In: National University of Singapore, Mar. 2018.
- [27] T. Moan. *Finite Modelling and Analysis of Marine Structures*. Sept. 2003.
- [28] D. Myrhaug. “Lecture note: Marine Dynamics”. In: NTNU, 2009.
- [29] NOOMAS. *LR-040613-1-OV Lokalitetsrapport Andal Regnr. 11513*. 2013.
- [30] Norsk Standard. *NS 9415, Marine fish farms. Requirements for site survey, risk analyses, design, dimensioning, production, installation and operation*. 2009. (downloaded: 17.09.2018).
- [31] NTNU. “Lecture note: Drag Forces in Dynamic Analysis”. In: TMR4305 - Advanced Analysis of Marine Structures - Norwegian University of Science and Technology, Sept. 2018.
- [32] S. Olsen. *Giganten ”Ocean Farm 1” blir liten sammenlignet med SalMars nye havmerd*. Apr. 2018. URL: <https://ilaks.no/giganten-ocean-farm-1-blir-liten-sammenlignet-med-salmars-nye-havmerd/>.
- [33] SINTEF. *Offshore salmon fish farming*. (accessed: 15.10.2018). Mar. 2016. URL: <https://www.sintef.no/en/projects/offshore-salmon-fish-farming/>.
- [34] SSB. *Akvakultur*. (accessed 30.11.2018). Nov. 2008. URL: <https://www.ssb.no/en/jord-skog-jakt-og-fiskeri/statistikker/fiskeoppdrett>.

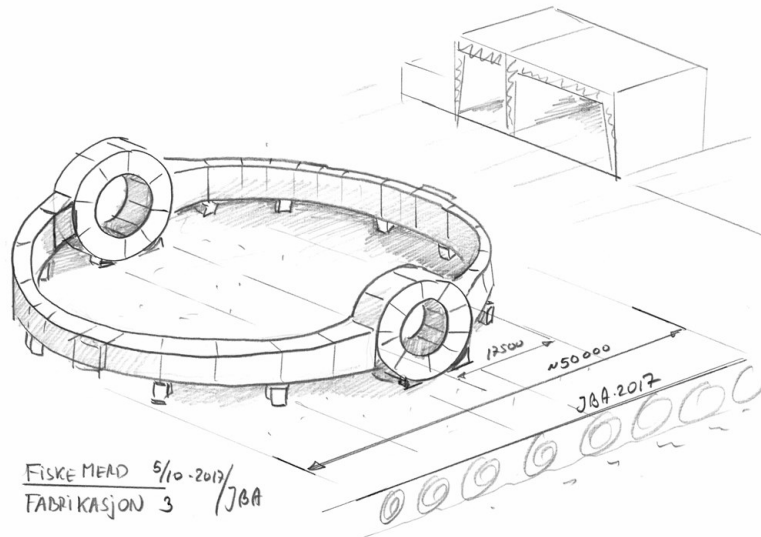
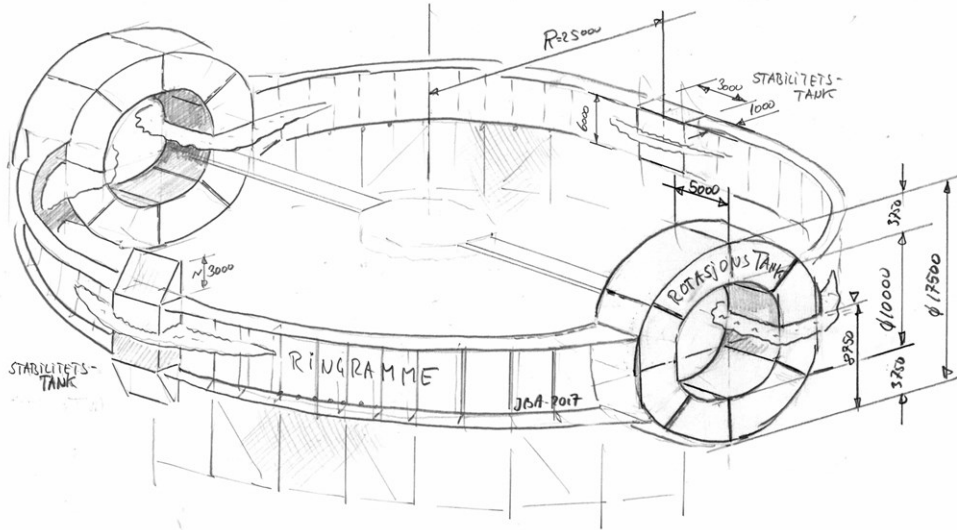
Design Drawings

A.1 Global Design

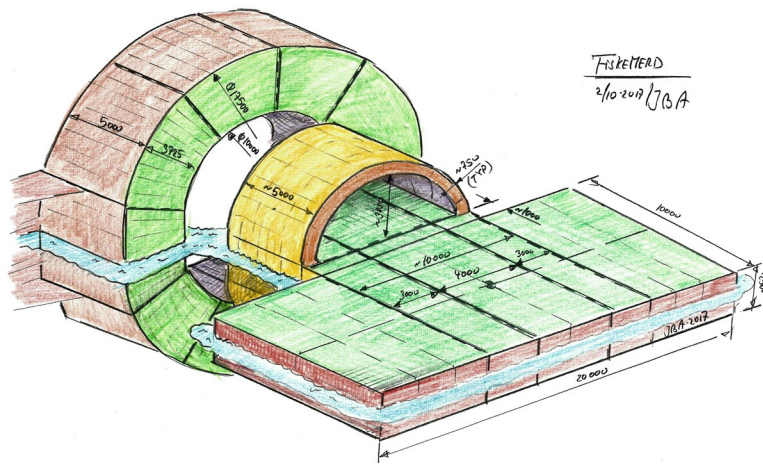
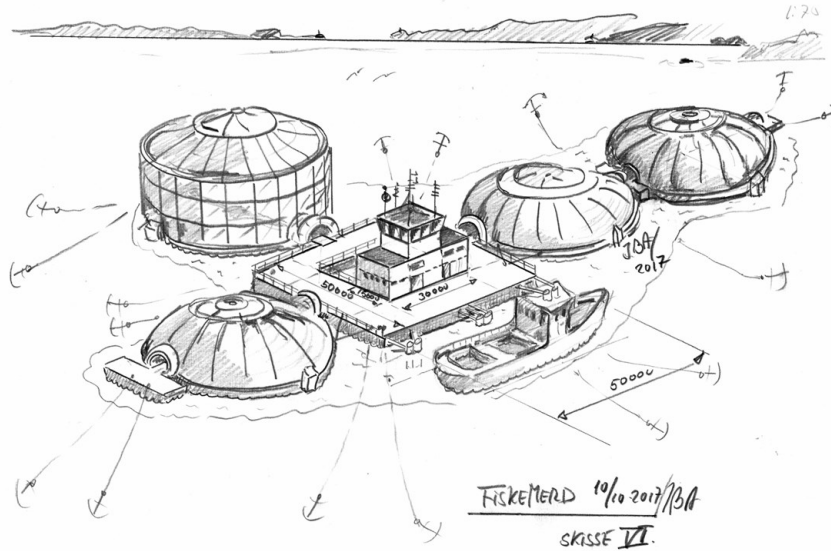


Fiske MEND 27/4-2017/JBA

REV. 1 26/10-2017/JBA



FISKE MEND 5/10-2017/JBA
FABRIKASJON 3



Appendix B

Load case numbering

Period/Direction	3	3.5	4	4.5	5	5.5	6	6.5	7	7.5	8	8.5	9	9.5	10	11	11	12	12	13	13	14	14	14	15	15	16	16	17	17	18	18	19	19.5	20
0	2	3	4	5	6	7	8	9	10	11	12	13	14	15	16	17	18	19	20	21	22	23	24	25	26	27	28	29	30	31	32	33	34	35	36
15	37	38	39	40	41	42	43	44	45	46	47	48	49	50	51	52	53	54	55	56	57	58	59	60	61	62	63	64	65	66	67	68	69	70	71
30	72	73	74	75	76	77	78	79	80	81	82	83	84	85	86	87	88	89	90	91	92	93	94	95	96	97	98	99	100	101	102	103	104	105	106
45	107	108	109	110	111	112	113	114	115	116	117	118	119	120	121	122	123	124	125	126	127	128	129	130	131	132	133	134	135	136	137	138	139	140	141
60	142	143	144	145	146	147	148	149	150	151	152	153	154	155	156	157	158	159	160	161	162	163	164	165	166	167	168	169	170	171	172	173	174	175	176
75	177	178	179	180	181	182	183	184	185	186	187	188	189	190	191	192	193	194	195	196	197	198	199	200	201	202	203	204	205	206	207	208	209	210	211
90	212	213	214	215	216	217	218	219	220	221	222	223	224	225	226	227	228	229	230	231	232	233	234	235	236	237	238	239	240	241	242	243	244	245	246

Results From ULS Analysis

C.1 Results ULS - Stress Peak

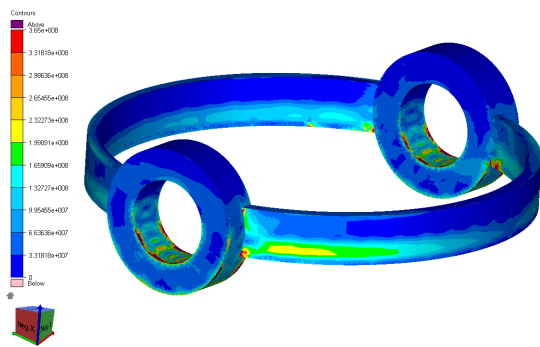


Figure C.1: Load case 2.02 ULSA maximum von Mises stress

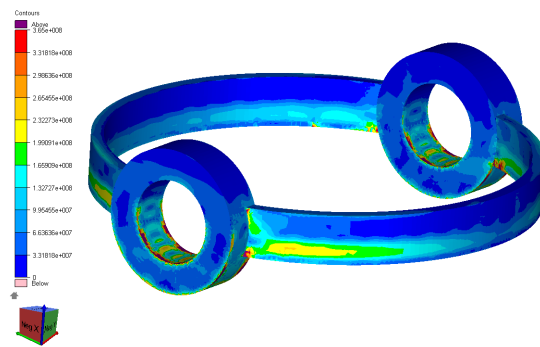


Figure C.2: Load case 2.03 ULSA maximum von Mises stress

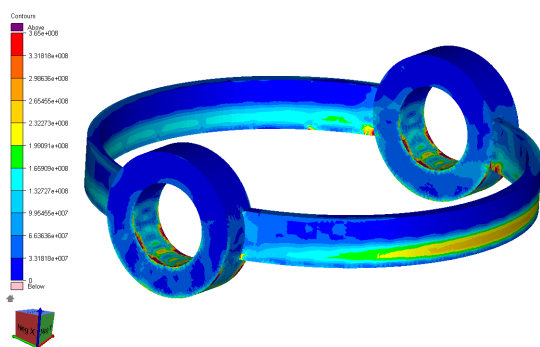


Figure C.3: Load case 2.04 ULSA maximum von Mises stress

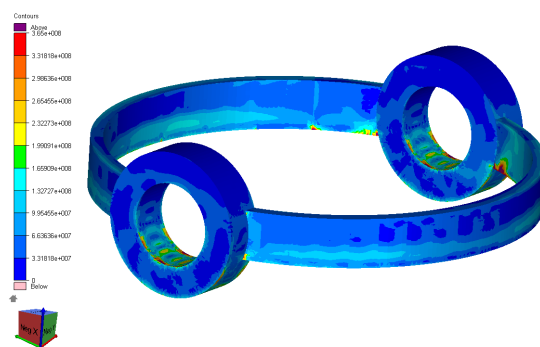


Figure C.4: Load case 2.07 ULSA maximum von Mises stress

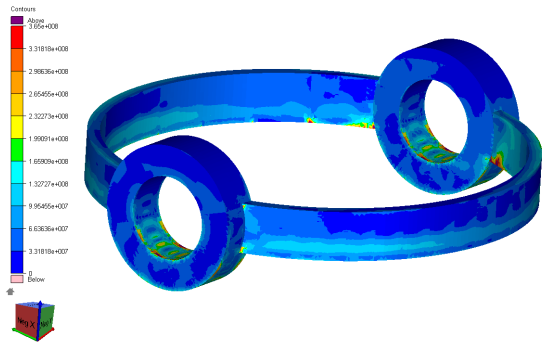


Figure C.5: Load case 2.08 ULSA maximum von Mises stress

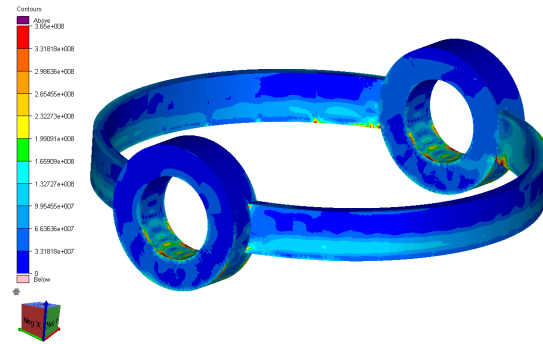


Figure C.6: Load case 2.09 ULSA maximum von Mises stress

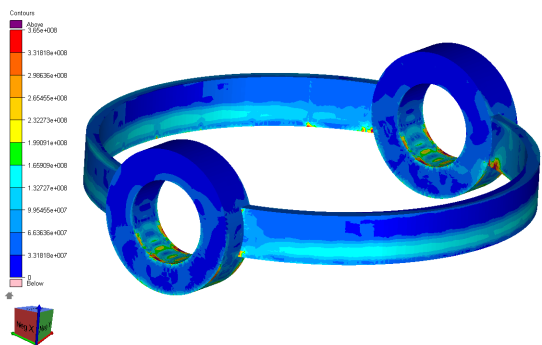


Figure C.7: Load case 2.10 ULSA maximum von Mises stress

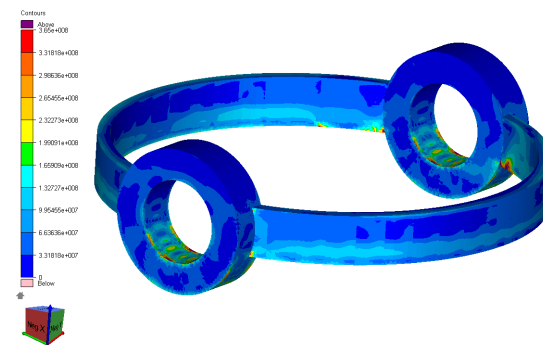


Figure C.8: Load case 2.11 ULSA maximum von Mises stress

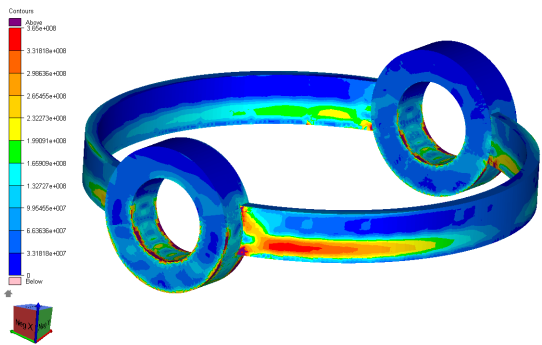


Figure C.9: Load case 2.02 ULSB maximum von Mises stress

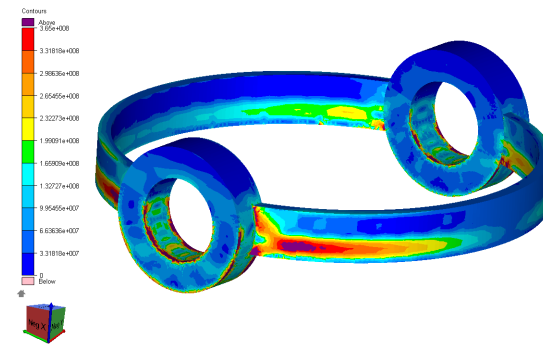


Figure C.10: Load case 2.03 ULSB maximum von Mises stress

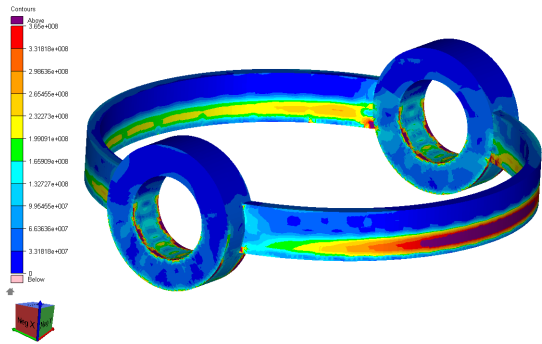


Figure C.11: Load case 2.04 ULSB maximum von Mises stress

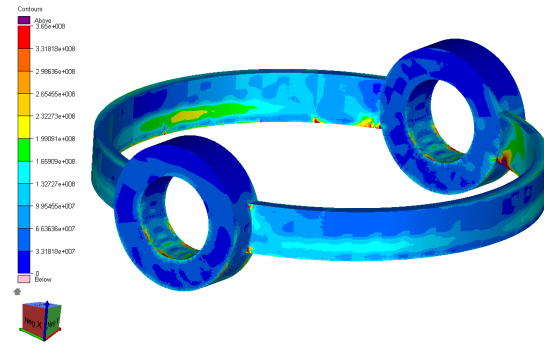


Figure C.12: Load case 2.07 ULSB maximum von Mises stress

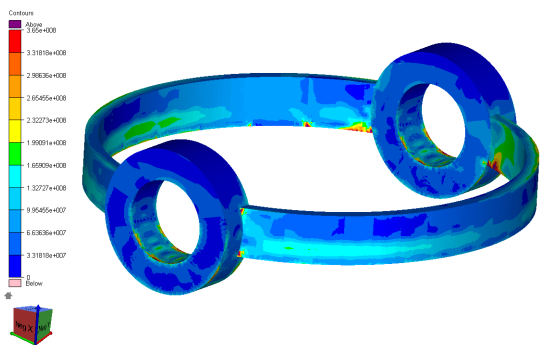


Figure C.13: Load case 2.08 ULSB maximum von Mises stress

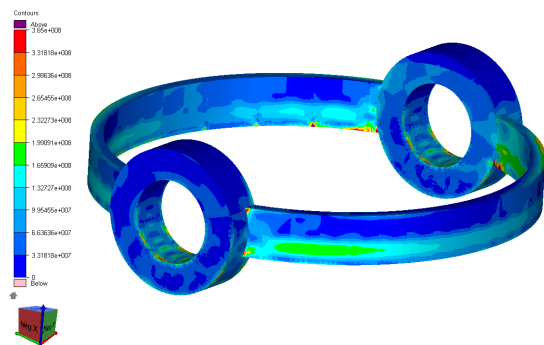


Figure C.14: Load case 2.09 ULSB maximum von Mises stress

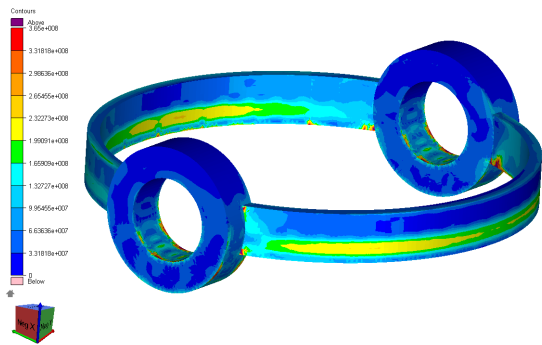


Figure C.15: Load case 2.10 ULSB maximum von Mises stress

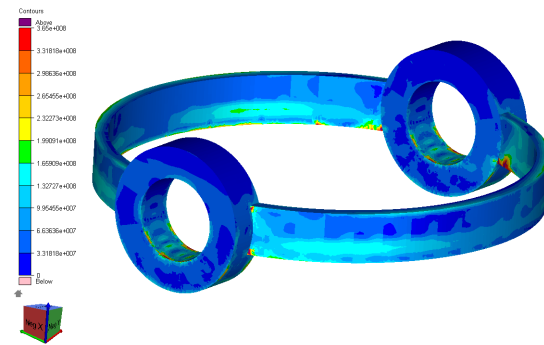


Figure C.16: Load case 2.11 ULSB maximum von Mises stress

C.2 Results ULS - Statistical Response

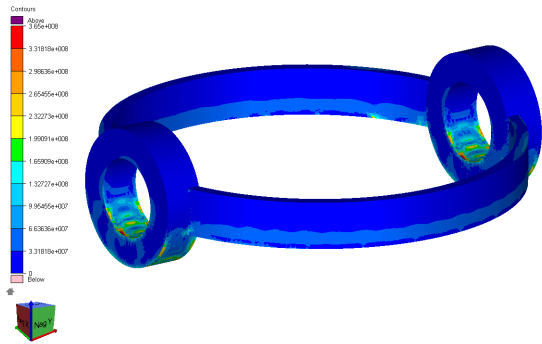


Figure C.17: Load case 1.03 ULSA maximum von Mises stress

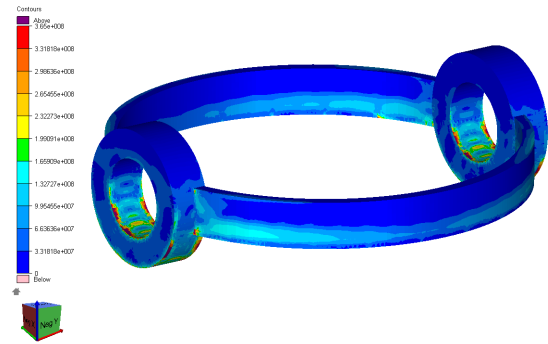


Figure C.18: Load case 1.04 ULSA maximum von Mises stress

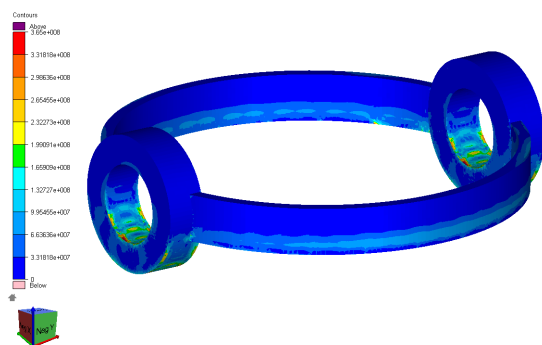


Figure C.19: Load case 1.05 ULSA maximum von Mises stress

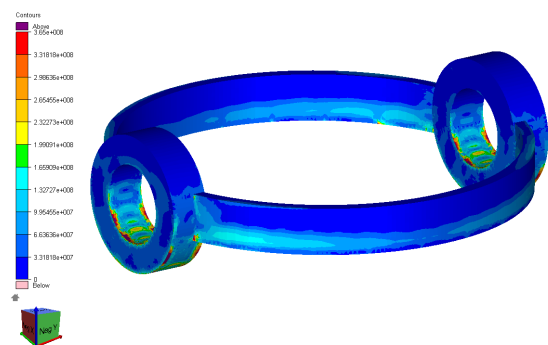


Figure C.20: Load case 1.06 ULSA maximum von Mises stress

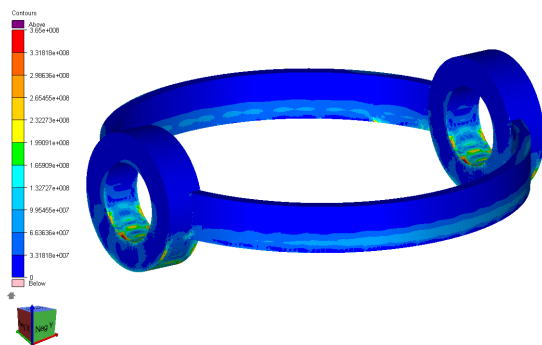


Figure C.21: Load case 1.07 ULSA maximum von Mises stress

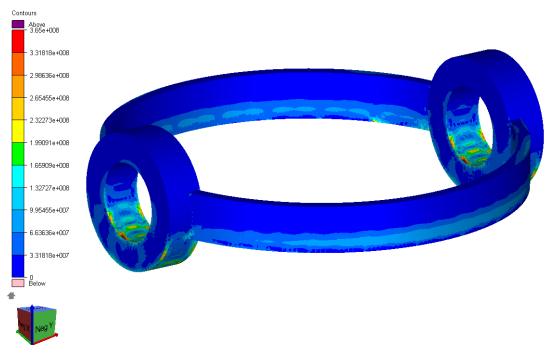


Figure C.22: Load case 1.08 ULSA maximum von Mises stress

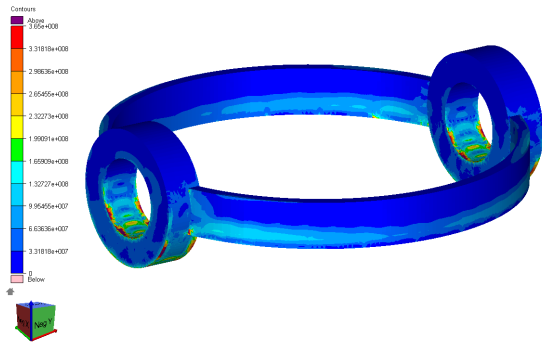


Figure C.23: Load case 1.09 ULSA maximum von Mises stress

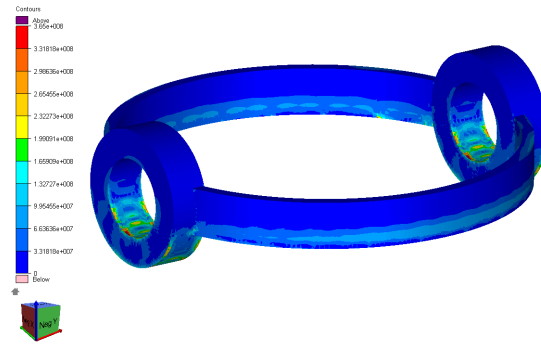


Figure C.24: Load case 1.10 ULSA maximum von Mises stress

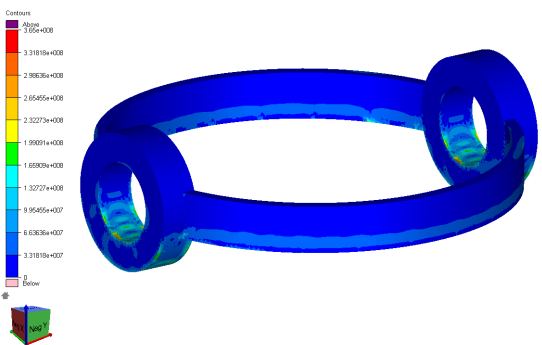


Figure C.25: Load case 1.03 ULSB maximum von Mises stress

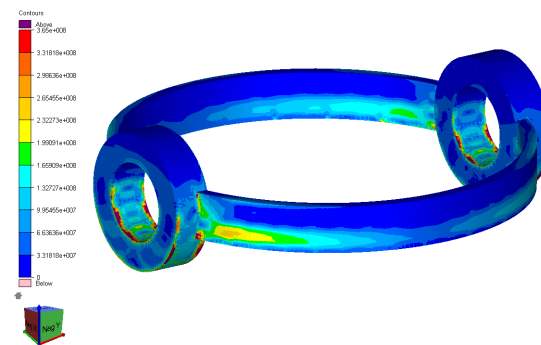


Figure C.26: Load case 1.04 ULSB maximum von Mises stress

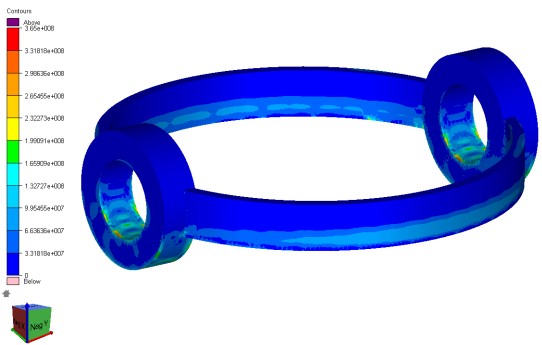


Figure C.27: Load case 1.05 ULSB maximum von Mises stress

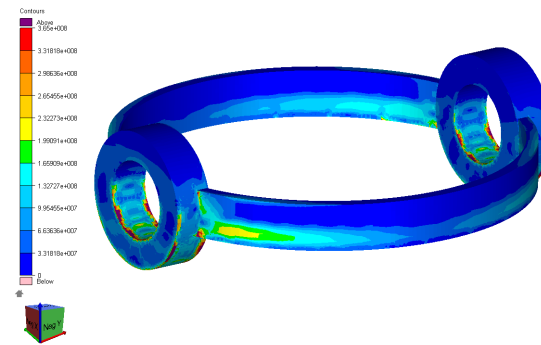


Figure C.28: Load case 1.06 ULSB maximum von Mises stress

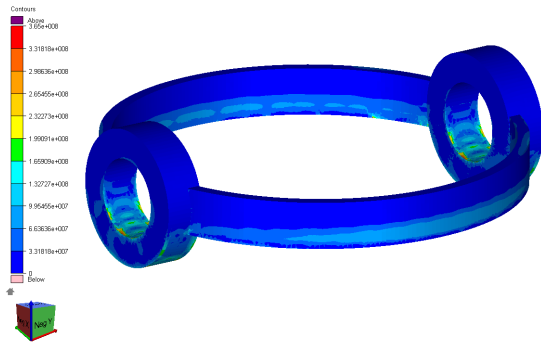


Figure C.29: Load case 1.07 ULSB maximum von Mises stress

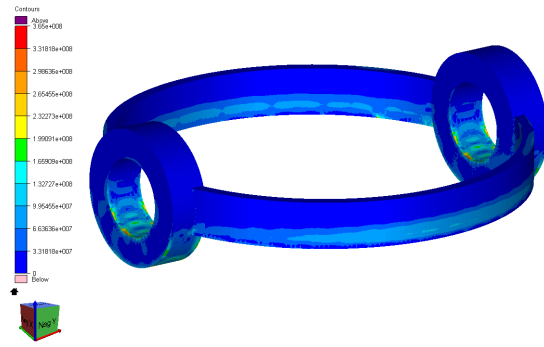


Figure C.30: Load case 1.08 ULSB maximum von Mises stress

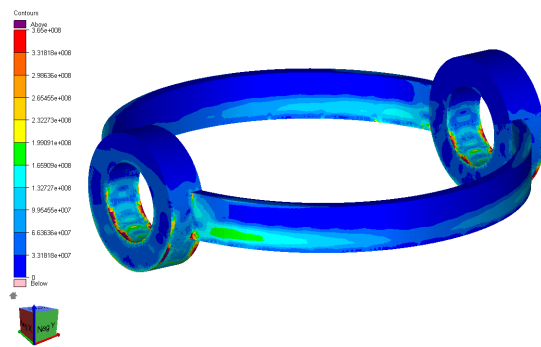


Figure C.31: Load case 1.09 ULSB maximum von Mises stress

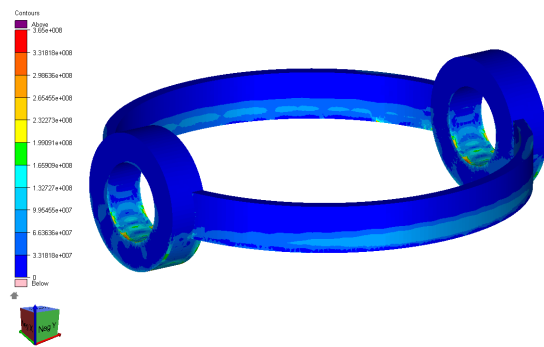


Figure C.32: Load case 1.08 ULSB maximum von Mises stress

Appendix D

Detailed Calculations of Statistical Design Waves

	MAX STDDEV	Description	Most prob	N	Load max	RAO-Value	Amplitude	Period
Section 1	6.58E+05	SECL1011 Dir=0.0 JW7	5.09E+06	1798	5807990.88	1.02E+06	2.84	7.5
Section 2	4.94E+05	SECL1012 Dir=45.0 JW5	3.88E+06	2264	4409432.22	1.46E+06	1.51	13.5
Section 3	3.08E+05	SECL1013 Dir=0.0 JW7	2.37E+06	1643	2706852.67	7.31E+05	1.85	7.5
Section 4	5.03E+05	SECL3013 Dir=90.0 JW7	3.90E+06	1817	4446241.96	8.55E+05	2.60	10
Section 5	4.01E+05	SECL3021 Dir=0.0 JW7	3.12E+06	1969	3552626.92	1.06E+06	1.68	7.5
Section 6	6.53E+05	SECL3023 Dir=90.0 JW7	5.06E+06	1810	5768460.36	1.12E+06	2.57	10
Section 7	1.33E+07	SECL3024 Dir=90.0 JW7	1.03E+08	1697	117434532.56	2.08E+07	2.82	10
Section 8	4.87E+05	SECL3031 Dir=0.0 JW7	3.75E+06	1625	4278427.06	1.50E+06	1.42	7.5
Section 9	8.09E+05	SECL3033 Dir=90.0 JW7	6.27E+06	1842	7147433.81	1.36E+06	2.62	10
Section 10	1.38E+07	SECL3034 Dir=90.0 JW7	1.07E+08	1708	121700627.76	2.16E+07	2.82	6.5

